Fall 2015

Identification of functional group characteristics and physicochemical properties of atrazine degrading Pseudomonas sp. strain ADP biofilm

Victoria Azula Henry
University of Iowa

IDENTIFICATION OF FUNCTIONAL GROUP CHARACTERISTICS AND PHYSICOCHEMICAL PROPERTIES OF ATRAZINE DEGRADING *PSEUDOMONAS* SP. STRAIN ADP BIOFILM

by

Victoria Azula Henry

A thesis submitted in partial fulfillment
of the requirements for the Doctor of
Philosophy degree in Chemical and
Biochemical Engineering
in the Graduate College of
The University of Iowa

December 2015

Thesis Supervisors: Associate Professor Julie L. P. Jessop
Associate Dean Tonya L. Peeples

Graduate College
The University of Iowa
Iowa City, Iowa

CERTIFICATE OF APPROVAL

PH.D. THESIS

This is to certify that the Ph.D. Thesis of

Victoria Azula Henry

has been approved by the Examining Committee for the thesis requirement for the Doctor of Philosophy degree in Chemical and Biochemical Engineering at the December 2015 graduation.

Thesis Committee:
Tonya L. Peeples, Thesis Supervisor

Julie L. P. Jessop, Thesis Supervisor

David W. Murhammer

Amanda J. Haes

Alexander R. Horswill

To My Daughter Justice with Love

I have learned that success is to be measured not so much by the position that one has reached in life as by the obstacles which he has overcome while trying to succeed.

Booker T. Washington
Up From Slavery

ACKNOWLEDGMENTS

It has been a long journey, but with God's grace, the support of family, friends, mentors, advisors, and the College of Engineering, I've been able to make it through. I am grateful for being awarded the opportunity to pursue a Ph.D. at the University of Iowa in the Chemical and Biochemical Engineering Department. In Christ's name, all things are possible.

I would like to thank my mother, Janice Simon, for instilling in me the value of a sound education. She created an environment where I was allowed to dream big and aggressively pursue goals. I would like to thank my elementary teacher, Mrs. Gloria Williams, for exposing me to a grand world beyond Williams Delight. I am thankful for the consistent support of my entire family, including Leona, Chichi, Laverne, Pauline, Sharlene, Sharmane, Videncia, Mario, Larry, Lawrence, Johnson, Julian, and all the others. Knowing that they believed in my goals, allowed me to continue trying, even when I became restless. My family away from home, New Creations International Church; Pastor Anthony Smith, First Lady Gwen, and all their members, thank you for welcoming my daughter and I into your family and making us feel at home from our very first visit. I love you all.

The many calls, text messages, and emails from my mentors Dr. Leroy Magwood, Dr. Vanere Goodwin, Dr. Thomas Zimmerman, Dr. Kris Lord, Dr. Alexander Lodge, Kent Hutchinson, and Deandrea Watkins, gave me direction at times when I felt lost. The many laughs, shared stories, and support of my friends, Gbenga Ajiboye, Maryam Tigadourn, Anup Pudasiani, Maisha Toussaint, Tiffany Fagan, and Ralph Hazelwood, made my cold days in Iowa feel much warmer.

A special thank you to my research advisors, Dr. Tonya Peeples and Dr. Julie Jessop for their continual support of my thesis. The many meetings, reports, emails, text messages, and

constant writing back and forth, was greatly appreciated. Thank you for believing in me and my research project. Thank you to Dr. Mani Subramanian, Dr. David Murhammer, Dr. Amanda Haes and Dr. Alexander Horswill for serving on my committee for the past four years. Dr. Chris Coretsopoulos, Natalie Porter, and Linda Wheatley, your friendly demeanor and welcoming conversations meant the world to me. I am grateful for having the best research group, consisting of Felipe Nicolau, Kurtz Seipel, Richard Gonzalez, Michael Delcau, and Sage Schissel. All the undergraduates that I have worked with, including Jose Guizar, Elizabeth Smith, Jessica Phillips, and Abigail Haas; thank you.

I am very thankful for my NOBCChE family and wonderful executive team, Mary Nyaema, Brigitte Vanle, Victoria Parker, Rondine Allen, Tiffany Fagan, Deandrea Watkins, Tracy Peterson, Dr. Daniel Quinn and Dr. Tonya Peeples. I've had many memorable experiences at UI and in Johnson County with this team.

Last but not least, a very special thank you to my right hand, companion, and co-pilot for the past 13 years, the beautiful and intelligent Justice Veira. Thank you for understanding the sacrifices being made and having unwavering patience; I love you and am very grateful that God has blessed me with a daughter as special as you. Thank you all!!

ABSTRACT

Microbial biofilms are significant in a variety of settings including the human microbiome, infectious disease, industrial processes, and environmental remediation. Due to the ubiquitous nature of biofilms, there is a great interest in understanding cellular activities within the biofilm matrix. Biofilm cells are able to better withstand environmental stress, experience increased horizontal gene transfer, and live longer. The purpose of this research is to grow *Pseudomonas* sp. strain ADP as a biofilm and examine the chemical and physical characteristics the microbe undertakes in a sticky extracellular matrix.

ADP is the organism of choice because of its ability to metabolize atrazine. Cells are grown in a drip biofilm reactor and flow cells under varying time lapse to gain insight to biofilm formation. Some cells are grown with atrazine as the sole nitrogen source, while others are grown in a nutrient-rich medium to compare cells response under nutrient-limited conditions with atrazine particles in the matrix. As a positive control, *Escherichia coli* are grown in a similar manner.

Raman spectroscopy was the main analytical technique used to evaluate the chemical and molecular characteristics of this system. Scanning electron microscopy is used to examine cellular distribution, and several assays are performed for molecular composition analysis. Raman analysis in the fingerprint region revealed distinct differences between free cells and cells in biofilm. Soluble extracellular polymeric substances (EPS) were found to be more prevalent than tightly bound EPS and lightly bound EPS in the biofilm matrix. Comparison of relative peak intensity ratios suggests that it is possible to track atrazine degradation by means of intermediates using Raman spectroscopy. SEM micrographs revealed EPS role as an immobilizing agent when in contact with compounds,

such as atrazine. Further research is needed to determine if atrazine can bind to EPS fractions outside the presence of cells and whether its affinity to EPS is mostly attributed to physical conditions, due to the architecture of biofilm, or chemical, based on functional groups presents.

The results obtained from this research will contribute to the development of a less invasive microscale approach to address the acquisition and induction of biotransformation activity occurring in xenobiotic degrading systems. The extracellular interactions observed can be used to further characterize biofilm-mediated bioremediation. Results have contributed to the Raman spectra library for microorganisms and organic compounds.

.

PUBLIC ABSTRACT

Microbial biofilms are significant in a variety of settings including the human microbiome, infectious disease, industrial processes, and environmental remediation. Due to the ubiquitous nature of biofilms, there is a great interest in understanding cellular activities within a biofilm matrix. As cells adhere to a surface and multiply, they produce a sticky extracellular matrix that serves as a protection barrier against adverse factors such as antibiotics, protozoan grazing, and host immune response. This protection barrier may be beneficial in bioremediation but wreak havoc on the human body. The purpose of this research is to gain insight into the molecular and chemical distribution occurring within a biofilm matrix by characterizing *Pseudomonas* sp. strain ADP biofilm. ADP is the organism of choice because of its potential in bioremediation applications. ADP completely metabolizes atrazine, a widely used herbicide that is often found as a pollutant in the environment.

Unique to this work is the application of Raman spectroscopy as the main analytical technique. Applying Raman spectroscopy to examine the chemical changes occurring within the system is a promising microscale approach to address the acquisition and induction of biotransformation activity occurring. Newly obtained spectra have contributed to the Raman spectra library for microorganisms and organic compounds.

Success of this research will lead to a firmer grasp of scientific fundamentals associated with microbial biofilms for pollutant degradation. This will ultimately lead to improved remediation applications, to reduced pollutant-associated illnesses, and to general methodologies for analysis of biofilms.

TABLE OF CONTENTS

LIST OF TABLES

LIST OF FIGURES

CHAPTER 1: INTRODUCTION

Project Description

Industrial microbiology and biochemical engineering research studies commonly evaluate freely suspended planktonic cells; however, in natural environments most bacteria congregate at interfaces to form polymicrobial aggregates, such as films, mats, flocs, sludge, or biofilms.[1, 2] Interfaces for attachment include air-liquid interfaces, filters, artificial implants in the human body, food processing equipment, and industrial pipelines.[3-8] Microbes are encapsulated within a sticky extracellular matrix that serves as a protection barrier against adverse factors such as environmental stressors, antibiotics, protozoan grazing, and host immune response.[1, 9, 10] Through chemotaxis and cell-cell communication, organisms in a biofilm matrix are able to position themselves in a manner that is most beneficial for the overall survival of the matrix. This community organization provides the organisms with increased bioavailability of nutrients, or in some cases, pollutants for xenobiotic degrading cells.[2, 11] The increase in survival and microbial adaptions presents benefits for biofilm-mediated bioremediation, but can be detrimental in the human body.[2, 12] Understanding the complex nature of the biofilm matrix may enhance current biotechnology applications and enable specially designed strategies for biofilm removal.

Specific Aims

The purpose of this research project is to gain insight into the molecular and chemical distribution occurring within a biofilm matrix by identifying functional group characteristics and physicochemical properties of the atrazine degrading bacterium, *Pseudomonas* sp. strain ADP, biofilm. Unique to this work is the application of Raman spectroscopy as the main analytical technique to address the acquisition and induction of biotransformation activity. Proposed hypotheses are 1) Raman scattering can be used to identify and distinguish members

of biofilm communities and 2) Raman scattering can be used to evaluate the persistence of atrazine and metabolites in flow systems. To test hypotheses and to further explore the molecular and chemical distribution occurring within a biofilm matrix, we addressed the following specific aims:

1. Establish Raman spectroscopy as an effective analytical approach to identify and distinguish bacteria in biofilm.
2. Determine the physicochemical properties of extracellular polymeric substances and its contribution to *Pseudomonas* sp. strain ADP biofilm.
3. Determine extracellular interaction with atrazine, when used as a nutrient source to grow ADP biofilm.
4. Use Raman scattering to track atrazine degradation within a biofilm matrix.
5. Identify atrazine-induced gene expression within a biofilm matrix compared to planktonic cells.

Background

Biofilms

A biofilm is a community of microorganisms that coexist in a sticky matrix adhered onto surfaces in moist environments where nutrients are present. Upon initial attachment, cells multiply and remain entrapped in the matrix, resulting in an increase in cell density (Figure 1:1). Through cell-to-cell communication, also known as quorum sensing, cells in biofilm release signaling molecules, called autoinducers, that enable the community to sense cell density.[13] Once the concentration of autoinducers reaches a threshold, the activation of genes responsible for extracellular polymeric substance (EPS) secretions and biofilm formation is initiated.[9] This phenomenon enables cells to position themselves in a manner that is most beneficial for the survival of the biofilm, allowing opening of channels/pores for adequate solute transport.[2]

EPS comprises the major portion of the sticky extracellular matrix that encapsulates cells and allows for protection against environmental stressors, such as antibiotics, protozoan grazing, and host immune response. For this reason, cells survive and are more resistant to environmental stress when in the protective environment of the biofilm rather than in the planktonic state. Compared to stationary suspended cells, continuously fed biofilms are much more metabolically active.[14] The robust nature of bacteria in a biofilm matrix may be detrimental in the human body due to antibiotic resistance; however, organisms' resilience in this matrix may be beneficial in bioremediation, especially in the treatment of recalcitrant compounds.

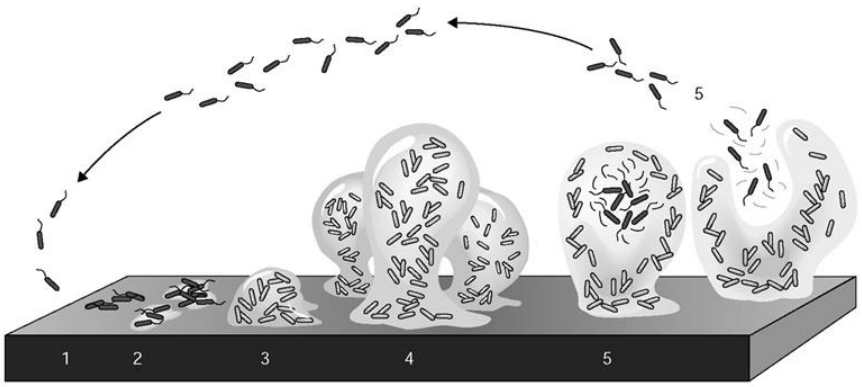

Figure 1:1: A schematic of bacterial biofilm formation.[15] At Stage 1, bacteria cells attach to the surface. At Stage 2, cells multiply and produce EPS, resulting in more firmly adhered (irreversible) attachment. Then Stage 3 is early development of architecture. At Stage 4, a mature biofilm with open channels form. Then in Stage 5, the sloughing away of cells occurs, resulting in cell dispersion to different location.

Source: Stoodley, P.; Sauer, K.; Davies, D. G.; Costerton, J. W., Biofilms as complex differentiated communities. *Annual Review of Microbiology* **2002**, 56, 187-209.

Atrazine

Atrazine [2-chloro-4-(ethylamino)-6-(isopropylamino)-1,3,5-triazine] is a rather mobile compound that remains active in the environment for several months after application. It was chosen as the model environmental pollutant due to its widespread usage in the United States. For the last 50 years, farmers have applied atrazine on 67% of all corn acreage, 65% of sorghum, and 90% of sugarcane acreage, which resulted in the use of over 70 million pounds of atrazine to prevent broad leaf and grassy weeds from forming amongst desired crops.[16, 17] EPA's regulation limits 3 ppb in groundwater; however, with exceedingly high usage of atrazine-containing herbicides, it is common for areas to exceed these limitations occasionally.[18] In August 2009, the Natural Resources Defense Council noted an increase in atrazine levels in water supplies of Midwestern and Southern towns; similar findings hold for soils and rainfall.[19] Wolf Creek, Iowa had a water supply that contained 10 ppb of atrazine, which is over three times EPA's limit.[19] In 2008, communities in Kansas and Indianapolis were reported to have up to 45 ppb in finished filtered water systems.[20]

Because atrazine is classified as a group C-possible human carcinogen, endocrine disrupter compound (EDC) showing impaired reproduction with reduced viability of offspring effects, and potent disrupter of cell chromosome structure, release into the environment is of growing concern.[21, 22] Studies have revealed a decrease in testosterone and estrogen in frogs that have been exposed to atrazine, as well as suppressed spermatogenesis and male frogs taking on female characteristics.[22] Ten percent of exposed male frogs that were chemically castrated were able to mate with non-exposed frogs and produce viable eggs.[23] In humans, intrauterine growth retardation, small-for-gestational age births, spontaneous abortion, and reduced semen quality have been associated with exposure to atrazine.[24] Women in Illinois are found to be more at risk for missed periods and intermenstrual bleeding than those in Vermont due to exposure to atrazine

in drinking water.[24]

With a half-life of 9 to 100 days in non-aquatic environments, depending on the nature of soil and microbes present, a half-life of 41 to 237 days in aquatic environment, and unfavorable effects on wetland inhabitants and mammals, it is imperative to remove atrazine from the environment quickly.[25, 26] Biofilm remediation presents a potentially efficient manner of immobilizing and degrading pollutants.

Pseudomonas sp. strain ADP

Through experimentation with a mixed bacterial culture at a herbicide spill site, a strain of *Pseudomonas* sp., denoted as ADP, was found to mineralize atrazine as its sole nitrogen source and metabolized much more than required for its nitrogen assimilation.[27] Further research demonstrated that media containing 1,000 ppm of atrazine was cleared, and 80% of the s-triazine ring carbon atoms were transformed to carbon dioxide. When an aliquot of ADP culture was transferred to sterile liquid medium containing 100 ppm atrazine, immediate growth was observed.[27] By HPLC analysis, within 25 hours all of the atrazine was completely metabolized (Figure 1:2).[27] As a control, heat-killed bacteria were also placed in sterile medium containing atrazine, and barely any decrease in atrazine was noticeable.[27] Under varying growth conditions in spherical stirred tank batch reactors and shake flasks, suspended ADP consistently showed similar growth rates when exposed to atrazine.[28] As the concentration of atrazine increased, the growth rate of ADP increased. Thorough investigation of this bacterium has led to its use as a reference strain. Several other bacteria, such as *Rhodococcus*, can metabolize s-triazines, but do not sufficiently degrade atrazine.[27]

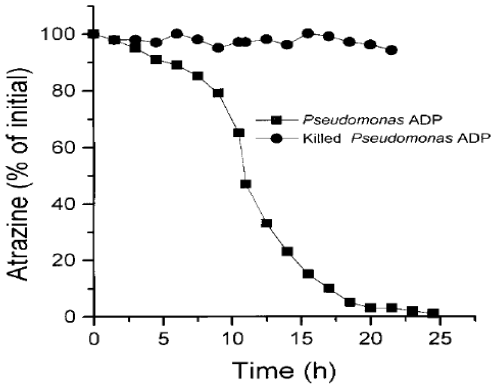

Figure 1:2: Degradation of 100 ppm atrazine in liquid medium containing *Pseudomonas* sp. strain ADP.[27]

Source: Mandelbaum, R. T.; Allan, D. L.; Wackett, L. P., Isolation and Characterization of a Pseudomonas Sp that Mineralizes the S-Triazine Herbicide Atrazine. *Applied and Environmental Microbiology* **1995**, 61, 1451.

Metabolic Pathway for Atrazine Degradation

Through a series of hydrolytic reactions, ADP metabolizes atrazine to ammonia and carbon dioxide (Figure 1:3).[29] The six-step degradation pathway is encoded in the 108-kbp plasmid, pADP-1 (Figure 1:4).[30] Genes atzA,-B, and -C and their encoded enzymes AtzA, -B, and –C are responsible for the degradation of atrazine by the removal of chlorine and aminoalkyl side chains to yield cyanuric acid.[30] Enzyme AtzA catalyzes the hydrolytic dechlorination of atrazine to hydroxyatrazine. AtzB catalyzes the deamidation of hydroxyatrazine to N-isopropylammelide. Then AtzC acts on N-isopropylammelide and breaks it down to cyanuric acid.[30] Genes atzA, -B, and -C are on different replicons as single transcriptional units surrounded by insertion-sequences (IS) elements, occupying nearly half of the plasmid sequence

in the 47 kb region.[31] These genes are not at any fixed location on the plasmid, thus making that portion of the plasmid rather unstable due to rearrangements resulting from loss of atzA,-B, and/or –C.[31] For this reason, ADP often loses its ability to degrade atrazine, causing the frequent appearance of Atr- derivatives (cells that can no longer metabolize atrazine).[30] However, a study showed that after 320 generations of ADP under atrazine selection pressure as the sole nitrogen source, a new population evolved that could grow faster and degrade atrazine more rapidly due to the tandem duplication of the atzB gene by homologous recombination mediated by IS elements.[31] The mobility of the IS elements not only aided the dispersal of atrazine degrading gene but also improved the fitness of the atrazine degrading population.[32]

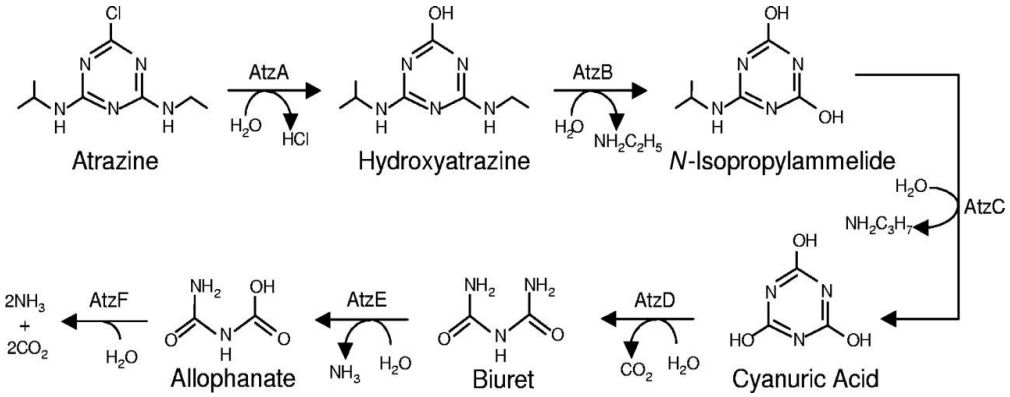

Figure 1:3: Schematic of the catabolic pathway for atrazine degradation by *Pseudomonas* sp. strain ADP with enzymes involved and intermediate metabolites included.[29]

Source: Martinez, B.; Tomkins, J.; Wackett, L. P.; Wing, R.; Sadowsky, M. J., Complete nucleotide sequence and organization of the atrazine catabolic plasmid pADP-1 from Pseudomonas sp. strain ADP. *Journal of Bacteriology* **2001**, 183, 5684.

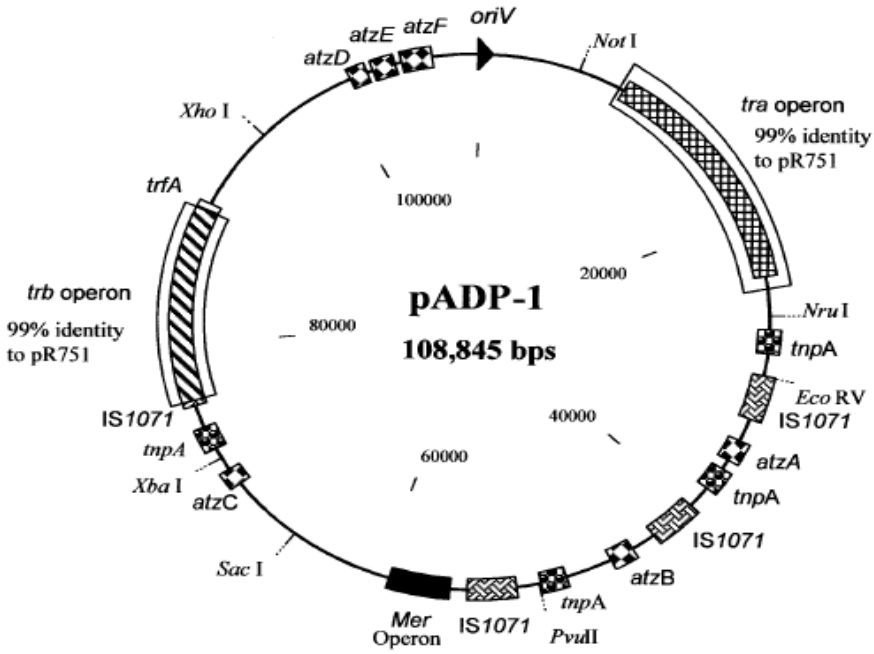

Figure 1:4: The catabolic plasmid, pADP-1, from *Pseudomonas* sp. strain ADP.[29]

Source: Martinez, B.; Tomkins, J.; Wackett, L. P.; Wing, R.; Sadowsky, M. J., Complete nucleotide sequence and organization of the atrazine catabolic plasmid pADP-1 from *Pseudomonas* sp. strain ADP. *Journal of Bacteriology* **2001**, 183, 5684.

Genes atzD -E, and –F, on the other hand, are nicely organized in an operon under a LysR-type transcriptional regulator, atzR. AtzD furthers the catabolic breakdown of cyanuric acid to biruet.[30] Then AtzE catalyzes the conversion of biruet to allophanate, and finally AtzF facilitates conversion of allophanate to ammonia (Figure 1:3).[29] Genes atzD, -E, and –F do not appear to have the genetic instability of atzA, -B, and –C. The atzR-atzDEF cluster is physically separated from the unstable 47 kb region containing atzA,-B,-C by two large gene clusters. For this reason, DeSouza et al. were able to demonstrate that Atr- is still capable of degrading cyanuric acid to carbon dioxide and ammonia even when it is unable to catabolize atrazine.[33] Another study showed that after 120 generations of ADP, under cyanuric acid induced pressure,

with cyanuric acid as the sole nitrogen source, a new population evolved which grew faster on cyanuric acid and had similar cyanuric degrading ability as the initial population.[31] The gain in fitness under cyanuric pressure resulted in loss of the 47 kb region containing atzABC genes, thus indicating a genetic burden under cyanuric acid pressure. ADP has a tendency to lose genes that constitute a genetic burden under unfavorable conditions, which is evident by the rapid loss of atz genes when cultures are grown on rich media without atrazine pressure.[31]

Raman spectroscopy

Raman spectroscopy enables rapid identification of chemical bonds present in an organic compound through measurement of vibrational, rotational, and other low-frequency modes in molecules. In one scan at low resolution, a Raman spectrum can reveal major cellular components and relative abundance simultaneously, without adding any chemical markers.[34] Macromolecules such as nucleic acids, proteins, lipids, and carbohydrates emit strong Raman signals, thus making Raman microspectroscopy an excellent tool for examining microbes.[35] This analytical technique measures molecular vibrations resulting from change in polarizability of a molecule upon interaction with light from a source, usually a laser.[36] A laser light is very different from white light, whereas the light emitted is monochromatic, is directional, and collimated. When focused on a sample, photons interact with matter by absorption, transmission, or scattering. This scattering may be elastic (Rayleigh scattering) or inelastic (Raman scattering).[37] Only a small fraction of light, approximately 1 in 10^7 photons, are Raman scattered at frequencies different than the frequency of incident photons.[36] The majority of scattered light is Rayleigh scattered, having the same wavelength corresponding to the laser light.

Raman spectroscopy relies on Raman scattering and uses filters to remove Rayleigh scattered photons. For polarizable molecules, the incident photon energy excites an electron into a higher virtual state and then the electron decays back to a lower level, emitting a scattered

photon (Figure 1:5). The virtual state can be considered a very short lived distortion of the electron cloud caused by the oscillating electric field of the light, rather than a true quantum state of the molecule. In Raman scattering, the electron decays to a vibrational energy level above, which is termed Stokes scattering, or below the initial state, termed anti-Stokes scattering. At ambient temperatures, Stokes scattering signal is stronger than anti-stokes and is therefore more observable with Raman spectroscopy. The measured energy difference or frequency shift between the incident and scattered photons is the Raman shift (cm^{-1}). Although the Stokes Raman values are actually negative frequency shifts, by convention positive numbers are reported. The observed bands, corresponding to specific energy transitions arising from molecular vibrations, provide a molecular fingerprint unique to each compound. The normalized peak height and relative peak intensity ratios can give the relative abundance of molecular species in a sample.

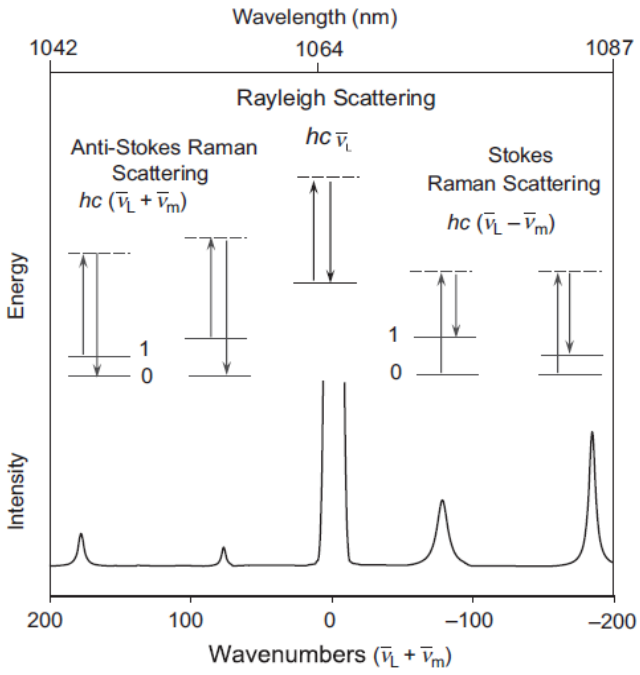

Figure 1:5: A schematic of Rayleigh, anti-Stokes Raman Scattering, and Stokes Raman scattering. The laser excitation frequency (ν_L) is represented by the upward arrows and is much higher in energy than the molecular vibrations. The downward arrows represent the frequency of the scattered photon and are unchanged in Rayleigh scattering but are of either lower or higher frequency in Raman scattering. The dashed lines indicate the virtual state. [38]

Source: Larkin, P., In *IR and Raman spectroscopy*; Amsterdam; Boston: Elsevier: Amsterdam; Boston, **2011**.

Limited sample preparation is required, without additives and dyes; and varying geometries/film thicknesses may be analyzed.[39, 40] Similar to confocal laser scanning microscopy, three-dimensional distributions of substances may be recorded with high spatial resolution; however, Raman spectroscopy can combine both optical and spectral analyses to monitor structure and chemical changes.[41] Unlike infrared spectroscopy, Raman spectroscopy can be used in aqueous environments and generates sharper and more distinguishable bands of specific molecules.[35, 42, 43] Over the past several years, Raman spectroscopy has been more widely used for the analysis of biological samples because it offers the potential of non-

destructive analysis and can rapidly distinguish cells.[44, 45]

Previously, Raman spectroscopy has been used in free-cell analysis for rapid detection and characterization of microbes, taxonomic comparison, detecting differences between populations, and analyzing composition of cells grown on morphologically differentiated cultures.[34, 35, 39, 40, 44-46] Fully hydrated biofilms have also been examined, and EPS characterization on different carriers explored.[41, 47] In this study, the chemical bond changes occurring in a pollutant degrading biofilm will be analyzed.

Research Gaps Addressed

There is still much to learn about *Pseudomonas* sp. strain ADP as it exists in a biofilm matrix, with limited research to reference in literature. Mandelbaum, Martinez, Watkett, De Souza, Govantes, Katz, Clausen, Devers and Changey have contributed much to the understanding of atrazine degradation by ADP cells in suspension.[27, 29, 30, 33, 48-50] Few researchers have studied ADP biofilm growth kinetics and atrazine degradation rate in biofilm reactors. A recent study suggested that biofilm systems may facilitate bioremediation by enhanced gene transfer among biofilm organisms and increased bioavailability of pollutants for degradation resulting from bacterial chemotaxis.[2] Herzberg observed higher atrazine degradation rate due to double flux of atrazine in biofilm grown on granulated activated carbon (BGAC) in a fluidized bed reactor.[51] Mass balance calculations for atrazine showed that the amount of atrazine degraded in the BGAC reactor was 2 orders of magnitude higher than influent loading rate due to degradation of both influent and pre-adsorbed atrazine.[51] Biglione compared growth rates of suspended ADP and ADP biofilm in spherical stirred tank reactors and found a 2 order of magnitude larger growth rate in suspended cells with comparable atrazine degradation rates.[52] Biofilms appeared to produce less cells than suspensions, but increased extracellular products.[52] There is no other published literature on ADP biofilm beyond the work

of Biglione and Herzberg. Although both research groups explored atrazine degradation rates within ADP biofilm under different growth conditions, neither characterized ADP biofilms.

In this dissertation, functional group characteristics and physicochemical properties of atrazine degrading ADP biofilms were explored to gain insight to molecular and chemical distribution of compounds within a biofilm matrix. Surface morphology of young and mature biofilms under nutrient-rich and nutrient-limited conditions containing atrazine as the sole nitrogen source was examined. Molecular distribution within the biofilm matrix was observed using Raman spectroscopy. Extracellular matrix was extracted, fractioned and further analyzed. Lastly, attempts were made to identify atrazine induced gene expression in biofilm compared to free cells. Advances were made in developing Raman analytical techniques for collecting chemical information from microbial biofilm systems. Raman spectroscopy is still a relatively new technique in the application of microbial systems, requiring protocol development to produce consistent, reproducible, and high quality spectra.

In Chapter 2, we demonstrate the sensitivity and feasibility of applying Raman spectroscopy for the analysis of complex microbial systems by collecting and differentiating spectra of free cells, biofilm, EPS, and cells from biofilm. In Chapter 3, to unmask the ambiguity typically associated with EPS, EPS was further fractionated and Raman spectra collected to gain insight into the molecular contribution to the biofilm matrix. Then atrazine was used as a nutrient source to grow biofilm, and particle allocation within the extracellular matrix was examined using scanning electron microscopy (SEM) in Chapter 4. Raman spectra of atrazine and metabolites are also presented to lay the groundwork for tracking atrazine degradation using Raman spectroscopy. In Chapter 5, attempts were made to detect atrazine induced gene expression in free cells compared to cells in a biofilm to better characterize the degradation capacity within a biofilm matrix. Chapter 6 presents several possibilities for future

studies to evaluate the ADP system and to extend the Raman and SEM analytical strategies for biofilm analysis.

CHAPTER 2: DIFFERENTIATING *PSEUDOMONAS* SP. STRAIN ADP CELLS IN SUSPENSIONS AND BIOFILMS USING RAMAN SPECTROSCOPY AND SCANNING ELECTRON MICROSCOPY

Introduction

To explore the biofilm system with Raman spectroscopy, it was necessary to first establish reference spectra by collecting preliminary data of ADP planktonic cells and biofilm. Compared to freely suspended cells, biofilms produce and exhibit an altered phenotype with respect to growth rate, gene transcription, and metabolic activity.[2, 14] When autoinducers reach a threshold among sessile cells, the activation of genes responsible for biosurfactant synthesis, competence, and secretion of extracellular polymeric substances (EPS) is initiated causing changes in phenotype.[9, 14] Therefore, it is hypothesized that Raman scattering can be used to identify and distinguish bacteria in biofilms from freely suspended planktonic cells. Through measurement of molecular vibrations resulting from change in polarizability of molecules upon interaction with light, Raman spectroscopy enables rapid identification of chemical bonds present. In one scan, a Raman spectrum can reveal major cellular components and relative abundance simultaneously.

In this study, a comparative analysis of planktonic cells versus cells in biofilms was conducted. Key Raman signals contributing to some of the biochemical properties present in biofilms are identified, and these features demonstrate how signals may vary among bacterial species. Scanning electron microscopy (SEM) imaging is used to provide additional information about surface morphology present and the EPS matrix. These initial baseline experiments provide insight into the cellular matrix in the biofilm and explores the use of Raman spectroscopy in distinguishing physiology among cells of the same species.

Materials and Methods

Cultures and Reagents

Pseudomonas sp. strain ADP was purchased from Deutsche Sammlung von Mikrooganismen und Zelkulturen (Braunschweig, Germany) and stored at -80°C in Tryptic Soy Broth with glycerol (1:1) as a cryoprotectant. Maxium efficiency *Escherichia coli* Dh5α competent cells were purchased from Life Technologies (Grand Island, New York) and stored similarly to ADP. EDTA (10 mM) used for EPS extraction was purchased from Fisher Scientific (Pittsburgh, Pennsylvania). Fixatives for SEM imaging, glutaraldehyde, cacodylate, osmium tetroxide, and hexamethyldisilazane (HMDS), were used as purchased from Sigma Aldrich (St. Louis, Missouri).

Raman Analysis

Raman microscopy was used to acquire spectra of free cells, biofilms, EPS, and cell pellets from biofilms to aid in identifying the corresponding chemical composition. A Thermo Nicolet Almega XR Raman spectrometer equipped with an Olympus BX 51 model microscope and Thermo Scientific OMNIC 8 software was used for Raman analysis. One µm x-y resolution and 2 µm depth resolution was achieved with a 100 µm pinhole and a thermoelectric-cooled charged coupled device (CCD) camera with a front-illuminated open electrode format. Samples were illuminated with a frequency-doubled 532 nm Nd:Yv04 laser emitting approximately 10 mW laser power at the sample. Video images were taken by a CCD camera and stored and processed using the OMNIC 8 software.

Spectra were recorded, peaks identified, and baseline corrections for relative peak intensity ratios were processed with the OMNIC 8 software. All spectra were normalized relative to the nucleic acid peak at ~800 cm^{-1}. Raman band assignments for free cells, biofilms, EPS, and pellets from biofilm were identified by comparison of published

molecular assignments of biological samples, Table 2:1. The relative molecular distribution in each sample was determined by calculating the relative peak intensity ratio. Three measurements, one each from three similar samples, were averaged and the standard deviation and normal distribution 95% confidence interval were calculated. Interpretation of differences between spectra was carried out by comparing relative peak intensity ratios of constituents including nucleic acids, phenylalanine, carbohydrates, amide I, and amide III.

Free Cell Preparation

Bacteria were thawed at room temperature, then diluted (1:10) in Luria Bertani (LB) medium and grown overnight in 250 mL shake flasks (Erlenmeyer flasks) at 30°C and 200 rpm. One mL of *E.coli* and ADP culture were inoculated separately in 9 mL of LB and incubated at 30°C overnight with 200 rpm shaking. Overnight cell cultures in LB grew from a 0.2 to approximately 7.0 optical density (OD_{600}). Following incubation, suspended cells were centrifuged at 4°C and 2000 g for 10 min to remove the medium. Cell pellets were washed 3 times and resuspended in sterile deionized water; lastly, the suspension was diluted to 1.0 OD. [34] By reducing cell concentration to approximately 1.0 OD, it was easier to focus on individual cells to produce clear Raman signals without fluorescence saturating the detector.

For Raman analysis, 10 µL samples of cells in suspension were air dried onto a quartz microscope slide. Even though Raman spectroscopy can be used in aqueous environments, Raman signal-to-noise ratios were low for liquid samples due to the constant movement of cells into and out of the sampling volume during the accumulation times. Air drying cells in suspension onto quartz slides created a static environment that allowed scattered photons to be easily collected from single cells, thus producing spectra with higher signal-to-noise ratios and more easily distinguishable peaks. Using the 10x objective with 0.25 NA, specimens

were brought into focus, individual cells were magnified and Raman spectra were collected with the 100x objective with 0.90 NA. The accumulation time for each sample was 60 s with 4 accumulations, and 6th order polynomial fluorescence correction was applied. Digital images were taken through the microscope attached to the Raman spectrometer with the 100x objective (Figure 2:1).

Table 2:1: Approximate Raman bands for cells. Abbreviations: C, U, T, A, and G stand for cytosine, uracil, thymine, adenine, and guanine, respectively.

Bands (cm^{-1})	Assignment
720, 727	Adenine[44, 53]
778-782	Nucleic acids (cytidine, uracil)[34]
784	Nucleic acids (C,T)[53]
785	Cytosine, uracil (ring, stretching)[44, 54]
813, 829, 852, 859	Tyrosine[40, 44, 53]
1004	phenylalanine[34, 44, 53]
1030-1130	Carbohydrates, mainly –C-C- (skeletal), C-O, δ(C-O-H)[34]
1125-1127	C-C str, C-O-C gycosidic link, ring breath, symm; C-N str[40]
1129	C-N and C-C stretching[44]
~1130	=C-C= (unsaturated fatty acids in lipids)[34]
1230-1295	Amide III [34, 44]
1200-1400	Amide III[41]
~1320	Protein (amide III); CH deformation [34]
1323	Adenine/DNA (deformed)[53]
1340	Nucleic acids (A,G)[53]
1345	CH deformation[40]
1400-1420	COO- symmetry[40]
1440-1460	C-H_2 deformation[34, 44]
1450	Lipids (CH_2 bending)[53]
1575, 1576	Guanine, adenine (ring stretching)[41, 44]
1580, 1583	Nucleic acids (A,G)[40, 53]
1650-1680	Amide I[4, 44, 53]

A

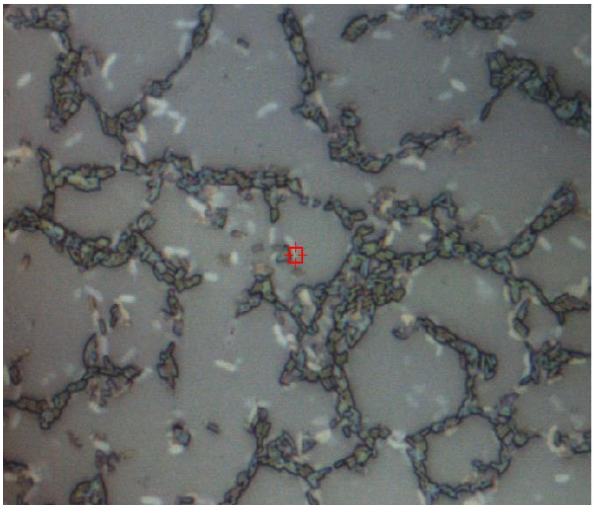

B

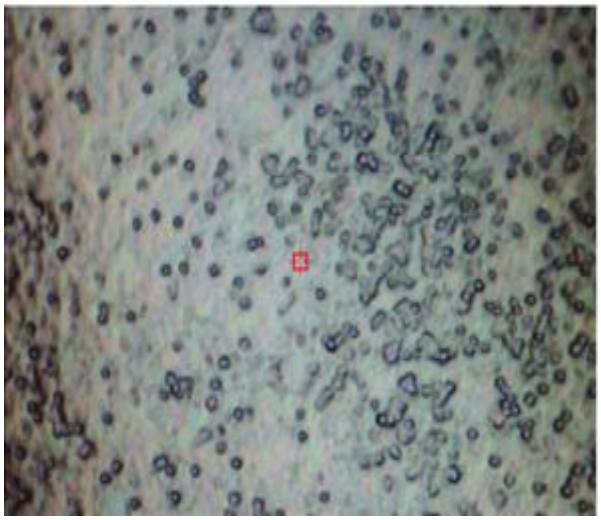

Figure 2:1: Raman optical micrograph of A) overnight *Pseudomonas* sp. strain ADP free cells dried onto quartz slide and B) washed 5 day old biofilm dried on quartz slide. The red box is the cross hairs used to focus on point of interest for laser excitation.

Biofilm Preparation

Biofilms were grown in a four-channel Teflon drip biofilm reactor made by the University of Iowa Medical Shop. Each channel had a polycarbonate lid, 0.25 µm bacterial vent, and a rubber inlet stopper. Through experimentation with different materials, Teflon was found to be best for growing biofilms since it is inert with respect to cells, thermally resistant to temperatures as high as 121°C, and chemically resistant to detergents, acids, and bases. Standard microscope glass slides (75 mm x 25 mm x 1 mm), quartz slides (76 mm x 25 mm x 1 mm), or glass coverslips (0.13-0.16 mm thick) were placed flat on the bottom of each channel to provide a surface for cells to adhere and grow. Each chamber was inoculated with 10 mL of overnight cell broth, containing a 10% inoculum of ADP cells suspended in LB medium. The system was held in batch mode initially for 6 h to allow the cells time to adhere to each substratum. Two peristaltic Masterflex pumps with four pump heads attached were used to pump medium into each chamber for 5 days at a flow rate of 0.8 mL/min through size 13 tubing (0.8 mm ID). The reactor was kept at a 10° inclined angle to maintain steady effluent flow. Waste containers were placed 2 ft below the reactor to prevent backflow of waste material and minimize movement of exiting bacteria backward into the reactor.

Following the 5-day run, biofilms were harvested by gentle scraping and washing with sterile deionized water. For Raman analysis, biofilms were placed onto quartz microscope slides and air dried. Biofilms were viewed similarly to free cells, i.e., bringing sample into focus with the 10x objective and then magnifying and focusing on cells with the 100x objective (Figure 2:1B). The same exposure time and accumulation were used as for the free cells.

Tubing and associated containers were sterilized as per Tolker-Nielsen with modifications.[55] Briefly, tubing was rinsed with 0.5% sodium hypochlorite at 4.5 mL/min for 5 min, and allowing sodium hypochlorite solution to remain in the line for 2 h. Sodium hypochlorite was flushed from the system by pumping sterile deionized water through the tubing three times at 4.5 mL/min and filling the lines with air between each pass for 30 min. Sterile deionized water was then pumped through the system overnight at 0.2 mL/min. Lastly, a solution of 1% hydrogen peroxide was pumped through tubing at 0.8 mL/min for 10 min to remove any remaining biomass. All associated glassware for feed and effluent, in addition to the biofilm reactor, were autoclaved for 20 min at 121ºC.

EPS Extraction

EPS was extracted as described by Sandt et al. with some modifications.[41] Briefly, biomass was separated from the culture medium by centrifugation at 2000 g for 10 min and washed 3 times with 0.9% NaCl solution. The biomass was then resuspended in 10 mM EDTA (pH 8.3) at room temperature for 2 h to remove divalent cations, Ca^{2+} and Mg^{2+}, which are responsible for the crosslinking of charged compounds in the EPS matrix.[56] The supernatant was dialyzed against deionized water for 2 days with a 10 kDA MWCO Snakeskin® dialysis tube (ThermoScientific, Rockford IL). For Raman analysis, 20 µL of dialyzed EPS in solution was air dried onto quartz slides. Each sample was brought into focus using the 10x objective and data were collected using the 100x objective. Raman spectra were obtained in a manner similar to that used for free cells. The cell pellets collected after the centrifugation of dialyzed EPS were smeared onto quartz slides and Raman spectra collected as described above.

Fixation for SEM

Biofilms were grown as previously described on glass coverslips in the drip biofilm reactor. Intact biofilms on glass coverslips were placed in sterile tissue plates and fixed for 1 h with 2.5 % glutaraldehyde in 0.1 M cacodylate buffer. Samples were rinsed in 0.1 M cacodylate buffer and further fixed with 1% osmium tetroxide in 0.2 M cacodylate buffer to add mechanical stability and increase electron density for SEM imaging. Samples were then rinsed with distilled water and sequentially dried in ethanol. To prevent surface tension phenomena associated with ethanol evaporation, samples were immediately rinsed in hexamethyldisilazane (HMDS) to chemically dry specimens. Samples were then mounted onto aluminum stubs using silver colloidal paint and allowed to dry overnight in a desiccant. Once dried, samples were gold-palladium sputter coated to further boost the secondary electron emission of the specimen prior to examination with a Hitachi S4800 scanning electron microscope operated at 1.5 kV. SEM images collected using 45,000x magnification and slow scan speed. All chemicals used for fixation were handled with caution in the fume hood as described in the MSDS.

Results and Discussion

Here, we present the first Raman spectrum of ADP planktonic cells and biofilm with putative peak assignments from published Raman assignments of single bacterial cells. The first high-resolution SEM image of ADP in the biofilm matrix is also presented, which aided in our analysis of EPS contribution to the biofilm matrix and interpretation of Raman data.

Free Cells

Raman spectra of individual ADP cells grown in liquid media were collected to compare against ADP cells grown within a biofilm. The Raman spectra obtained from a single cell in an air-dried sample contained approximately 20 sharp bands (Figure 2:2) and

had higher signal-to-noise ratios, than spectra from cells in liquid media. As a positive control and to compare data with published work, *E.coli* was also examined (Figure 2:2A). Tentative band assignments for molecular components of a single cell from the literature are presented in Table S1.[4, 34, 35, 40, 41, 44, 54] The *E.coli* spectrum was comparable to the spectrum found in the literature,[35] having most notably the Raman bands at 787, 1001, and 1667 cm^{-1}. Because a smaller spot size and more accumulations were used, a clean spectrum with high signal-to-noise ratios was obtainable. The overall shape of the spectrum is almost identical to the spectrum that has been published, with minor variations in the relative intensity of phenylalanine to carbohydrate at 1001 and 1055 cm^{-1}, respectively. Minor variations are expected when working with multicomponent systems such as cells since there are many factors such as age, growth phase, and source of nutrients that may alter spectral characteristics.[44]

This Raman technique enabled the distinction between ADP and *E.coli* cells. Visual differences between *E.coli* and ADP occurred in the fingerprint regions at 747, 1126, and 1308-1392 cm^{-1} (Figure 2:2A-B), which from previous reports[34, 35, 41] are attributed to adenine, carbohydrate, and amide III content, respectively. By calculating the relative peak intensity ratios in each sample (Tables 2:2 and 2:3), we are able to estimate the relative amount of selected molecular components, as well as obtain a comparison that is independent of instrumental variations Figure 2:3. Theoretically, the Raman peak intensity is directly proportional to the concentration of the represented bond and thus the chemical constituents. Comparing the relative intensity ratio of nucleic acids (C,U) to adenine $\left(\frac{I_{791}}{I_{725}}\right)$, *E.coli* has a peak ratio approximately 3 times greater than ADP's ratio (Table 2:4). The phenylalanine to

carbohydrate peak ratio $\left(\frac{I_{1001}}{I_{1124}}\right)$ for *E.coli* is more than 2 times that of ADP. The amide I to nucleic acids (A, G) content $\left(\frac{I_{1661}}{I_{1575}}\right)$ is noticeably different as well, with a relative peak ratio for *E.coli* that is almost 2 times greater than ADP. Both strains were grown on identical media and processed the same way; however, each species produces different proteins and expresses variant genes in the presence of nutrients, which corresponds to the observed spectral differences.

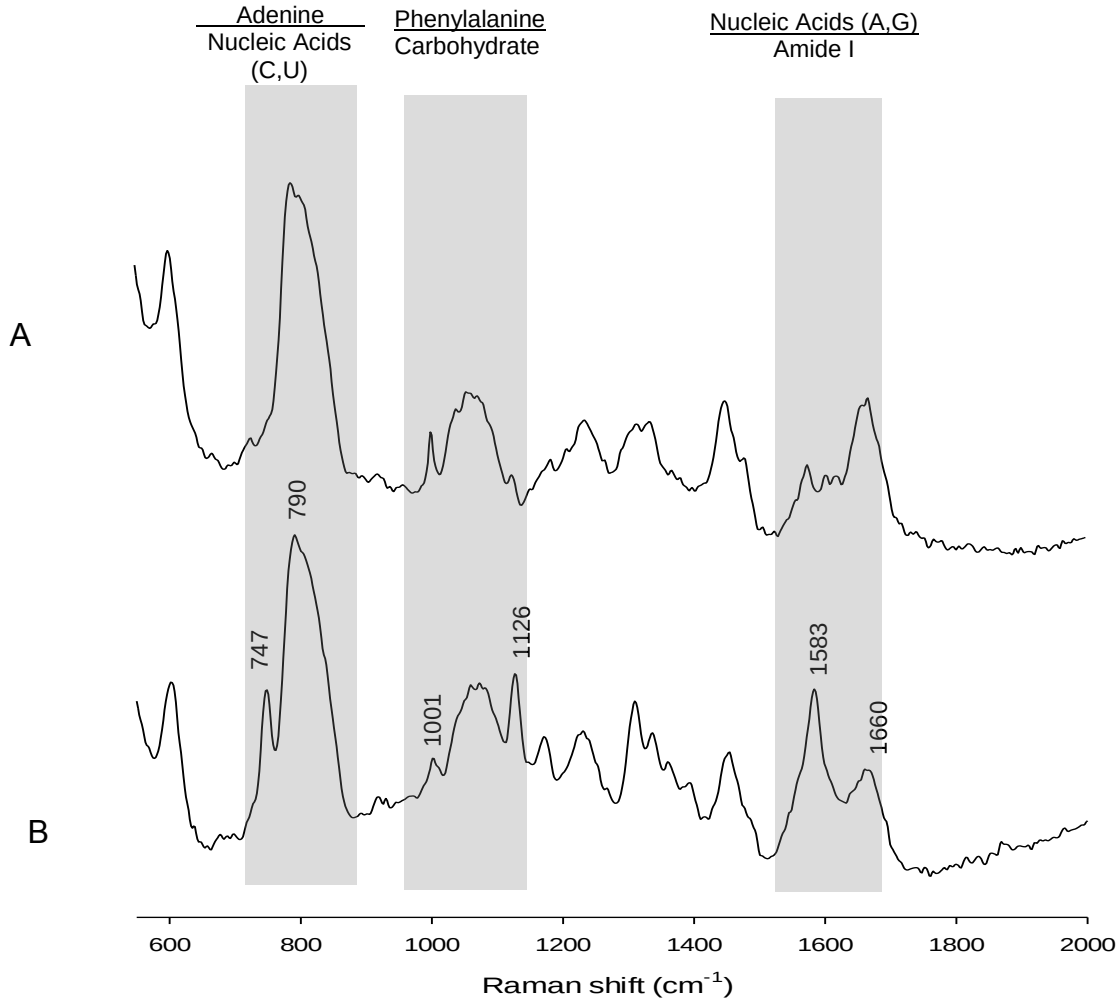

Figure 2:2: Comparison of normalized Raman spectra of A) *Escherichia coli* and B) *Pseudomonas* sp. strain ADP, collected with 532 nm laser, 60 seconds accumulation, and 0.6 µm spot size. Notice differences in nucleic acid content at 747 cm^{-1}, reduction in phenylalanine (1001 cm^{-1}) relative to neighboring carbohydrates in ADP, and variation in relative peak intensities at 1580 and 1160 cm^{-1}.

Table 2:2: Relative peak intensity ratios of molecular components in three different samples of *Escherichia coli* free cells.

	E.Coli 1		*E.Coli* 2		*E.Coli* 3		Mean		Std Dev	95% Conf Interval (n=3)
Band Assignments	Ratio	Value	Ratio	Value	Ratio	Value	Ratio	Value	Value	Value
Nucleic acids (C,U)/Adenine	$\frac{I_{787}}{I_{727}}$	8.49	$\frac{I_{791}}{I_{721}}$	7.15	$\frac{I_{795}}{I_{727}}$	7.00	$\frac{I_{791}}{I_{725}}$	7.55	0.82	± 0.93
Phenylalanine/ Carbohydrates	$\frac{I_{1001}}{I_{1122}}$	2.33	$\frac{I_{1001}}{I_{1126}}$	1.49	$\frac{I_{1001}}{I_{1125}}$	1.66	$\frac{I_{1001}}{I_{1124}}$	1.83	0.44	± 0.50
Amide I/ Nucleic acids (A, G)	$\frac{I_{1668}}{I_{1575}}$	1.97	$\frac{I_{1659}}{I_{1576}}$	1.66	$\frac{I_{1657}}{I_{1575}}$	1.73	$\frac{I_{1661}}{I_{1575}}$	1.785	0.16	± 0.19

Table 2:3: Relative peak intensity ratios of molecular components in three different samples of *Pseudomonas* sp. strain ADP free cell.

	ADP 1		ADP 2		ADP 3		Mean		Std Dev	95% Conf Interval (n=3)
Band Assignments	Ratio	Value	Ratio	Value	Ratio	Value	Ratio	Value	Value	Value
Nucleic acids (C,U)/Adenine	$\frac{I_{791}}{I_{747}}$	2.04	$\frac{I_{788}}{I_{748}}$	3.15	$\frac{I_{787}}{I_{744}}$	2.62	$\frac{I_{789}}{I_{746}}$	2.61	0.55	± 0.63
Adenine/ Nucleic acids (C,U)	$\frac{I_{747}}{I_{791}}$	0.49	$\frac{I_{748}}{I_{788}}$	0.32	$\frac{I_{744}}{I_{787}}$	0.38	$\frac{I_{746}}{I_{789}}$	0.40	0.09	± 0.10
Phenylalanine/ Carbohydrates	$\frac{I_{1001}}{I_{1130}}$	0.45	$\frac{I_{1003}}{I_{1125}}$	0.95	$\frac{I_{1001}}{I_{1126}}$	0.64	$\frac{I_{1002}}{I_{1127}}$	0.68	0.26	± 0.29
Nucleic Acids (A,G)/ Amide III	$\frac{I_{1339}}{I_{1307}}$	0.80	$\frac{I_{1337}}{I_{1311}}$	0.97	$\frac{I_{1332}}{I_{1307}}$	0.79	$\frac{I_{1337}}{I_{1309}}$	0.85	0.11	± 0.12
COO- symmetry/ Amide III	$\frac{I_{1395}}{I_{1307}}$	0.48	$\frac{I_{1387}}{I_{1311}}$	0.59	$\frac{I_{1396}}{I_{1307}}$	0.57	$\frac{I_{1392}}{I_{1308}}$	0.55	0.06	± 0.07
Lipids (CH_2) /Amide III	$\frac{I_{1450}}{I_{1307}}$	0.71	$\frac{I_{1450}}{I_{1311}}$	1.20	$\frac{I_{1444}}{I_{1307}}$	1.05	$\frac{I_{1448}}{I_{1308}}$	0.99	0.25	± 0.29
Amide I/ Nucleic Acids (A,G)	$\frac{I_{1666}}{I_{1583}}$	0.58	$\frac{I_{1657}}{I_{1580}}$	1.11	$\frac{I_{1666}}{I_{1583}}$	1.06	$\frac{I_{1663}}{I_{1582}}$	0.92	0.30	± 0.33

Table 2:4: Comparison of relative peak intensity ratios of selected molecular components of *Pseudomonas* sp. strain ADP to *Escherichia coli*. The ± values represent the 95 % confidence intervals (n=3).

	Pseudomonas sp. strain ADP		*Escherichia coli*	
Band Assignments	Ratio	Value	Ratio	Value
Nucleic acids (C,U)/Adenine	$\frac{I_{789}}{I_{746}}$	2.6 ± 0.6	$\frac{I_{791}}{I_{725}}$	7.5 ± 0.8
Phenylalanine/Carbohydrates	$\frac{I_{1001}}{I_{1126}}$	0.7 ± 0.3	$\frac{I_{1001}}{I_{1124}}$	1.8 ± 0.4
Amide I/Nucleic acids (A,G)	$\frac{I_{1662}}{I_{1583}}$	0.9 ± 0.3	$\frac{I_{1661}}{I_{1575}}$	1.8 ± 0.2

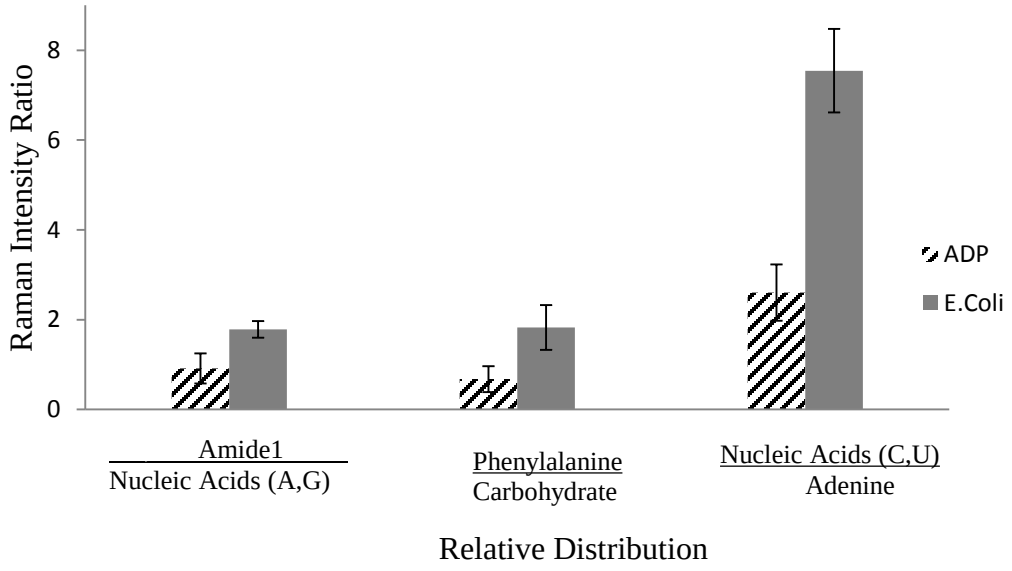

Figure 2:3: Relative Raman peak intensity ratios of ADP in comparison to *E.coli*. Notable difference in the nucleic acid region. The errors bars represent 95% confidence intervals (n=3).

Biofilm

The Teflon drip biofilm reactor proved to be effective in the cultivation of mature biofilms. ADP cells grew well as a biofilm on smooth glass surfaces in the four channel reactor, i.e., there was no need to chemically etch substrata to increase surface adhesion. After 24 h with continuous flow of medium, cells began to come together and aggregate on the surface, but no extracellular matrix was visible (Figure 2:4). By Day 5, the biofilms were rich in EPS with dense webs of EPS encapsulated cells, and an intricate web-like architecture (Figure 2:5). Rod-shaped cells, approximately 1.0-2.0 µm in length, produced elongated EPS fibers that coated cell exteriors, bound neighboring cells together, and formed micro structures within open terrestrial spaces between cells. These mats of biomass with open channels are consistent with the definition of a mature biofilm.[57]

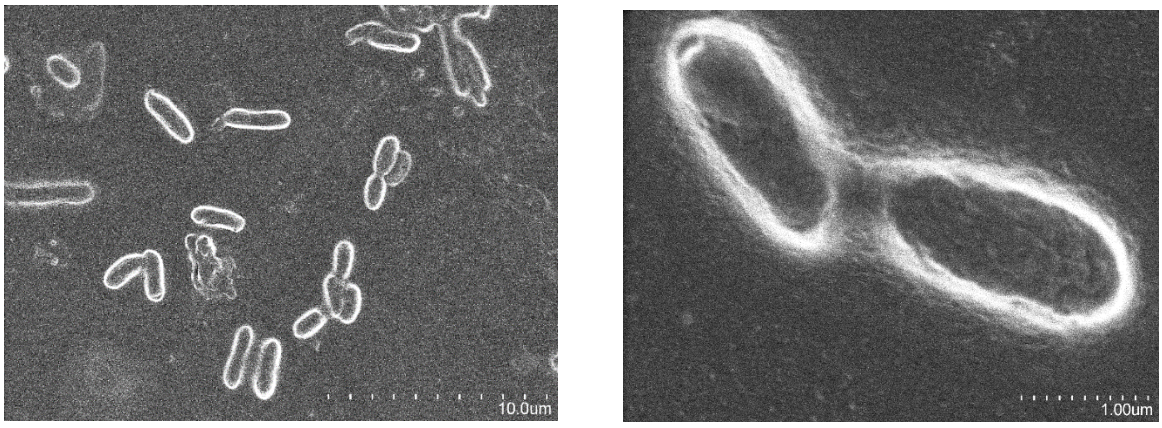

Figure 2:4: SEM image of 24 hour old *Pseudomonas* sp. strain ADP biofilm grown on LB medium. Cells are beginning to aggregate on substrata but extracellular secretion is not visible. A) Micrograph image with 10 µm scale, B) Magnified view of individual cells coming close together on 1µm scale.

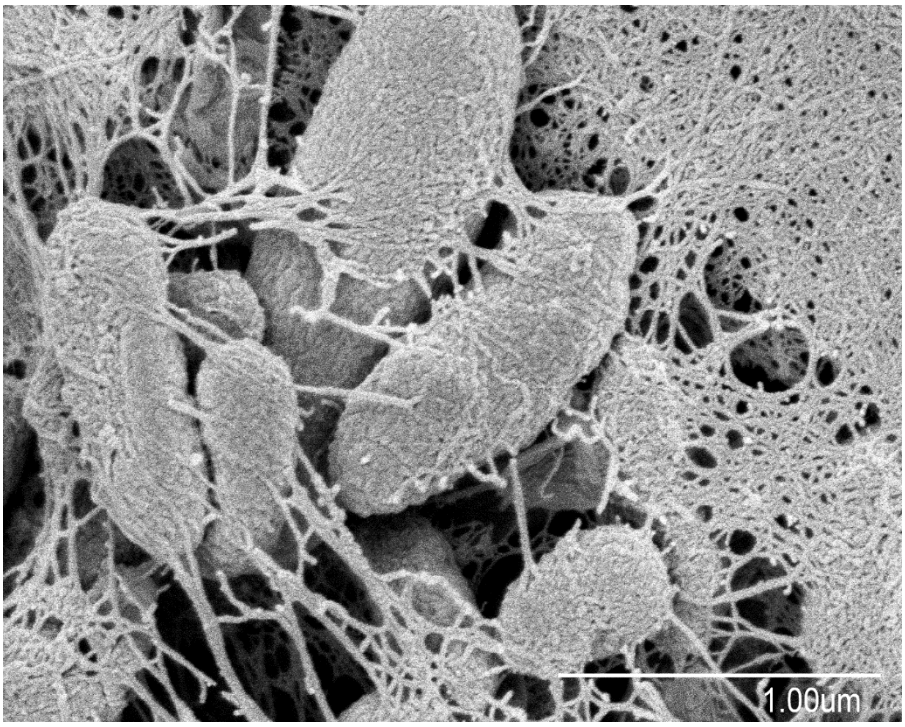

Figure 2:5: SEM image of 5 day old *Pseudomonas* sp. strain ADP biofilm at 15,000x magnification. Extracellular polymeric substances dominate the biofilm matrix, creating web-like structure surrounding cells and spreading throughout the matrix creating intricate architecture.

Raman analysis of mature biofilms revealed similarities to free cells in regards to molecular compounds present, but with differences in molecular distribution (Figure 2:6A-B). When comparing relative peak intensity ratios (Figure 2:7) in the nucleic acid region $\left(\frac{I_{789}}{I_{752}}\right)$, ADP biofilms have a ratio more than 2 times higher than that for free cells (Table 2:5). The biofilm matrix can act as a recycling center, retaining lysed cells components, such as DNA.[1] On the other hand, the relative abundance of phenylalanine to carbohydrates $\left(\frac{I_{1008}}{I_{1132}}\right)$ is 15% higher in the free cells than in the biofilm. The peak ratios of lipids to

amide III $\left(\frac{I_{1455}}{I_{1313}}\right)$ and amide I to nucleic acids (A, G) peak intensity ratios $\left(\frac{I_{1672}}{I_{1586}}\right)$ are comparable in both the free cell and biofilm, suggesting similar abundances of molecular components in those regions.

Table 2:5: Relative peak intensity ratios of molecular components in three different samples of *Pseudomonas* sp. strain ADP biofilm.

	Biofilm 1		Biofilm 2		Biofilm 3		Mean		Std Dev	95% Conf Interval (n=3)
Band Assignments	Ratio	Value	Ratio	Value	Ratio	Value	Ratio	Value	Value	Value
Adenine/ Nucleic acids (C,U)	$\frac{I_{753}}{I_{786}}$	0.77	$\frac{I_{754}}{I_{792}}$	0.89	$\frac{I_{749}}{I_{788}}$	0.75	$\frac{I_{752}}{I_{789}}$	0.80	0.08	± 0.08
Phenylalanine/ Carbohydrates	$\frac{I_{1006}}{I_{1133}}$	0.63	$\frac{I_{1008}}{I_{1134}}$	0.52	$\frac{I_{1006}}{I_{1129}}$	0.57	$\frac{I_{1510}}{I_{1132}}$	0.57	0.06	± 0.06
Nucleic Acids (A,G)/ Amide III	$\frac{I_{1341}}{I_{1310}}$	0.82	$\frac{I_{1342}}{I_{1313}}$	1.01	$\frac{I_{1337}}{I_{1314}}$	0.68	$\frac{I_{1340}}{I_{1312}}$	0.84	0.16	± 0.19
COO- symmetry/ Amide III	$\frac{I_{1399}}{I_{1310}}$	0.59	$\frac{I_{1411}}{I_{1313}}$	0.43	$\frac{I_{1391}}{I_{1314}}$	0.47	$\frac{I_{1400}}{I_{1312}}$	0.50	0.09	± 0.10
Lipids (CH_2)/Amide III	$\frac{I_{1449}}{I_{1312}}$	1.09	$\frac{I_{1463}}{I_{1312}}$	1.08	$\frac{I_{1453}}{I_{1314}}$	1.11	$\frac{I_{1455}}{I_{1313}}$	1.09	0.01	± 0.01
Amide I/ Nucleic Acids (A,G)	$\frac{I_{1667}}{I_{1590}}$	0.91	$\frac{I_{1679}}{I_{1590}}$	0.73	$\frac{I_{1671}}{I_{1582}}$	0.82	$\frac{I_{1672}}{I_{1586}}$	0.82	0.09	± 0.10

EPS Contribution.

To aid in understanding the Raman spectra of cells in mature biofilms, EPS was extracted, and both EPS and the remaining cell pellets were spectrally examined. In the SEM image of the mature biofilm, EPS appeared to be the dominating component (Figure 2:5). SEM imaging of the 5 day old biofilm showed masses of EPS adhered closely to cells producing dense web-like structures within the matrix. Raman analysis of EPS, confirmed that the biofilm signal (Figure 2:6B) may largely be attributed to EPS (Figure 2:6C). The relative peak intensity ratios of EPS are presented in Table 2:7. However, the presence of EPS was not the sole reason for chemical differences between the biofilm and free cell spectra. Both EPS and the biofilm have peak ratios for adenine to nucleic acids (U, G) $\left(\frac{I_{752}}{I_{794}}\right)$ greater than the same ratio for the free cells, 31% and 51% higher, respectively (Figure 2:7). The relative peak intensity ratios of phenylalanine to carbohydrate $\left(\frac{I_{1006}}{I_{1130}}\right)$ are comparable in EPS and the biofilm. However, there is a 31% difference in amide I to nucleotides relative peak intensity ratio $\left(\frac{I_{1669}}{I_{1588}}\right)$ between EPS and the biofilm. Also, after adding the free cell spectrum to the EPS spectrum, the resulting spectrum was very similar to the cell in biofilm spectrum (Figure 2:8). These results suggest that EPS secretion contributed to, but is not the sole reason, for chemical differences between the biofilm and free cell spectra.

Table 2:6: Relative peak intensity ratios of molecular components in three different samples of extracellular polymeric substances (EPS) extracted from *Pseudomonas* sp. strain ADP biofilm. No peak was detected at 1319 cm^{-1} in samples 2 and 3. ND represents none detected.

	EPS 1		EPS 2		EPS 3		Mean		Std Dev	95% Conf Intvl (n=3)
Band Assignments	Ratio	Value	Ratio	Value	Ratio	Value	Ratio	Value	Value	Value
Adenine/ Nucleic acids (C,U)	$\frac{I_{755}}{I_{795}}$	0.89	$\frac{I_{851}}{I_{803}}$	0.26	$\frac{I_{749}}{I_{789}}$	0.58	$\frac{I_{752}}{I_{794}}$	0.58	0.31	±0.35
Phenylalanine/ Carbohydrates	$\frac{I_{1009}}{I_{1134}}$	0.50	$\frac{I_{1006}}{I_{1129}}$	0.61	$\frac{I_{1004}}{I_{1129}}$	0.66	$\frac{I_{1006}}{I_{1130}}$	0.59	0.08	±0.09
Nucleic Acids (A,G)/ Amide III	$\frac{I_{1340}}{I_{1319}}$	0.68	$\frac{I_{1337}}{I_{1319_{ND}}}$	ND	$\frac{I_{1334}}{I_{1319_{ND}}}$	ND	$\frac{I_{1340}}{I_{1319}}$	0.68	ND	ND
COO- symmetry/ Amide III	$\frac{I_{1406}}{I_{1319}}$	0.39	$\frac{I_{1391}}{I_{1319_{ND}}}$	ND	$\frac{I_{1403}}{I_{1319_{ND}}}$	ND	$\frac{I_{1406}}{I_{1319}}$	0.39	ND	ND
Lipids (CH_2)/Amide III	$\frac{I_{1459}}{I_{1317}}$	0.93	$\frac{I_{1445}}{I_{1317_{ND}}}$	ND	$\frac{I_{1447}}{I_{1317_{ND}}}$	ND	$\frac{I_{1459}}{I_{1317}}$	0.93	ND	ND
Amide I/ Nucleic Acids (A,G)	$\frac{I_{1674}}{I_{1591}}$	0.66	$\frac{I_{1669}}{I_{1586}}$	1.41	$\frac{I_{1665}}{I_{1586}}$	1.29	$\frac{I_{1669}}{I_{1588}}$	1.12	0.40	±0.46

Pellets

The Raman spectra of cell pellets remaining after EPS extraction from the biofilm were collected to determine how the molecular distribution of cellular components varied when cells were grown in a biofilm rather than motile planktonic cells (Figure 2.6D). The lower nucleic acid region $\left(\frac{I_{799}}{I_{750}}\right)$ is 30% lower in pellets removed from the EPS matrix than free cells from the liquid suspension (Figure 2:7). The phenylalanine to carbohydrate peak intensity ratio $\left(\frac{I_{1006}}{I_{1130}}\right)$ is 19% higher in pellets than free cells. The amide I to nucleotides (A, G) content $\left(\frac{I_{1672}}{I_{1586}}\right)$ is almost twice as high in pellets. These notable differences may be attributed to particular gene expression in response to increased cell density, stimulating EPS secretion. Through quorum sensing, some bacteria have the ability to monitor their own cell density and coordinate particular gene expression responsible for EPS secretion.[9] Due to several factors, including growth conditions, cell-cell communication, and gene regulation, cells from the mature biofilm behave differently than motile planktonic cells, which were evident in Raman spectra and captured in the peak ratio calculations in Table 2.8.

Table 2:7: Relative peak intensity ratios of molecular components in three different samples of pellets remaining after EPS extraction from *Pseudomonas* sp. strain ADP biofilm.

	Pellets Remaining 1		Pellets Remaining 2		Pellets Remaining 3		Mean		Std Dev	95% Conf Interval (n=3)
Band Assignments	Ratio	Value	Ratio	Value	Ratio	Value	Ratio	Value	Value	Value
Nucleic acids (C,U)/Adenine	$\frac{I_{751}}{I_{803}}$	0.25	$\frac{I_{751}}{I_{796}}$	0.31	$\frac{I_{749}}{I_{799}}$	0.28	$\frac{I_{750}}{I_{799}}$	0.28	0.03	±0.04
Phenylalanine/ Carbohydrates	$\frac{I_{1005}}{I_{1127}}$	0.70	$\frac{I_{1006}}{I_{1127}}$	0.92	$\frac{I_{1006}}{I_{1127}}$	0.89	$\frac{I_{1006}}{I_{1127}}$	0.84	0.12	±0.13
Nucleic Acids (A,G)/ Amide III	$\frac{I_{1341}}{I_{1312}}$	0.88	$\frac{I_{1337}}{I_{1314}}$	0.97	$\frac{I_{1339}}{I_{1310}}$	0.86	$\frac{I_{1339}}{I_{1312}}$	0.90	0.06	±0.07
Amide III	$\frac{I_{1378}}{I_{1312}}$	0.52	$\frac{I_{1372}}{I_{1314}}$	0.61	$\frac{I_{1366}}{I_{1310}}$	0.45	$\frac{I_{1372}}{I_{1312}}$	0.53	0.08	±0.09
COO- symmetry/ Amide II	$\frac{I_{1395}}{I_{1312}}$	0.54	$\frac{I_{1399}}{I_{1314}}$	0.51	$\frac{I_{1386}}{I_{1310}}$	0.47	$\frac{I_{1393}}{I_{1312}}$	0.51	0.04	±0.04
Lipids (CH_2)/Amide III	$\frac{I_{1449}}{I_{1312}}$	1.07	$\frac{I_{1449}}{I_{1312}}$	1.11	$\frac{I_{1453}}{I_{1310}}$	1.21	$\frac{I_{1450}}{I_{1311}}$	1.13	0.07	±0.08
Amide I/ Nucleic Acids (A,G)	$\frac{I_{1669}}{I_{1584}}$	1.65	$\frac{I_{1669}}{I_{1586}}$	1.83	$\frac{I_{1669}}{I_{1584}}$	1.70	$\frac{I_{1669}}{I_{1585}}$	1.73	0.09	±0.10

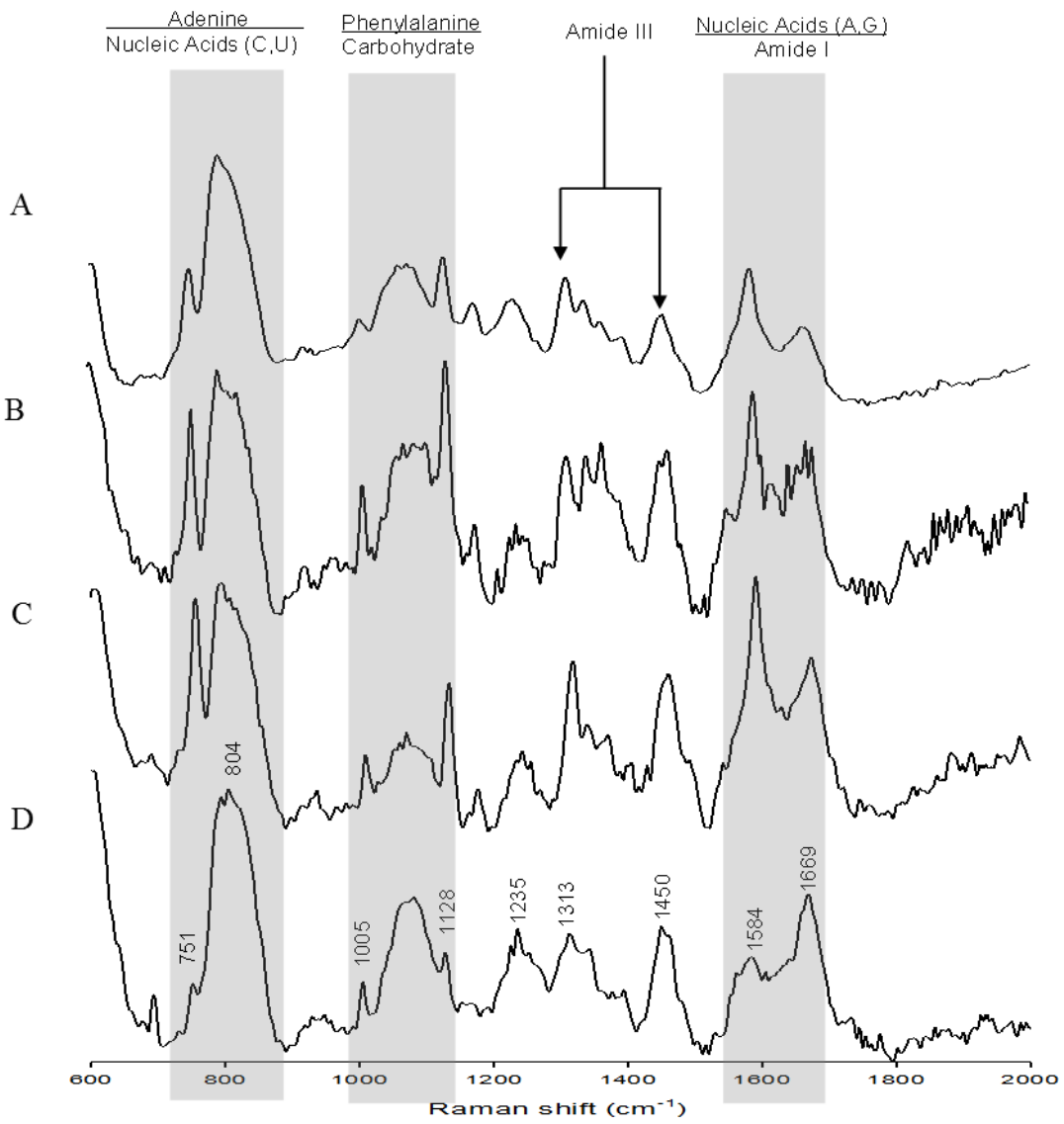

Figure 2:6: Normalized Raman spectra of *Pseudomonas* sp. strain ADP without baseline correction, collected with 532 nm laser, 60 seconds accumulation, and 0.6 μ**m** spot size. A) free cell, B) biofilm, C) extracted extracellular polymeric substance, and D) remaining pellets from biofilm. Notice change in relative intensity of peaks in nucleic acid region and phenylalanine/carbohydrate region. Spectra B and C have almost the same curve, with the exception of the amide III region, indicating that EPS is the dominating feature in a mature biofilm. Dissimilarities revealed in spectra A and D, show that EPS is not the sole contributing factor to differences between biofilm and planktonic microbes.

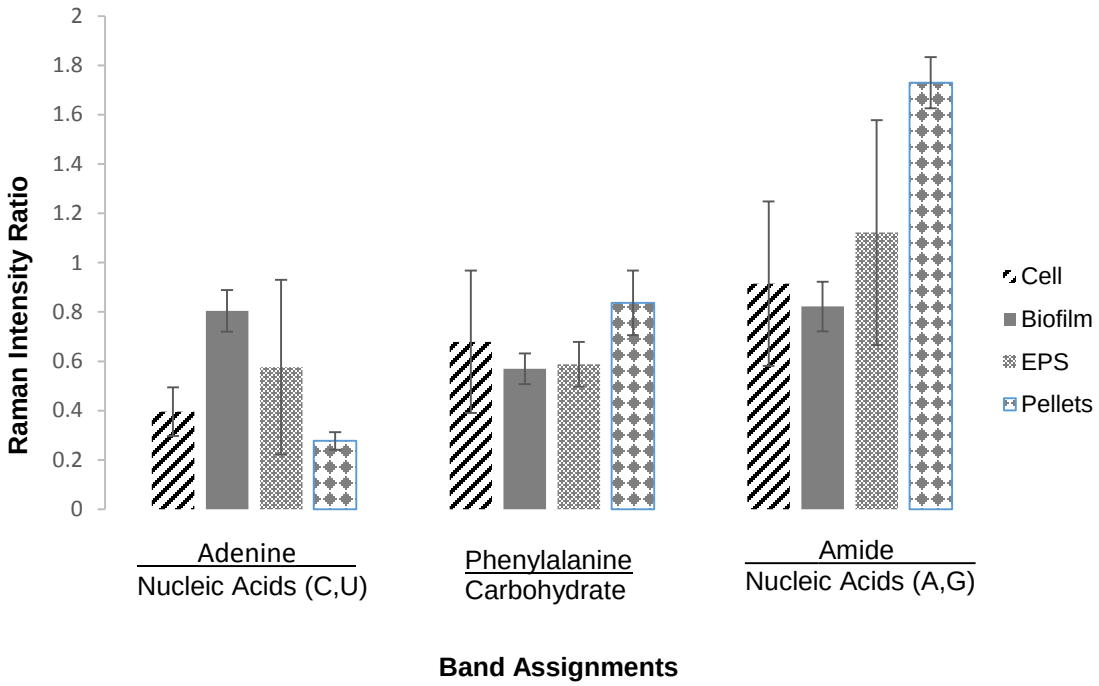

Figure 2:7: Relative Raman peak intensity ratios of *Pseudomonas* sp. strain ADP free cell, biofilm, EPS, and pellets remaining after EPS extraction. The errors bars represent 95% confidence intervals (n=3).

Table 2:8: Comparison of relative peak intensity ratios of *Pseudomonas* sp. strain ADP free cells to cells in biofilm, EPS, and remaining pellets after EPS extraction from biofilm. The ± values represent the 95 % confidence levels (n=3), n=1 for values including an asterisk.

	Free Cell		**Biofilm**		**EPS**		**Pellets**	
Band Assignments	Ratio	Value	Ratio	Value	Ratio	Value	Ratio	Value
Adenine/Nucleic acids (C,U)	$\frac{I_{746}}{I_{789}}$	0.4 ± 0.1	$\frac{I_{752}}{I_{789}}$	0.8 ± 0.1	$\frac{I_{752}}{I_{794}}$	0.6 ± 0.4	$\frac{I_{750}}{I_{799}}$	0.3 ± 0.04
Phenylalanine/Carbohydrates	$\frac{I_{1002}}{I_{1127}}$	0.7 ± 0.3	$\frac{I_{1007}}{I_{1132}}$	0.6 ± 0.1	$\frac{I_{1006}}{I_{1130}}$	0.6 ± 0.1	$\frac{I_{1006}}{I_{1127}}$	0.8 ± 0.1
Nucleic Acids (A,G)/ Amide III	$\frac{I_{1337}}{I_{1309}}$	0.9 ± 0.1	$\frac{I_{1340}}{I_{1312}}$	0.8 ± 0.2	$\frac{I_{1340}}{I_{1319}}$	0.7*	$\frac{I_{1339}}{I_{1312}}$	0.9 ± 0.1
COO-symmetry/ Amide III	$\frac{I_{1392}}{I_{1308}}$	0.5 ± 0.1	$\frac{I_{1400}}{I_{1312}}$	0.5 ± 0.1	$\frac{I_{1406}}{I_{1319}}$	0.4*	$\frac{I_{1393}}{I_{1312}}$	0.5 ± 0.04
Lipids (CH_2) /Amide III	$\frac{I_{1448}}{I_{1308}}$	1.0 ± 0.3	$\frac{I_{1455}}{I_{1313}}$	1.1 ± 0.01	$\frac{I_{1459}}{I_{1317}}$	0.9*	$\frac{I_{1450}}{I_{1311}}$	1.1 ± 0.08
Amide I/ Nucleic acids (A, G)	$\frac{I_{1663}}{I_{1582}}$	0.9 ± 0.3	$\frac{I_{1672}}{I_{1586}}$	0.8 ± 0.1	$\frac{I_{1669}}{I_{1588}}$	1.1 ± 0.5	$\frac{I_{1669}}{I_{1585}}$	1.7 ± 0.1

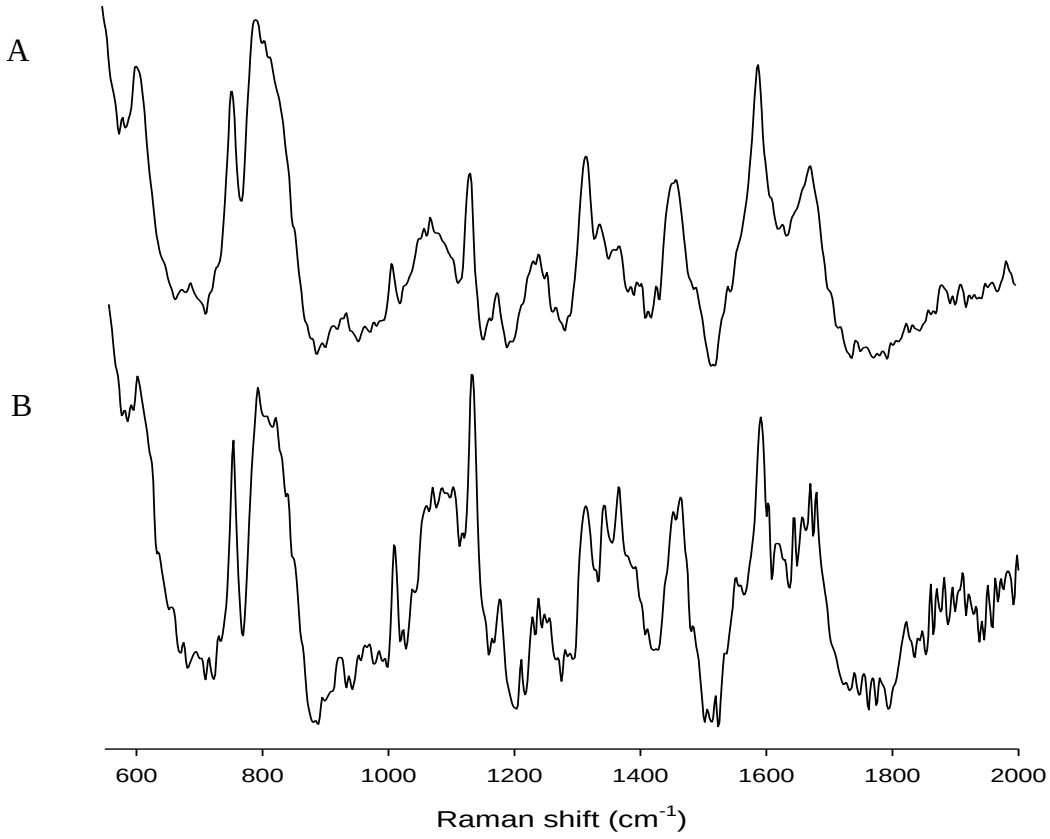

Figure 2:8: Normalized Raman spectra of *Pseudomonas* sp. strain ADP A) added free cell to EPS spectra B) cell in biofilm. Notice that the biofilm spectrum is almost equivalent to the free cell plus EPS spectrum, with the exception of difference in relative intensity at 1406 cm^{-1} in the amide III region. The similarities in spectra indicate that EPS is the major constituent in a mature biofilm.

Conclusion

By visual inspection of Raman spectra and comparison of relative peak intensity ratios, it is possible to detect differences in molecular components distribution of ADP free cells and ADP biofilms. Superior Raman spectra of microbes were obtained by removing water from samples, thereby reducing concentration, decreasing wavelength, and increasing sample accumulation time. This analytical approach was validated by comparing experimental Raman spectra of *E.coli* with published spectra.

Free cells of *E. coli* and ADP showed differences in relative peak intensity ratios greater than 2 fold. Cells of the same species, grown differently (i.e., freely in suspension or in biofilm) showed differences in nucleic acid, carbohydrate, and protein content in the fingerprint region. Following SEM imaging and EPS extraction from mature biofilms, differences were largely attributed to the presence of EPS in the matrix.

In Chapter 3, EPS fractions along with component analysis is addressed to gain insight to molecular contribution detected in Raman spectra. Molecular component analysis of EPS by peak identification and relative distribution will more precisely determine EPS contribution to the biofilm matrix. There is still much to be learned on the molecular level about various biofilm matrix polymers and their contribution to the integrity of the biofilm matrix.[1] Success of this research will ultimately lead to a firmer grasp of scientific fundamentals associated with microbial biofilms and the aid in the building of the Raman microbial library.

CHAPTER 3: FUNCTIONAL GROUP CHARACTERISTICS OF EXTRACELLULAR POLYMERIC SUBSTANCES IN *PSEUDOMONAS* SP. STRAIN ADP BIOFILM

Introduction

The formation and maintenance of structural microbial communities strongly depend on the presence of interconnecting extracellular polymeric substances (EPS).[10] EPS are high molecular weight biopolymers produced by microbes as they multiply and remain entrapped in the biofilm matrix, producing water-rich, three-dimensional architectures that allow the flow of nutrients into and out of the biofilm and protecting cells from dewatering and toxic substances.[58] Not only are EPS products of microbial secretions, they are also products of cellular lysis and hydrolysis of macromolecules.[56] A large range of polymers and molecular components, including DNA, carbohydrates, fats, and lipids, can be found in the extracellular matrix.

EPS matrices have been labeled 'the dark matter of biofilms' because of the ambiguity of biopolymers and difficulty in analyzing them.[1] There are many different types of EPS, such as slimes, sheaths, gels, capsular polymers, and colloids, depending on the association of the polymers with cells.[56] To make differentiation less difficult, Nielsen et al. separated EPS into two groups, bound and soluble EPS.[59] In bound EPS, polymers encapsulate cells, and organic material is attached to cells; while in soluble EPS (SEPS), soluble macromolecules and colloids, which are products of biological activity either through polymer synthesis, cell lysis and/or substrate hydrolysis, are adsorbed to the matrix.[56] Bound EPS consist of dynamic two layer structures composed of tightly bound EPS (TB-EPS) and lightly bound (LB-EPS) (see Figure 3:1).[60] TB-EPS are the inner layers closest to the cell that have shape and stability. LB-EPS are the looser outer layers without finite shape that sometimes give slushy, slime-like characteristics to biofilms. SEPS are

adsorbed weakly to cells and are assumed to be readily dispersed in solution.

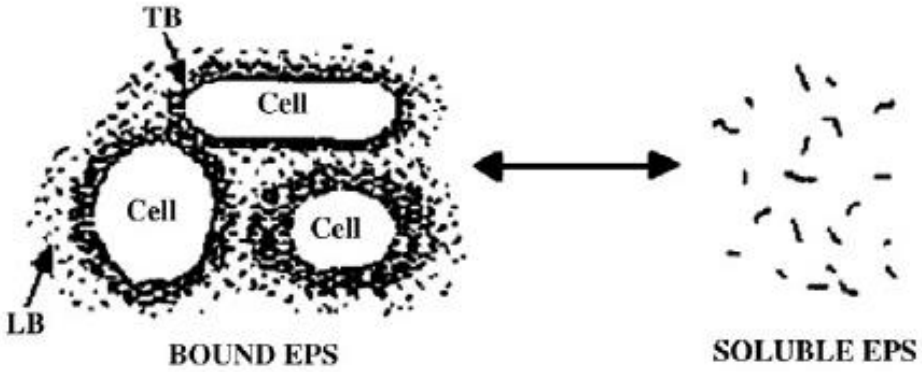

Figure 3:1: Sketch depicting the two types of EPS, bound and soluble EPS, that exist outside of cell congregates.[58] Bound EPS bind closely to cells, while soluble EPS are weakly attached to cells or dissolved in solution. Bound EPS consist of two layers: tightly bound EPS (TB-EPS) and lightly bound EPS (LB-EPS). TB-EPS are the layers closest to cells with structure and stability, and LB-EPS are looser, slimier layers without obvious edges.

Source: Sheng, G. P.; Yu, H. Q.; Li, X. Y., Extracellular polymeric substances (EPS) of microbial aggregates in biological wastewater treatment systems: A review. *Biotechnology Advances* **2010**, 28, 882-894.

EPS properties significantly influence the physicochemistry of microbial aggregates, including adsorption ability, surface charge, structure, and hydrophobicity.[47] The complex nature of biofilms and variability in composition, as a result of environmental and growth conditions, leads to conflicting data in literature, making it difficult to generalize EPS properties.[60] For this reason, it is beneficial to separate EPS from cells and perform more detailed studies to better characterize individual biofilm systems.

Raman spectroscopy provides a way to extract quickly biochemical information about EPS fractions. In Chapter 2, we demonstrated that EPS contributed significantly to

the Raman signal of ADP biofilms. In most biofilms, the extracellular matrix accounts for over 90% of the dry mass, while the organism accounts for less than 10%.[1] To distinguish the contributions of specific EPS components, further separations and characterizations were pursued. In this study, the molecular composition of EPS secreted in *Pseudomonas* sp. strain ADP (ADP) biofilm is characterized, and chemical bonds present are identified with Raman spectroscopy. Collecting the chemical fingerprint of EPS from ADP aids in understanding the biochemical properties of ADP biofilm, which may have positive implications for future biotechnology applications.

Materials and Methods

Cultures and Reagents

Pseudomonas sp. strain ADP was purchased from Deutsche Sammlung von Mikrooganismen und Zelkulturen, (Braunschweig, Germany) and stored at -80^{o}C in Tryptic Soy Broth with glycerol (1:1) as a cyroprotectant. EDTA (10 mM) was used for EPS extraction as purchased from Fisher Scientific (Pittsburgh, Pennsylvania).

Biofilm Preparation

Biofilms were grown in a four-channel Teflon drip biofilm reactor, as described in Chapter 2. Standard microscope glass slides (75 mm x 25 mm x 1 mm) were placed flat on the bottom of each channel to provide a surface for cells to adhere and grow. Frozen bacteria were thawed at room temperature, then diluted (1:10) in Luria Bertani (LB) medium and grown overnight in 250 mL Erlenmeyer shake flasks at 30^{o}C and 200 rpm. Each chamber was inoculated with 10 mL of overnight cell culture, containing a 10% inoculum of ADP cells suspended in LB medium. The system was held in batch mode for 6 h to allow the cells time to adhere to each substratum. Then LB medium was fed into the reactor for 5 d at a flow

rate of 0.8 mL/min with size 13 tubing (0.8 mm ID). Biofilms were harvested by gentle scraping into centrifuge tubes.

EPS Extraction

EPS was extracted using combined chemical and physical methods of Chen, Liang, and Castro with slight modifications (see Figure 3:2).[47, 60, 61] Each five-day-old biofilm was collected in centrifuge tubes, brought to 45 mL suspension with deionized water, and treated with ultrasound at 20 kHZ for 60 s.[47] The suspension was then centrifuged at 2,000 g for 15 min and 4°C. The supernatant, which is considered SEPS, was collected and filtered through a 0.45 µm filter and freeze dried. Sediments at the bottom of the centrifuge tube were resuspended to the initial 45 mL volume with deionized water to begin LB-EPS extraction. The suspension was incubated in an orbital shaker at 20 rpm for 1 h prior to centrifugation at 5,000 g and 4°C for 15 min. The supernatant was treated as LB-EPS, filtered, and freeze dried. Sediments at the bottom of the centrifuge tube were then resuspended in 10 mL PBS and 5 mL of 10 mM EDTA (pH 8.3) for 3 h at 4°C to extract TB-EPS.[60] EDTA helps to remove divalent cations, Ca^{2+} and Mg^{2+}, responsible for crosslinking of charged compounds in the EPS matrix to enhance efficiency of TB-EPS extraction.[59] Upon incubation, the suspension was centrifuged at 5,000 g for 15 min. Supernatant fluids were filtered, freeze dried, and stored at -20°C. The dry mass of each fraction was recorded after freeze drying for 3 days.

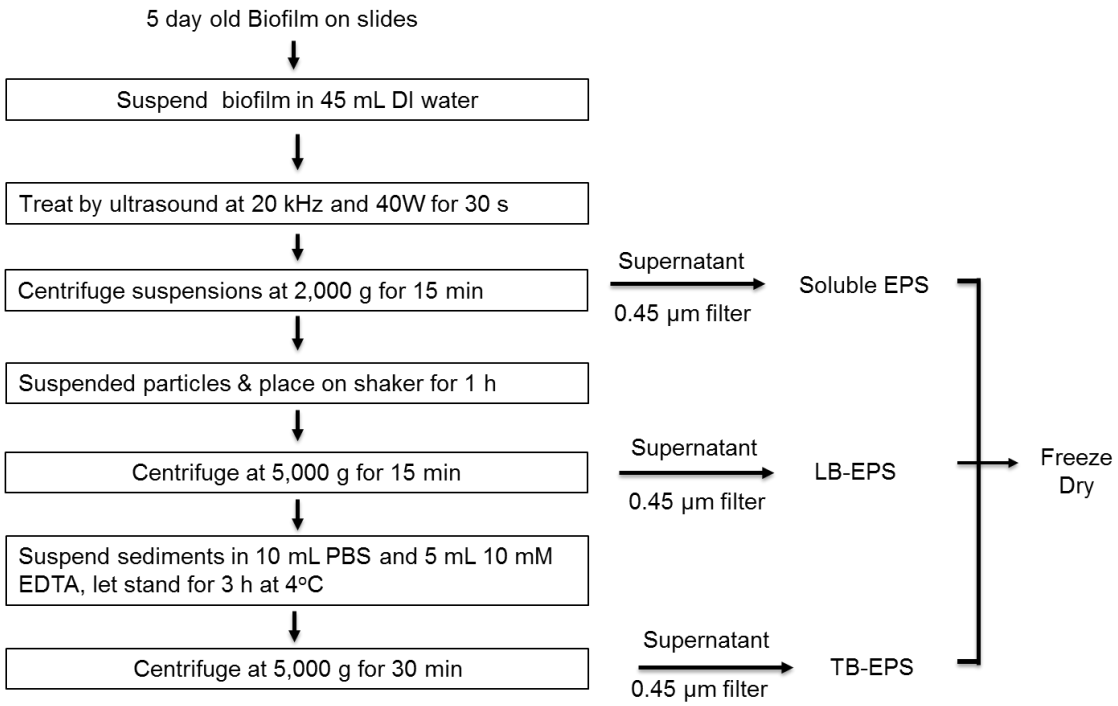

Figure 3:2: Schematic of EPS fractionation using sonication, centrifugation, and EDTA.

Chemical Analysis

Raman microscopy was used to acquire spectra of EPS fractions. A Thermo Nicolet Almega XR Raman spectrometer equipped with an Olympus BX 51 model microscope and Thermo Fisher Scientific OMNIC 8 software was used for Raman analysis as described in Chapter 2. Samples were illuminated with frequency-doubled 532 nm Nd:Yv04 laser emitting approximately 10 mW laser power at the sample.

Raman spectra of dried powders of EPS were collected with 100x objective with 0.90 NA, 60s exposure with 2 accumulations, and 6th order polynomial fluorescence correction applied. Spectra were recorded, peaks identified, and baseline corrections for relative peak intensity ratios were processed with OMNIC 8 software. Raman band assignments for EPS were identified by comparison of published molecular assignments of biological specimen

(Table 2:1). All spectra in the 600-2000 cm^{-1} fingerprint region were normalized to the lipids (CH_2 bending) peak at ~1450 cm^{-1}; and spectra in the 2500-3500 cm^{-1} C-H region where normalized to C-H stretching in fatty acids and proteins peak at ~2950 cm^{-1}. The relative molecular distribution in each sample was determined as described in Chapter 2 by calculating the relative peak intensity ratios.

Protein content for each EPS fraction was determined by modified Lowry assay (see Appendix E for calibration curve). RNA content was quantified using the Qubit assay for RNA high-sensitivity detection with the Qubit Fluorimeter 3.0.

Results and Discussion

Here, we present the relationships among three microbial products of *Pseudomonas* sp. strain ADP biofilm: tightly bound EPS (TB-EPS), lightly bound EPS (LB-EPS), and soluble EPS (SEPS). Chemical and molecular distribution are analyzed to aid in deciphering the complex nature of ADP biofilm. Lowery assays of protein content and RNA analysis further demonstrated the efficiency of using Raman spectroscopy for determining the relative distribution of multiple molecular components within one sample.

Raman Spectra of EPS

By comparison of relative peak intensity ratios, Lowry assay, and fluorimetry, SEPS was found to have the highest protein and RNA content of the three EPS fractions from ADP biofilm. Figure 3:3 shows qualitative Raman spectra of TB-EPS, LB-EPS, and SEPS, with some similarities and differences among all three spectra. The protein content of amide I to lipids (CH_2 deformation) $\left(\frac{I_{1669}}{I_{1452}}\right)$ and amide I to carbohydrate $\left(\frac{I_{1670}}{I_{1088}}\right)$ were 76% higher in SEPS compared to LB-EPS and TB-EPS. The relative peak intensity ratio of amide II to

carbohydrates $\left(\frac{I_{1578}}{I_{1088}}\right)$ was 64% higher in SEPS than TB-EPS. Secondary protein structures in the amide II region, ~1550 cm^{-1}, were minimally detected in LB-EPS. Adenine was detected at 720 and 726 cm^{-1} in LB-EPS and SEPS, respectively, while cytosine and uracil, were only detected in SEPS at 785 cm^{-1}. Trace amounts of tyrosine appeared as a doublet Raman band caused by Fermi resonance between the in-plane breathing mode of the phenol ring and an overtone of out-of-plane deformation mode at 830 and 850 cm^{-1} in SEPS, and buried tyrosine was detected at 859 cm^{-1} in LB-EPS. Phenylalanine was detected in SEPS and LB-EPS at 1001 and 1005 cm^{-1}, respectively, with a minute amount detected in TB-EPS relative to CH_2 deformation at ~1450 cm^{-1}. All three EPS fractions displayed peaks at ~1075 cm^{-1}, 1335, and 1450 cm^{-1}, which often represent carbohydrates, nucleic acids (A,G), and lipids (CH_2 deformation), respectively. However, the band assignment of the 1335 cm^{-1} peak in SEPS is questionable, because the peak appears as a Fermi doublet (1320 and 1335 cm^{-1}), which may be associated with a protein instead of nucleic acids. Often the Fermi doublet of tryptophan is found in proteins at 1340 and 1360 cm^{-1}.[62] The COO- moieties appear to be suppressed in SEPS by well-structured pentagonal water of hydrophobic hydration. Competition for hydration between hydrophobic (apolar) and charge (polar) moieties can be so severe as to suppress charge formation.[63] Both TB-EPS and LB-EPS have strong Raman band COO- symmetry at 920 cm^{-1}. The COO- moiety at 1413 and 1411 cm^{-1} is only detected in TB-EPS and LB-EPS, respectively, and lipids (CH_2 deformation) are detected in all three spectra at ~1450 cm^{-1}. Sandt et al. also detected the COO-moiety of carboxylic acid at 1400 cm^{-1} near the base and top of *Pseudomonas aeruginosa* PA01 biofilm colony.[41] Upon completion of the modified Lowry assay, SEPS was found to have the highest protein and RNA content (Figure 3:4), as supported by relative peak intensity ratios.

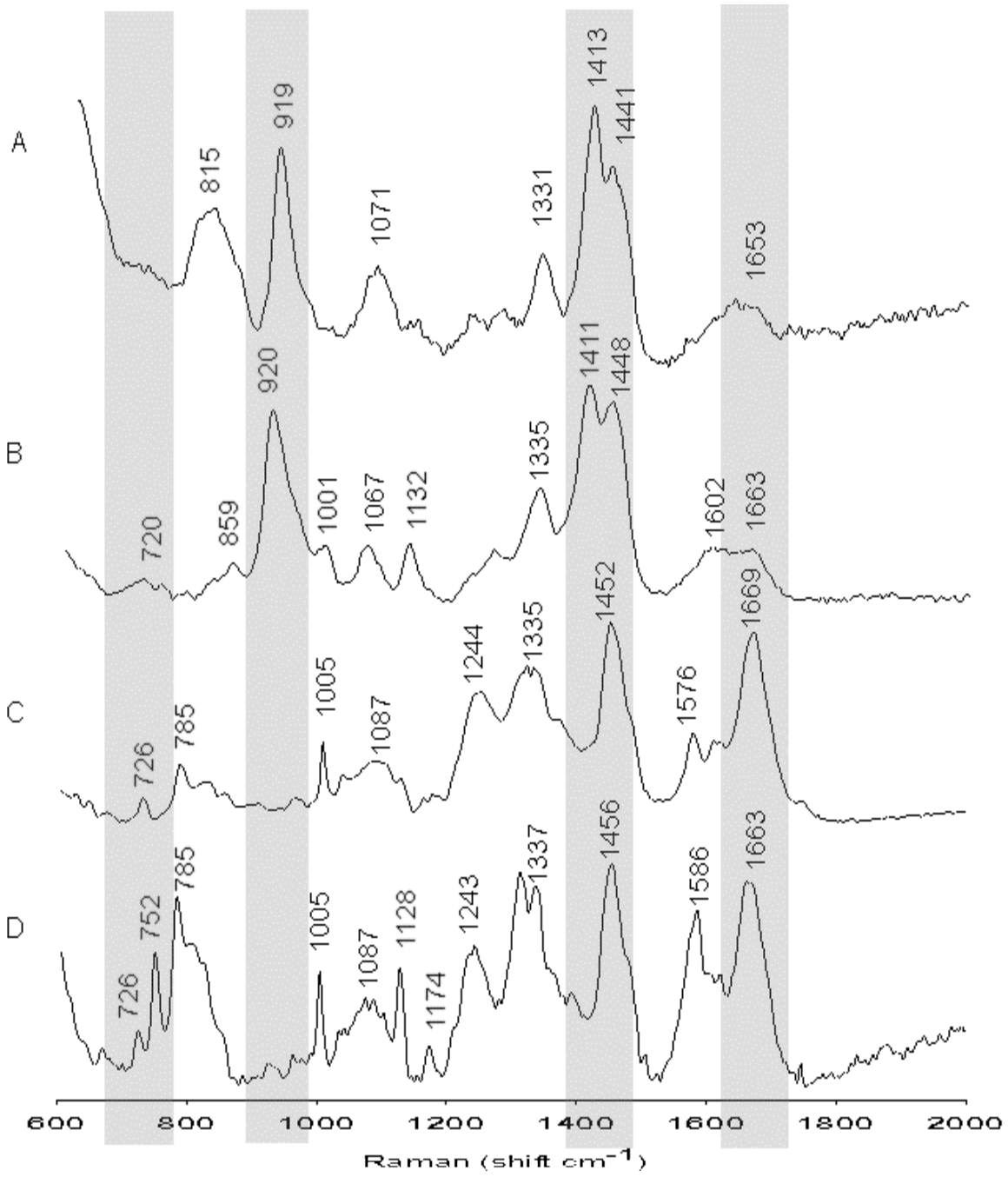

Figure 3:3: Normalized Raman spectra of EPS fractions in the 600-2000 cm^{-1} fingerprint region A) tightly bound EPS, B) lightly bound EPS, C) soluble EPS, and D) biofilm. Notice that Raman shifts of SEPS are present at the same locations in biofilm, with the exception of the 752 cm^{-1} peak.

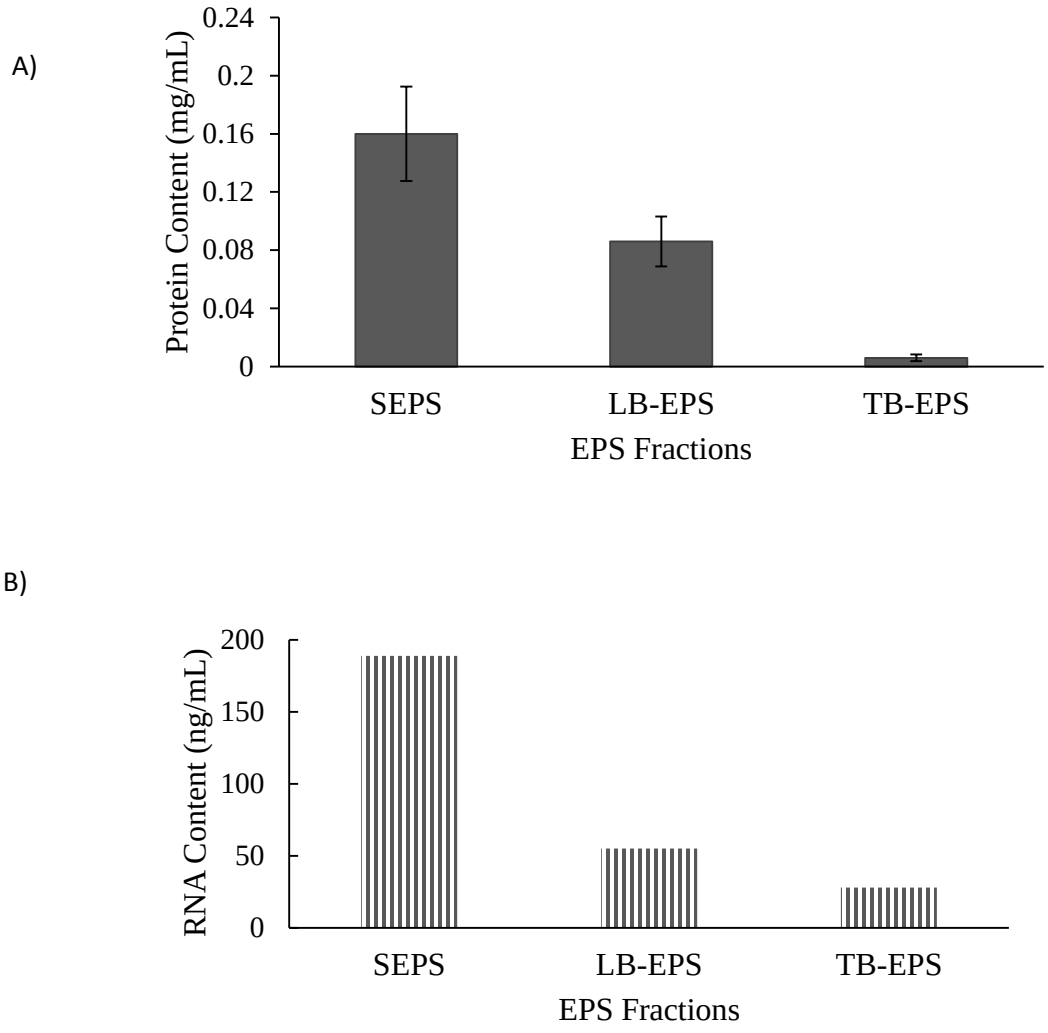

Figure 3:4: A) Protein and B) RNA content of soluble EPS, lightly bound EPS and tightly bound EPS by Lowry and Qubit assay, respectively. Notice that SEPS has the highest protein and RNA content. The errors bars represent 95% confidence intervals (n=3), n=1 for Qubit assay.

Table 3:1: Comparison of relative peak intensity ratios of secondary proteins relative to carbohydrate and lipid content in EPS fractions and biofilm. The ± values represent the 95% confidence levels (n=3), where n=1 for values including an asterisk. ND denotes areas where peaks were not detected.

	TB-EPS		LB-EPS		SEPS		Biofilm	
Band Assignments	Ratio	Value	Ratio	Value	Ratio	Value	Ratio	Value
Amide II/ Carbohydrates	$\frac{I_{1564}}{I_{1076}}$	0.4 ± 0.1	$\frac{I_{1570\ ND}}{I_{1068}}$	ND	$\frac{I_{1578}}{I_{1088}}$	1.2 ± 0.5	$\frac{I_{1585}}{I_{1075}}$	1.9 ± 0.3
Amide I/ Carbohydrates	$\frac{I_{1668}}{I_{1076}}$	0.6*	$\frac{I_{1663}}{I_{1068}}$	0.7 ± 0.6	$\frac{I_{1670}}{I_{1088}}$	2.8 ± 0.9	$\frac{I_{1664}}{I_{1075}}$	1.7 ± 0.7
Amide I/Lipids	$\frac{I_{1669}}{I_{1452}}$	0.2*	$\frac{I_{1663}}{I_{1448}}$	0.2 ± 0.1	$\frac{I_{1669}}{I_{1452}}$	1.0 ± 0.2	$\frac{I_{1663}}{I_{1456}}$	0.9 ± 0.1

EPS Contribution to Biofilm

By qualitative inspection of Raman spectra (Figure 3:3) and Raman peak intensity ratios calculations (Table 3:2), SEPS were found to be most comparable to biofilm. The Raman spectra contain similar Fermi doublet at 1337 and 1335 cm^{-1}, and similar peaks are detected at 785, 1005, and 1244 cm^{-1}. All spectra showed similar peaks at 1067-1087 cm^{-1}, accounting for carbohydrates. This data suggest that SEPS have biochemical compositions most similar to biofilm in comparison to TB-EPS and LB-EPS.

Per mass extracted, SEPS had the lowest dry weight (Table 3:2). Biofilms grown on standard glass microscope slides (75 mm x 22 mm x 1 mm) have a dry mass of 98 mg (± 0.1) per channel, n=4. The total amount of EPS, including SEPS, LB-EPS, and TB-EPS, accounts for 92.97% of the biofilm dry weight, Figure 3:5. SEPS, LB-EPS and TB-EPS were 2.27%, 6.88%, and 83.81%, respectively, of the biofilm total mass. Since SEPS have the highest protein and RNA content among the three fractions, but lowest dry mass, it appears as though LB-EPS and TB-EPS may largely be made up of carbohydrates and lipids. Similar findings have been reported of polysaccharides being most abundant in EPS, while proteins were more abundant in biofilm systems.[60]

Table 3:2: Combined final dry mass of EPS extracted from 5-day old *Pseudomonas* sp. strain ADP grown in four channel drip biofilm reactor.

EPS Fraction	Dry weight
SEPS	8.9 mg
LEPS	26.9 mg
TB-EPS	327.7 mg

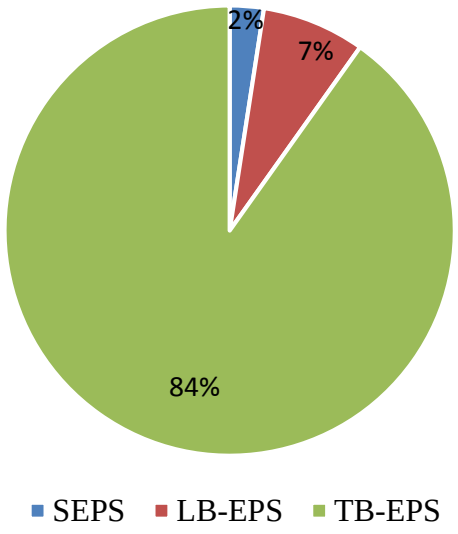

Figure 3:5: EPS contribution to the total biofilm mass. EPS makes up 93% of the 5-day old ADP biofilm dry weight. SEPS, LB-EPS, and TB-EPS account for 84%, 7 %, and 2% respectively.

Conclusion

In this study, EPS contribution to ADP biofilms have been investigated. Raman spectroscopy allowed direct analysis of specific components and molecular distribution among EPS fractions. The major components of EPS have strong Raman bands, allowing composition analysis of EPS fractions without having to make individual extractions. All EPS fractions showed similarities and differences, with SEPS having most similar characteristics to biofilm. Chemical assays revealed that proteins and RNA were most abundant in SEPS, which was supported with Raman analysis. Proteins also appeared to be more abundant in ADP biofilms relative to the carbohydrate and lipid content. Further studies in Chapter 4, involve growing ADP biofilm on minimal salt medium containing atrazine as the sole nitrogen source and determining the extent of particles affinity to the extracellular matrix.

CHAPTER 4: DETECTING ATRAZINE DEGRADATION IN *PSEUDOMONAS* SP. STRAIN ADP BIOFILM WITH RAMAN SPECTROSCOPY

Introduction

Through infiltration and surface runoff, atrazine is often found as a pollutant in concentrations exceeding the EPA limit of 3 ppb.[64] In nature, some microbial populations, including *Rhodococococcus*, *Anthrobacter*, *Klebsiella*, and *Agobacterium*, respond to synthetic chlorinated compound exposure by producing enzymes that degrade xenobiotic materials such as atrazine.[33, 65, 66] Some microbes mineralize atrazine into deethylatrazine (DEA) and deisopropylatrazine (DIA).[67] Others, such as *Pseudomonas* sp. strain ADP, completely degrade atrazine to carbon dioxide and ammonia. The degradation pathway of ADP free cells is well established; however, there is much to learn about how ADP cells interact with atrazine in a biofilm matrix. Previous efforts to study and apply the biocatalytic power of ADP in bioreactor systems led to the discovery that these cells form biofilms.[28]

Exploring the degradation capacity of ADP cells in a biofilm matrix may enhance current biotechnology applications involving atrazine. As a biofilm, metabolic activities are increased and xenobiotic usage is accelerated, owing to the numerous uses of biofilms in industrial applications.[2, 68] Microbes in biofilms are in close proximity to each other and experience increased horizontal gene transfer. Through chemotaxis and cell-cell communication, organisms in a biofilm matrix are able to position themselves in a manner that is most beneficial for the overall survival of the matrix, and the matrix increases the bioavailability of nutrients for the cells.[2, 11] The increase in survival and microbial adaptions presents a safe alternative to traditional remediation applications.[2, 12]

Mandelebaum, Martinez, Watkett, De Souza, Govantes, Katz, Clausen, and Changey have contributed much to the understanding of atrazine degradation by ADP cells

in suspension.[27, 29, 30, 33, 48, 49] In this study, atrazine degradation is characterized in ADP biofilms. Raman spectroscopy was used to detect atrazine degradation via intermediates and through comparison of relative peak intensity ratios. Scanning electron microscopy (SEM) was used to visualize the surface morphology and extracellular interaction within biofilms containing atrazine. Gas chromatography coupled with mass spectrometry (GC-MS) was used to track atrazine degradation over time.

In previous studies, HPLC, GC, and mass spectrometry were used to confirm the appearance of intermediate products resulting from atrazine degradation.[27, 29, 69] Late exponential ADP cells were resuspended in fresh medium containing 100 ppm ring labeled [^{14}C] atrazine and its radioactivity analyzed over time.[27] In less than 150 min, atrazine was completely degraded, and 80% carbon dioxide was generated. Analysis of culture medium by HPLC showed the appearance of intermediate products, and mass spectrometry confirmed hydroxyatrazine as one of the major products early in the degradation process.[27] Sadowsky et al. introduced N-isopropylammelide as a substrate and detected cyanuric acid by HPLC and GC-MS analysis.[69] Martinez et al. inserted a plasmid containing atzD from pADP-1, pBMZ1, into *E.coli* DH5α and monitored reactions with 3 mM cyanuric acid by HPLC. Cyanuric acid concentration decreased over time and biuret was resolved from reaction mixtures using an Adsorbosphere C18 reverse-phase HPLC column; mass spectroscopy confirmed biuret as a product.[29] In this study, Raman spectroscopy is proposed as a new approach to detect atrazine and its intermediate products, cyanuric acid and biuret. By collecting the Raman spectra of the effluent leaving the bioreactor, we hypothesized that the degradation capacity of wild type ADP biofilms could be characterized by detecting intermediate product(s).

Materials and Methods

Chemicals

Atrazine was donated by Monsanto (Muscatine, Iowa) and purchased from Cayman Chemicals (Ann Arbor, Michigan). Deuterated chloroform, deuterium labeled atrazine (atrazine-d5), hydroxyatrazine, biuret, and cyanuric acid were purchased from Sigma Aldrich (St. Louis, Missouri). Methanol, chloroform, and ethyl acetate were purchased from Fisher Scientific (Pittsburgh, Pennsylvania). Chemicals used for media preparation were reagent grade and purchased from Fisher Scientific (Pittsburgh, Pennsylvania), Sigma Aldrich, and Mallinckrodt (St. Louis, Missouri). All water used for experimentation was purified using Thermo Scientific Barnstead NANOpure DIamond ultrapure water system (Waltham, Massachusetts).

NMR Analysis

NMR spectroscopy was used to confirm the purity of atrazine on hand. Atrazine in stock was a 7-year-old sample donated by Monsanto. Ten milligrams of atrazine were dissolved in 700 µL of deuterated chloroform, then placed in dram vial with cap for analysis. NMR analysis was performed using a 300 Hz Avance Bruker NMR. Integration and areas were found using the Bruker Topsin 1.3 software.

Cultures

Pseudomonas sp. strain ADP was purchased from Deutsche Sammlung von Mikrooganismen und Zelkulturen (Braunschweig, Germany) and stored at -80^{o}C in Tryptic Soy Broth with glycerol (1:1) as a cyroprotectant. Frozen bacteria were thawed at room temperature, then diluted (1:10) in Luria Bertani (LB) medium and grown overnight in 250 mL Erlenmeyer flasks at 30^{o}C and 180 rpm. One mL of overnight ADP culture (~ 7.0 OD_{600}) was passed to 9.0 mL of minimal salt (MS) medium containing 1.6 g K_2HPO_4, 0.4 g KH_2PO_4,

0.2 g $MgSO_4 \cdot 7H_2O$, 0.1 g $CaCl_2$, and 1.0 g sodium citrate per liter of water. The medium was autoclaved for 20 min at 121°C and 15 psig. Salt and vitamin stock solutions were filtered sterilized (0.22 µm Nalgene filter top, Thermo Scientific, Waltham, Massachusetts) into medium by 10% volume, glucose was autoclaved at 121°C separately for 10 min and added by 5% volume, and 50 mg of atrazine was added to the medium from stock solution containing 20 mg atrazine per mL methanol.[52] Stock solution of atrazine was made in methanol because atrazine is poorly soluble in water (33 mg/L). Salt stock contained 2.5 g EDTA, 0.4 g $CuSO_4 \cdot 5H_2O$, 1.54 g $MnSO_4 \cdot H_2O$, 0.2 g $CoSO_4 \cdot 7H_2O$, 19.77 g $ZnSO_4 \cdot 7H_2O$, 9.15 g $FeSO_4 \cdot 7H_2O$, 0.18 g $Na_2B_4O_7 \cdot 10H_2O$, and 5.0 mL H_2SO_4 per liter of water. Vitamin stock contained 5.0 mg thiamine, 10.0 mg pyridoxine hydrochloride, 2.0 mg folic acid, 10.0 mg niacinamide, and 2.0 mg biotin per liter of water.[70] Glucose stock contained 10 g glucose per 100 mL of water. Ten percent inoculum of cells in liquid MS broth grew 24-72 h at 30°C and 180 rpm. MS cultures were later used to inoculate the biofilm reactor and shake flasks.

Biofilm Cultivation

Biofilms were grown in a four-channel Teflon drip biofilm reactor under continuous flow for 10 d with MS media containing 50 ppm atrazine as the sole nitrogen source for the first 5 d, then MS media not containing atrazine or other nitrogen source for an additional 5 d to encourage cells to mineralize atrazine already caught in the matrix. Each chamber was inoculated for six hours with 10 mL MS cell broth, measuring approximately 1.0 OD. The reactor was held in batch mode for 6 h to allow cells time to adhere to glass or quartz substrata. Flow was maintained with two peristaltic pumps at 0.8 mL/min. See Appendix B for more detail on reactor design and Chapter 2 for more detail on reactor setup. Standard glass microscope slides (75 mm x 25 mm x 1 mm) were placed on the bottom of Channels 1

and 2; two quartz microscope slides (38 mm x 25 mm x 1 mm) were placed in Channel 3 for Raman analysis of intact biofilm. For SEM imaging, biofilms were grown on two glass coverslips (22 mm x 22 mm and 0.13-0.16 mm thick) in Channel 4. The first coverslip was used for viewing of intact 5 d old biofilm grown continuously with atrazine. The second coverslip was used for analysis of 10 d biofilm, which was grown for 5 d with atrazine and an additional 5 d without atrazine. EPS was extracted from the 10 day biofilm as described in the Materials and Methods section in Chapter 3.

Raman Analysis

Raman microscopy was used to acquire spectra of atrazine, metabolites, effluent leaving the bioreactor and cell culture from shake flasks. A Thermo Nicolet Almega XR Raman spectrometer equipped with an Olympus BX 51 model microscope was used along with OMNIC 8 software for Raman analysis as described in Chapter 2. Samples were illuminated with a frequency-doubled 532 nm Nd:Yv04 laser. To track atrazine degradation by detection of intermediates, Raman spectra of bioreactor effluent were collected and compared against Raman spectra of reference samples of atrazine, hydroxyatrazine, cyanuric acid, and biuret. Multiple spectra were collected of effluent every 24 h over 10 d to probe for the appearance of intermediates by peak identification and calculations of relative peak intensity ratios.

Reference Sample Analysis

Reference Raman spectra of pure solid state atrazine and metabolites (i.e., hydroxyatrazine, cyanuric acid, and biuret) were collected with a 100x objective and 0.90 NA, with a spot size of 0.6 µm. Unaltered samples, as provided by manufacturers, were placed onto quartz microscope slides, brought into focus with a 10x objective, then illuminated, and their spectra collected with 100x objective. The exposure time for each

sample was 2 seconds with 2 accumulations, and 6th order polynomial fluorescence correction was applied. Spectra were normalized to the highest peak. Peaks were identified, and baseline corrections for relative peak intensity ratios were processed with Omnic 8 software. Comparison of relative peak intensity ratios aided in quantifying differences among spectra of atrazine and metabolites. Relative peak intensity ratios, along with Raman band positions, were used as a rubric for identifying the appearance of an intermediate(s) in effluent (Table 4:1 and Table 4:4).

To develop a calibration curve, atrazine was placed in sterile MS medium at varying concentrations (0-100 ppm). Five µL of atrazine in solution was air dried onto a quartz microscope slide and brought into focus with a 10x objective. Raman spectra were collected with a 50x objective and 0.90 NA, with a spot size of 0.6 µm. The exposure time for each sample was 30 seconds with 2 accumulations, and 6th order polynomial fluorescence correction applied.

Effluent Sample Preparation

Effluent exiting Channels 1 through 3 of the biofilm reactor was collected every 24 h for 10 d and stored at 4^{o}C until Raman analysis. For Raman analysis, 5 µL of effluent were air dried onto a quartz microscope slide, then samples were brought into focus using the 10x objective. Raman spectra were collected using a 50x objective, 30-60 seconds exposure time, and 2 accumulations; 6th order polynomial fluorescence correction was applied. Effluent exceeding 48 h was diluted with water to minimize background noise, increase signal to noise ratios, and allow for better viewing of individual particles from solutions. Influent of sterile MS media containing atrazine and MS media not containing atrazine entering into Channels 1 through 3 was analyzed similarly to effluent.

Biofilm Raman Analysis

Intact 5 and 10 d old biofilms, grown on quartz microscope slides, were mounted directly onto the microscope stage. Samples were brought into focus with the 10x objective, and spectra collected with the 100x objective.

Fixation for SEM

Atrazine was mounted onto an aluminum stub using silver colloidal paint and allowed to dry. Once dried, the sample was gold-palladium sputter coated to increase electron density prior to examination with the Hitachi S4800 SEM. Five day old biofilms grown under continuous flow of MS media containing 50 ppm atrazine were prepared for SEM imaging as described in the University of Iowa Central of Microscopy Research Facility protocol.[71] Briefly, intact biofilms on glass coverslips were fixed for 1 h with 2.5% glutaraldehyde in 0.1 M cacodylate buffer. Samples were rinsed in 0.1 M cacodylate buffer and further fixed with 1% osmium tetroxide in 0.2 M cacodylate buffer. Samples were then rinsed with distilled water and sequentially dried in ethanol. To prevent surface tension phenomena associated with ethanol evaporation, samples were immediately rinsed in hexamethyldisilazane (HMDS) to chemically dry specimens. Samples were allowed to air dry overnight in the fume hood, before being mounted onto aluminum stubs using silver colloidal paint, and gold-palladium sputter coated for 3 min. All chemicals used for fxation were handled with caution in the fume hood as described in the MSDS.

Images were collected with a Hitachi S4800 scanning electron microscope operating at 1.8 kV, 10 μA emission current, SE mix detector mode, under normal probe current, and ultrahigh resolution focus. Using the track ball to move the microscope stage, specimen on stubs were located in low magnification (10x) mode. Upon specimen location, high magnification (45,000x) was used to zoom in, and samples were brought into focus using

the fine/course adjustment knobs. Preparing for alignment, magnification was increased to 100,000x, and samples were brought into focus. The beam and aperture were aligned using the X/Y stigma align knobs on the control surface. X and Y astigmatisms were corrected with the X/Y stigma align knobs. Upon alignment, images were captured by increasing the magnification passed the desired magnification, and refocusing and adjusting the astigmatism. Magnification was then reduced to 45,0000x to capture the entire are of interest in slow scan speed. Ten day old biofilms grown for an additional 5 d without atrazine were examined in the same manner.

GC-MS Analysis

Atrazine degradation was quantified by gas chromatography (GC) coupled to mass spectrometry (MS). Effluent samples were taken every 24 hours for 10 days and processed using liquid-liquid extraction every 24 hours for 10 days with ethyl acetate. For liquid-liquid extraction, 0.5 mL of ethyl acetate was mixed with 1 mL of effluent. Atrazine, along with any other organic material that is more soluble in ethyl acetate than water, was separated out of the effluent into the organic phase containing ethyl acetate. After the solution settled into two liquid phases, the upper (organic) layer was transferred to a microcentrifuge tube. Dried extracts, collected after centrifugal evaporation, were resuspended in 1 mL of ethyl acetate and stored at -20^{o}C until GC-MS analysis. The extraction was repeated 3x by adding ethyl acetate to remaining effluent, mixing, and removing organic layers. Removal of all water content from samples prior to GC-MS analysis was very important; non-homogenous samples containing water are not permitted in this technique.

Shake Flasks Experiments

As a comparative analysis, shake flasks experiments were run in parallel to biofilm experiments to determine if microbes in a biofilm matrix degrades atrazine faster than free

floating planktonic cells. In 500 mL Erlenmeyer flasks, 45 mL MS media containing 50 ppm atrazine were inoculated with 5 mL of MS cell culture. Every 24 h for 10 d, 1 mL aliquots were removed to monitor cell growth and atrazine degradation. Shake flasks were maintained at 30^{o}C and 180 rpm. Glassware was autoclaved prior to use.

Results and Discussion

This study aims to model the degradation of atrazine in *Pseudomonas* sp. strain ADP biofilm using Raman spectroscopy, supported with GC-MS analysis and SEM imaging. Reference spectra of atrazine and metabolites (cyanuric acid and biuret) were first collected to identify characteristic peaks and peak ratios of interest for identifying the appearance and disappearance of intermediates in effluent. Unique Raman spectra of ADP biofilm and cells in suspension were observed and provided insight as to the biochemical changes occurring within the biofilm matrix. Peak ratios of ADP cells grown on rich media were compared to cells grown on nutrient-limited media containing atrazine as the sole nitrogen source. High resolution SEM images of atrazine and ADP biofilm matrix aided in the interpretation of Raman data collected. The degradation rate of atrazine with ADP was quantified using GC-MS analysis. Prior to experimentation, NMR analyses were performed on atrazine in stock to ensure samples were pure without any degradative products present.

Purity Test

Unaltered atrazine can maintain its integrity for years at room temperature without breaking down into subsequent products, as demonstrated by nuclear magnetic resonance spectroscopy. NMR collected of 7-year-old atrazine donated by Monsanto was compared to the National Institute of Advanced Industrial Science and Technology published NMR spectrum (Figure 4:1). The spectra were almost identical, showing what appeared to be two compounds at 3.4 ppm at a 7:3 ratio. The major peak at 1.20 ppm, corresponding to the

methyl groups in atrazine, was selected as the point of integration (9 hydrogen). Using 9 as the point of integration, from left to right, the subsequent areas are 0.52 (6.40 ppm), 1.21 (5.43 ppm), 1.01 (4.20 ppm), and 2.00 (3.44 ppm), respectively (Figure 4:2). At 3.4 and 4.2 ppm there should be only one quartet that integrates for 2 hydrogen and 1 hydrogen, respectively. Instead, there is an overlap of some sort, indicating the presence of impurities. CNMR also supports this finding. A pure sample of atrazine spectra should contain seven peaks representing the seven carbons present: three in the upper region and four in the lower area. Instead, on the right side, in the 20-60 ppm range, there appeared to be another sub peak neighboring a defined peak, which is indicative of the presence of another compound. To confirm that the older atrazine from Monsanto had not degraded, a spectrum was also collected of newly purchased atrazine from Cayman Chemicals, data not shown. All spectra were identical, thus implying that the second compound present in the NMR spectra may be a by-product resulting from synthesis. For the purposes of this research, solid state atrazine is simply referred to as pure atrazine, since the by-product is one from syntheses and not degradation.

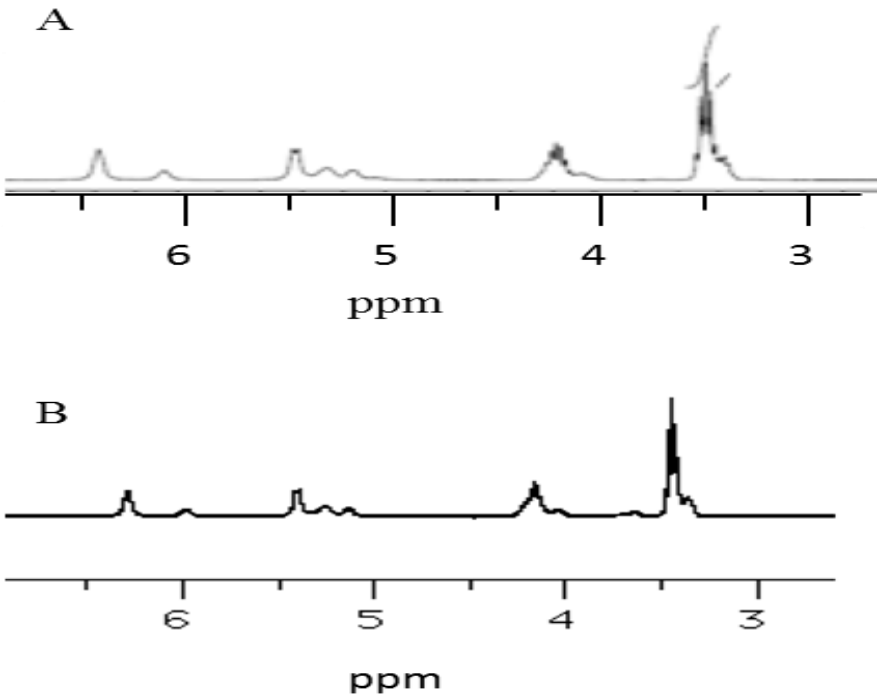

Figure 4:1: H-NMR of atrazine A) experimental spectra of aged atrazine compared to B) atrazine standard from the National Institute of Advanced Industrial Science and Technology. Spectra are identical, indicating that atrazine in its solid state without additives can retain its structure without decomposing for years.

Source: National Institute of Advanced Industrial Science and Technology Spectral Database for Organic Compounds SDBS. *http://riodb01.ibase.aist.go.jp/sdbs/cgi-bin/direct_frame_top.cgi* (accessed October 11, 2011).

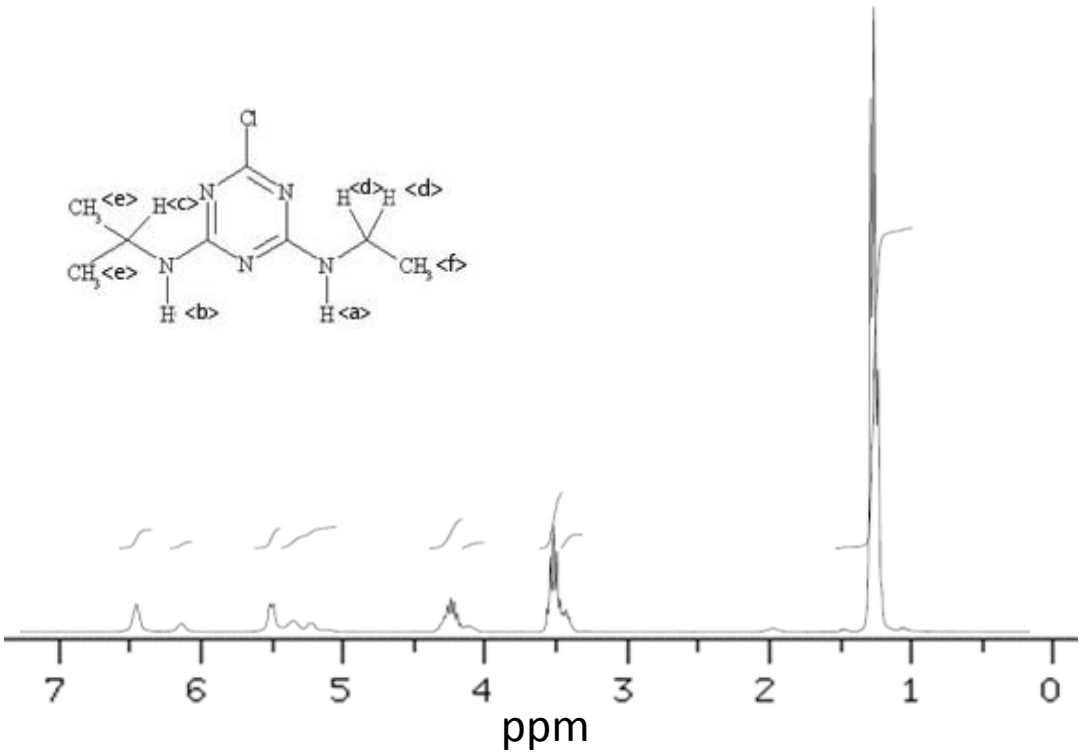

Assignment	Shift (ppm)	Integrated Area
A	6.40	0.52
B	5.43	1.21
C	4.20	1.01
D	3.44	2.00
E,F	1.20	9.17

Figure 4:2: H-NMR of atrazine, with peaks and integrated area assignments in table.

Raman Analysis of Atrazine and Intermediates

To track atrazine degradation by detection of intermediates with Raman spectroscopy, reference spectra of atrazine, cyanuric acid, and biuret were first collected. Pure solid powder granules of atrazine emit a Raman signal with 20 vibrational bands in the fingerprint region, 600-1800 cm^{-1} (Figure 4:3). The signal collected is comparable to the signal that has been previously published.[72] The averaged experimental Raman band assignments in Table 4:1 were all slightly higher, within 3-6 cm^{-1}, than published bands, with the exception of the NH and CH rocking at 1319 cm^{-1}). The experimental signal was collected with a 532 nm laser and 100x objective, while the published signal was collected with a 632.8 nm laser and 50x objective.

Raman spectra of atrazine, along with intermediates, cyanuric acid, and biuret revealed three distinct spectra in the fingerprint region (Figure 4:4). The peak assignments for atrazine using Varsanyi notation for six-membered rings to assign ring modes are presented in Table 4:1.[72] Prominent peaks in cyanuric acid were found at 705 and 1731 cm^{-1}, ring 4 (out-of-plane) bending vibration and C=O stretching vibrations of the keto form of cyanuric acid, respectively (Table 4:2).[73, 74] Free cyanuric acid in crystal form, as well as in neutral and acidic solutions, mainly exists as the keto (isocyanuric acid) form, while the enol form is most prevalent in alkali solution (Figure 4:5).[75] Raman bands unique to biuret, in comparison to cyanuric acid and atrazine, are 1511, 1627, and 1691 cm^{-1} (Table 4:3).

Relevant Raman bands for the detection of cyanuric acid and biuret in effluent samples are 707, 1513, 1691, and/or 1691 cm^{-1}. Peak ratio calculations of bands of interests were performed to identify values that signify the presence of atrazine and intermediates in effluent. If calculated peak ratio values of $\frac{I_{707}}{I_{1729}}$ and $\frac{I_{1513}}{I_{1691}}$ are approximately 0.93 and 1.38,

respectively, then cyanuric acid and/or biuret are/is present in samples (Table 4:4). Prominent peak ratios of $\frac{I_{649}}{I_{687}}$ and $\frac{I_{965}}{I_{1253}}$ signify the strong presence of atrazine in samples. By tracking the appearance of intermediates in the effluent, it is should be possible to use Raman spectroscopy to track atrazine degradation qualitatively.

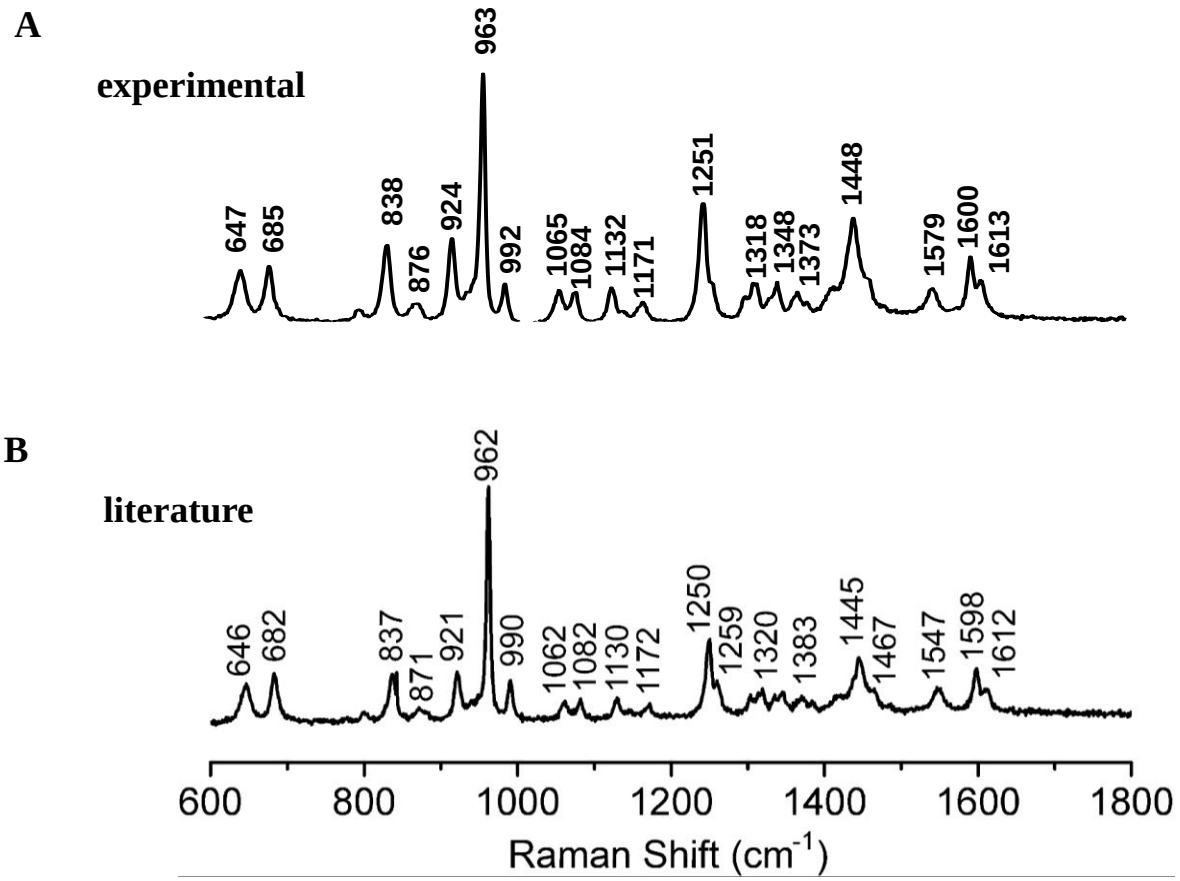

Figure 4:3: Uncorrected Raman spectra of solid atrazine A) obtained in lab and B)[61] published in literature. Peak identities of recorded spectra are comparable.

Source: Costa, J. C. S.; Ando, R. A.; Camargo, P. H. C.; Corio, P., Understanding the Effect of Adsorption Geometry over Substrate Selectivity in the Surface-Enhanced Raman Scattering Spectra of Simazine and Atrazine. *Journal of Physical Chemistry C* **2011**, 115, 4184.

Table 4:1: Raman band assignments for atrazine peaks in the fingerprint region (600-1800 cm^{-1}) in Varsanyi notation; twisting (τ), stretching (ν), wagging (ω), bending (δ), rocking (ρ), and ring mode (ϕ). The $\pm$ values represent the 95 % confidence levels (n=3).

Experimental	Published Measurements[72]	Band Assignments
649 ± 2	646	$_{\tau}(CH_2)$
687 ± 3	682	ϕ(6a)
840 ± 2	837	$_{\nu}$(C-C) + $_{\omega}(CH_3)$
877 ± 1	871	$_{\omega}(CH_3)$ + $_{\omega}(CH_2)$
925 ±3	921	$_{\tau}$ (CH_3)
965 ± 3	962	ϕ(12) and $_{\nu}$(C-C)
994 ± 2	990	ϕ(19b) + δ(NH) + $_{\nu}$(CN)
1065 ± 3	1062	$_{\nu}$(C-C) + $_{\omega}(CH_3)$ + δ(CH)
1083 ± 1	1082	$_{\nu}$(C-C) + $_{\omega}(CH_3)$
1135 ± 2	1130	$\delta(H_3C\text{-}C\text{-}CH_3)$ + $_{\omega}$(CH)
1173 ± 3	1172	ϕ(14) + δ(NH)
1253 ± 2	1250	δ(14) + $_{\tau}(CH_2)$
1319 ± 3	1320	δ(NH) + δ(CH)
1375 ± 1	1370	$\delta(CH_3)$ + δ(CH) + δ(NH)
1448 ± 3	1443	δ (CH_2) + $\delta(CH_3)$
1552 ± 3	1547	ϕ(8a) + δ(NH)
1602 ± 3	1598	ϕ(8b) + δ(NH)

Source: Costa, J. C. S.; Ando, R. A.; Camargo, P. H. C.; Corio, P., Understanding the Effect of Adsorption Geometry over Substrate Selectivity in the Surface-Enhanced Raman Scattering Spectra of Simazine and Atrazine. *Journal of Physical Chemistry C* **2011**, 115, 4184.

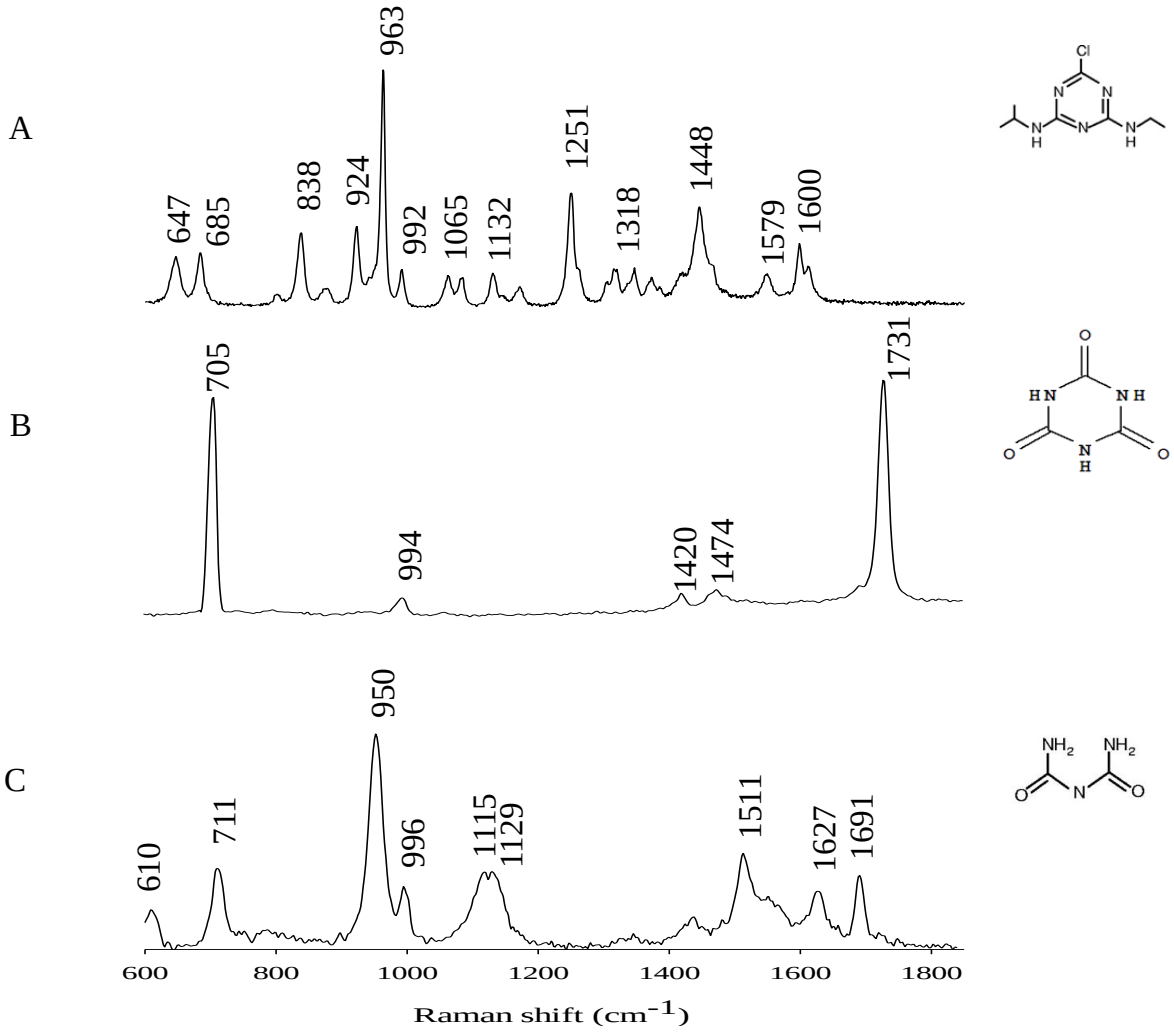

Figure 4:4: Raman spectra collected with 532 nm laser, 30 seconds accumulation, and 0.6 µm spot size of pure powder granules of A) atrazine, B) cyanuric acid, and C) biuret. Raman spectra shows differences in atrazine chemical fingerprint from intermediates, cyanuric acid and biuret. Notice peak 1731 cm^{-1} is unique to cyanuric acid and peaks 1511, 1627, and 1691 cm^{-1} are unique to biuret.

Table 4:2: Tentative Raman band assignments for cyanuric acid. The ± values represent the 95 % confidence levels (n=3).

Bands (cm^{-1})	Assignment[73]
707 ± 2	Out-of-plane bending ring
995 ± 1	Ring breathing mode I[75]
1421 ± 1	Weak ring stretching
1474 ± 3	Not assigned
1729 ± 2	C=O stretching of the keto form

Table 4:3: Tentative Raman band assignments for biuret. The ± values represent the 95 % confidence levels (n=3).

Bands (cm^{-1})	Assignment[73]
712 ± 2	CN stretching
951 ± 1	NH_2 deformation
998 ± 1	NH_2 deformation
1117 ± 7	Not assigned
1132 ± 4	Not assigned
1513 ± 5	Not assigned
1628 ± 1	NH_2 deformation[76]
1691 ± 2	C=O stretching

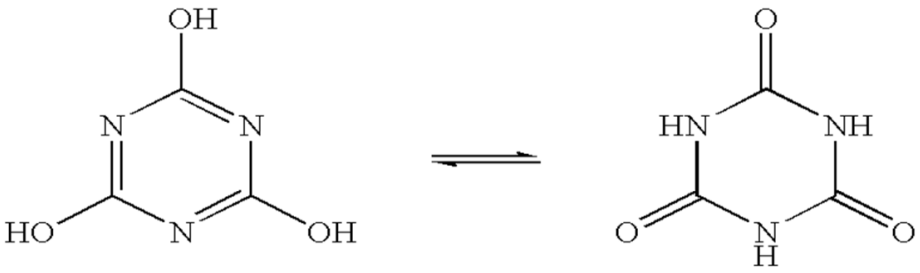

Cyanuric Acid
(enol form)

Isocyanuric Acid
(keto form)

Figure 4:5: The chemical structures of tautomers, cyanuric acid and isocyanuric acid. The keto-enol isomerization reaction is endothermic, indicating that the keto form is more stable than the enol form; not considering solvent effects.[75] Thus, the keto form of cyanuric acid is most prevalent in the solid crystalline state of cyanuric acid.

Table 4:4: Relevant peak intensity ratios to identify intermediate products in effluent. The ± values represent the 95 % confidence levels (n=3). UA represents unassigned group and ND is no peak detected.

	Atrazine		Cyanuric Acid		Biuret	
Band Assignments	Ratio	Value	Ratio	Value	Ratio	Value
$\tau(CH_2)/\ \phi$ (6a)	$\frac{I_{649}}{I_{687}}$	0.9 ± 0.1	$\frac{I_{649}}{I_{687}}$	ND	$\frac{I_{649}}{I_{687}}$	ND
ϕ (12) and ν(C-C)/ δ(14) + τ (CH_2)	$\frac{I_{965}}{I_{1253}}$	1.7 ± 0.6	$\frac{I_{965}}{I_{1253}}$	ND	$\frac{I_{965}}{I_{1253}}$	ND
ϕ (4) / ν(C=0)	$\frac{I_{707}}{I_{1729}}$	ND	$\frac{I_{707}}{I_{1729}}$	0.9 ± 0.04	$\frac{I_{707}}{I_{1729}}$	ND
UA/ν(C=0)	$\frac{I_{1513}}{I_{1691}}$	ND	$\frac{I_{1513}}{I_{1691}}$	ND	$\frac{I_{1513}}{I_{1691}}$	1.4 ± 0.2

Biofilm

Ten day old biofilms were grown under continuous flow conditions on standard glass microscope slides in a 4-channel Teflon drip reactor. MS media containing atrazine as the sole nitrogen source flowed through the reactor for the first 5 days, then MS media not containing any nitrogen source followed for an additional 5 d. On Days 5 and 10 bacteria were still viable, as established on nutrient-rich agar plates. SEM images showed web-like EPS structures on Day 5 (Figure 4:6a,b). The architecture of the biofilm was made of microstructures with open channels, which is consistent with the definition of a mature biofilm.[57] Elongated rod-shaped cells of approximately 1.00-2.00 µm in length could be found embedded in the matrix surrounded with particles. Atrazine particles appeared to adhere more to the EPS matrix rather than the cell. Pure solid-state atrazine on its own appeared as 1-4 µm crystalline structures (Figure 4:6c). However, particles in the biofilm matrix, resulting from the continuous flow of atrazine suspended in MS media, were spherical particles.

By Day 10, it appeared that the biofilm was at the late stage of existence, Stage 5. As discussed in Chapter 1, biofilm development occurs in 5 stages.[15] At the final stage, Stage 5, the sloughing away of cells occurs, resulting in the biofilm breakdown.[15] Fewer cells were detected in the SEM image of the 10 day biofilm (Figure 4:7) compared to the 5 day biofilm (Figure 4:6a,b). The EPS matrix was no longer visible in the 10 day biofilm and signs of an intact architecture were not present. This phenomenon may have occurred for two reasons: 1) the age of the biofilm or 2) the removal of atrazine from the matrix. Over time, due to environmental factors and bacteria age, all biofilms reach Stage 5 where old architecture breaks down as cells slough away. Shear stress and nutrient limitation due to lack of permeability through the matrix are some natural environmental stressors that

encourage breakdown.

Because atrazine was not present in the medium on Days 6-10, it is most likely that the absence of atrazine facilitated cellular dispersion. Not only does atrazine serve as a nutrient source, but also as an additional substrata that increased surface adhesion for cells. It is plausible that when atrazine was removed from the MS media under continuous flow conditions, that some of the particles already caught in the matrix began to wash away, taking along the EPS structure to which it was adhered, thus causing the architectural breakdown of the biofilm. If the biofilm matrix has a larger capacity to immobilize atrazine particles than to degrade particles, then that would explain why minimal cell development occurred even though there was evidently still atrazine present in the matrix (Figure 4:7). The degradation capacity of the biofilm matrix is further explored in the effluent and GC-MS analysis sections of this chapter.

A

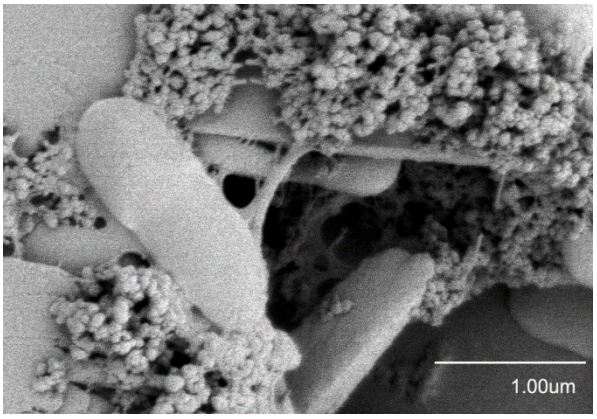

B

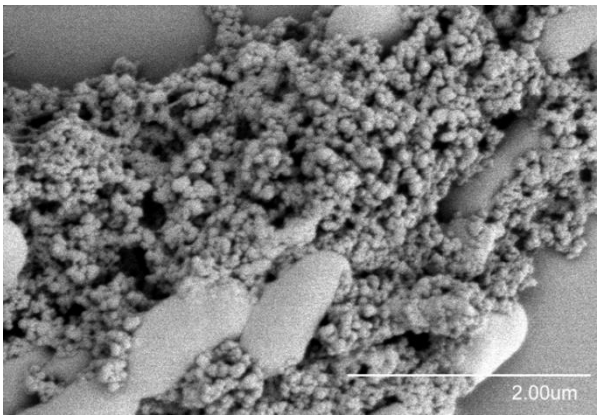

C

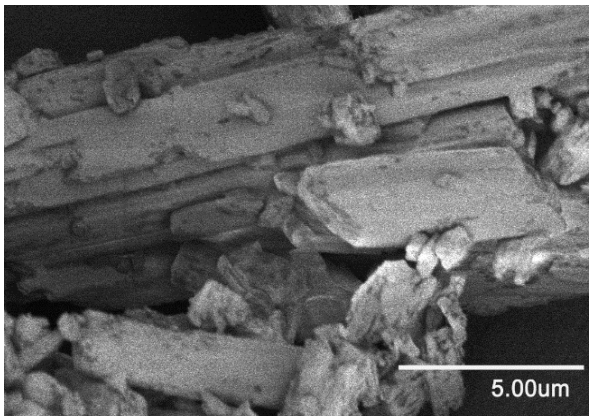

Figure 4:6: SEM image of A), B) 5-day old biofilm grown on atrazine enriched medium, and C) pure solid-state atrazine not contained in medium. The atrazine particles adhered to web-like architecture between cells in images A and B. Atrazine goes from crystalline structures in C) to spherical structures in the biofilm matrix.

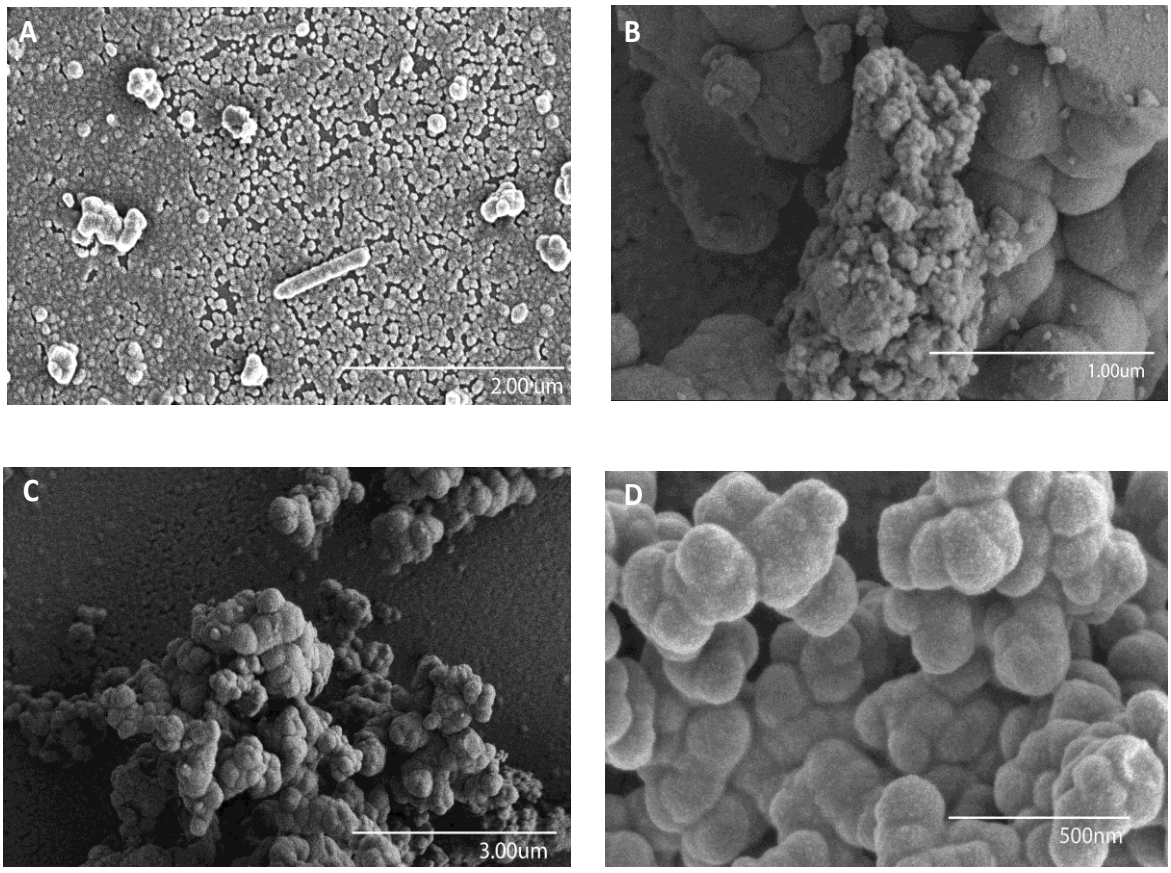

Figure 4:7: SEM images of 10 day old biofilm grown on minimal salt medium containing 50 ppm atrazine for the first 5 days and minimal salt medium without atrazine on days 6-10. There is minimal cell detection and no signs of the extracellular matrix. Image shows A) single cell surrounded by debris, B) agglomeration in the biofilm matrix, C) particulates in the matrix, and D) increased magnification of agglomerate in search of EPS matrix.

Raman Analysis of Biofilms

In Chapter 2, it was established that Raman spectroscopy can be used to differentiate free cells from cells in biofilms. Here, we demonstrate that Raman spectroscopy can also be used to distinguish cells of the same species grown under different nutrient conditions. The Raman spectra of ADP 5 day biofilm grown on nutrient limited medium containing atrazine, 10 day biofilm grown with and without atrazine, and 5 day biofilm grown on nutrient rich, LB medium, revealed three distinct chemical fingerprints (Figure 4:8). In the 5 day biofilm grown on MS medium containing atrazine, similar cellular components as detected in the 5 day biofilm grown with LB medium were detected (Figure 4:8 a,b). Similarly, nucleic acids were identified at 752 and 786 cm^{-1}, carbohydrates at 1125 cm^{-1}, amide III at 1242 and 1311 cm^{-1}, adenine and guanine at 1590 and amide I at 1660 cm^{-1}.

Unique to the 5 day MS biofilm were the detection of tyrosine at 821 cm^{-1} and change in the phenylalanine band width at 999 cm^{-1}. The phenylalanine band in bacteria arising from amino acids at approximately 1000 $cm^{-1} \pm 5$ cm^{-1} is usually detected as an intense narrow peak. There are several reasons which may account for changes in Raman band widths, such as conformational changes, molecular interaction with external factors, and a change in hydrogen bonding.[62] Both the 5-day biofilm grown on LB and the 5-day biofilm grown on MS containing atrazine were prepared in the same manner for Raman analysis. Temperatures and pressures were the same, and the same laser power and spot size were applied for data acquisition. Phenylalanine is known to be less susceptible to conformational changes; therefore, it is believed that neighboring reactions occurring from a change in medium and the presence of a nearby additional amino acid and tyrosine, which was not detected in the biofilm grown on LB, are the reasons why the Raman band width at 999 cm^{-1} increased.

Looking at the relative peak intensity ratios, it is clear that the relative distribution of molecular components are different between both 5 day MS biofilm and 5 day LB biofilm. Even though both specimens were classified as mature biofilms on day 5 containing intact EPS, samples were maintained under different growth conditions. Changes in the nitrogen source, carbon source, salts, and vitamins will result in changes in organisms' assimilation; thus stimulating changes in the more complex components formed within the organism, as evident in the Raman spectra.

The 10 day biofilm, which was grown identically to the 5 day MS biofilm for the first 5 days, emitted a very different Raman spectrum by comparison (Figure 4:8b,c). Unlike the 5 day MS and 5 day LB biofilms, the 10 day MS biofilm was not classified as a mature biofilm. Intact extracellular architecture with open channels was not visible by SEM imaging. Roughly three Raman bands were detected at 788, 1126, and 1513 cm^{-1}. As in the case of the 5-day MS and 5-day LB biofilms, nucleic acids and carbohydrates were detected at 788 and 1126 cm^{-1} respectively. However, an unassigned peak at 1513 cm^{-1} was also detected. In addition, characteristic amide I and nucleic acids (A,G) peaks, ~ 1590 and 1660 cm^{-1}, went unmeasurable. Comparing data to the Raman band assignments of cellular components (Table 2:1), there is no direct evidence linking the 1513 cm^{-1} band to a specific cellular component. Therefore, it is believed that some intermediate associated with atrazine degradation, most likely biuret, resulted in the 1513 cm^{-1} shift (Figure 4:5).

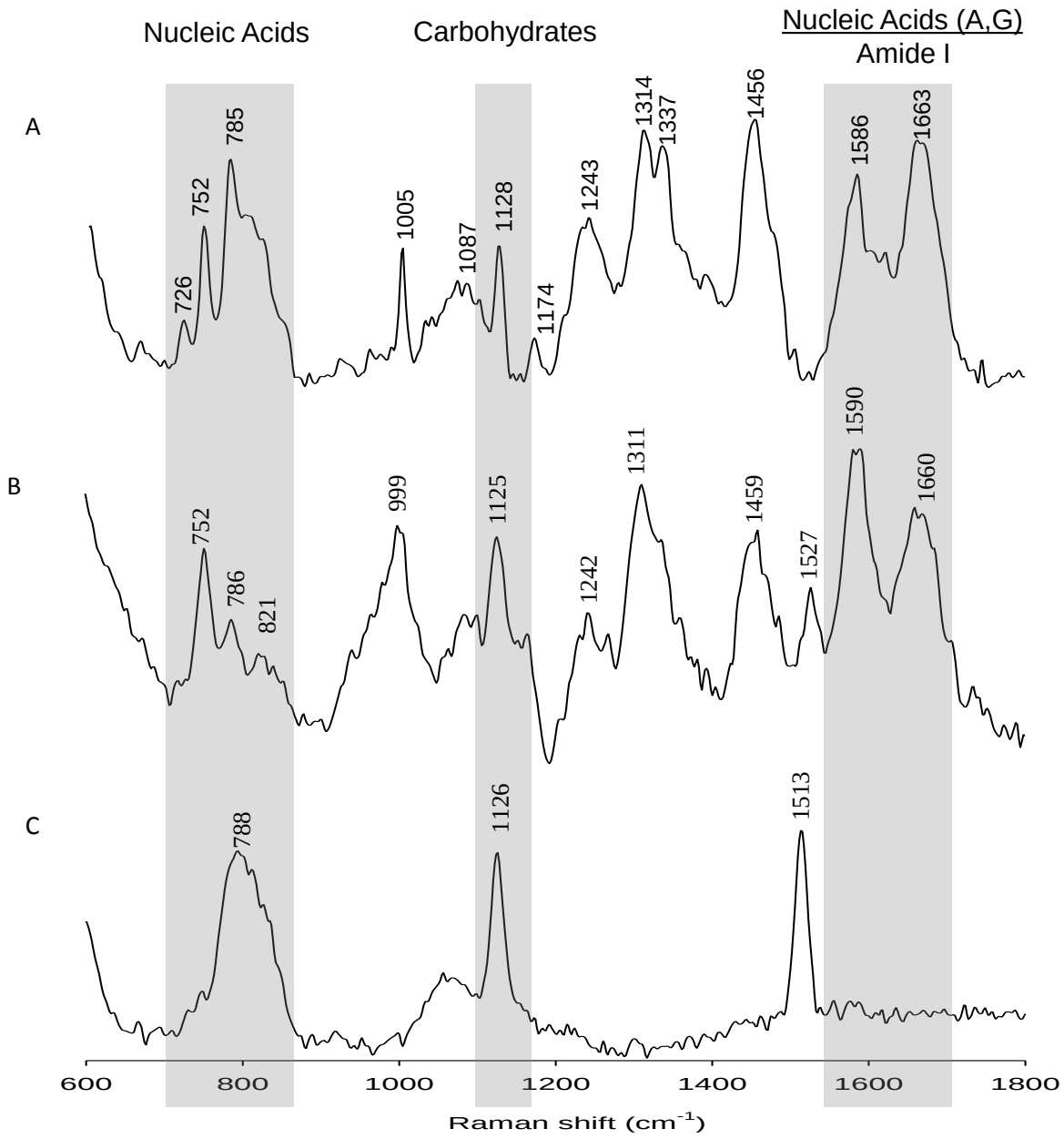

Figure 4:8: Raman spectrum collected with 532 nm laser, 60 seconds accumulation, and 0.6 µm spot size of 5-day *Pseudomonas* sp. strain ADP biofilm grown on A) LB medium and B) MS medium containing atrazine, C) Raman spectrum of 10 day ADP biofilm grown on MS medium.

Raman Analysis of EPS Fractions

From SEM imaging, it was apparent that atrazine was more adsorbent to EPS than to cells contained in the biofilm matrix (Figure 4:6). To further evaluate the extent of atrazine's affinity to EPS, EPS were extracted from 10 d biofilm to determine which fraction atrazine had the strongest affinity for. After 5 days of flow with MS media containing 50 ppm atrazine, followed by an additional 5 days of flow with MS media not containing atrazine, atrazine appeared to be present in all three EPS fractions (Figure 4:9a,b,c,e). Without direct comparison of relative peak intensity ratios among the three spectra it is difficult to determine at this time, precisely, which fraction has the highest atrazine content. However, of the three fractions, SEPS was the only product that showed signs of atrazine characteristic peak, 963 cm^{-1}. The prominent Raman band in atrazine (triazine ring mode 12 and C-C stretching), 963 cm^{-1}, shifted to 989 cm^{-1} and broadened in SEPS. The increase in the peak ratio $\frac{I_{991}}{I_{923}}$ in LB-EPS relative to atrazine and disappearance of 963 cm^{-1} means the triazine ring is not as dominant and some intermediate products may be present in LB-EPS. In the EPS layer closest to the cell, TB-EPS, atrazine's prominent peak, 963 cm^{-1} was not detected and more cellular components were detected in comparison to SEPS and LB-EPS. The COO- moiety was detected at 1418 cm^{-1} and adenine at 1322 cm^{-1}. The peak ratio $\frac{I_{1129}}{I_{1627}}$ in TB-EPS is comparable to biuret. Atrazine was not detected in the pellets remaining after EPS extraction (Figure 4:9d,e). Separate to the unassigned peak at 602 cm^{-1}, the Raman spectrum of the cell pellets bared similarities of a typical spectrum of a cell. Combining these results, atrazine appeared to be present only in EPS fractions, with signs of intermediates being present in LB-EPS and TB-EPS.

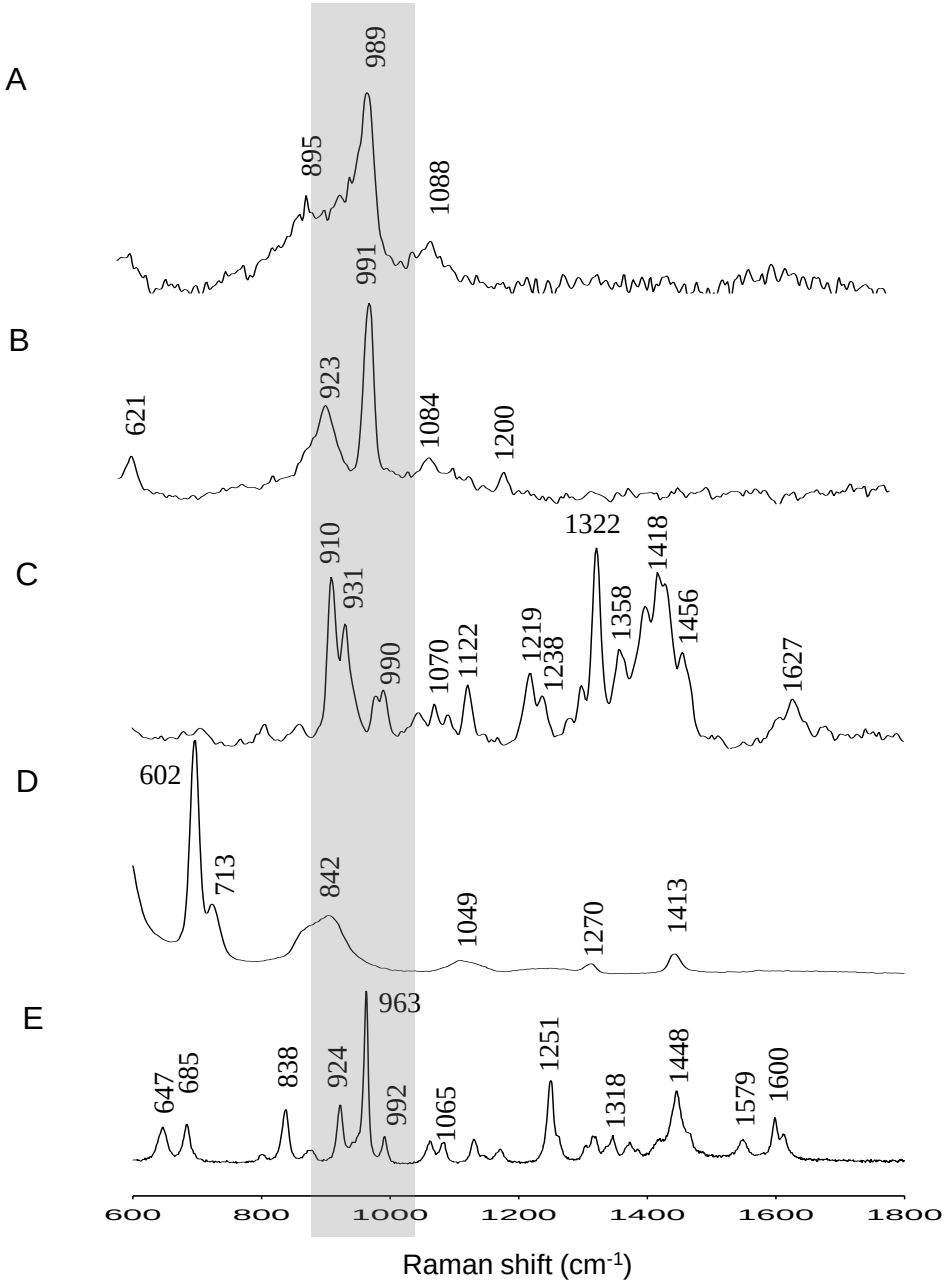

Figure 4:9: Normalized Raman spectra collected with 532 nm laser and 0.6 µm spot size of microbial products from a 10-day *Pseudomonas* sp. strain ADP biofilm grown on minimal salt medium A) soluble EPS, B) lightly bound EPS, C) tightly bound EPS, D) pellets, and E) atrazine.

Raman Analysis of Free Cells

Similar to the LB biofilm and MS biofilm, the Raman spectra of ADP cells grown on MS media containing 50 ppm atrazine and ADP cells grown on LB media, generated two distinct spectra (Figure 4:10). This confirms that Raman spectroscopy is sensitive enough to detect phenotypic differences amongst cells of the same species under different induced metabolic pathways. Cellular components were distinguishable in both spectra, but the relative distribution of components varied (Figure 4:11). In theory, the Raman peak intensity is directly proportional to the concentration, within a limited range, of the represented bond, in our case cellular components. Comparing the relative intensity ratio of phenylalanine to carbohydrate, $\frac{I_{1002}}{I_{1127}}$, ADP on MS has a peak ratio 12 % higher than ADP grown on LB media (Table 4:5). The lipids to amide III ratio, $\frac{I_{1440}}{I_{1304}}$, is 88% higher in the ADP on MS spectra and the amide I to nucleic acids (A,G) ratio, $\frac{I_{1663}}{I_{1582}}$, is 62 % higher in the ADP on MS spectra. Carbonyl stretching was detected at 1742 cm^{-1} in only the ADP on MS media spectra. Adenine content at 747 cm^{-1} was only detected in the ADP cell grown on LB. Both samples were prepared the same way for Raman analysis. Overnight suspended cells were washed 3x to remove media, resuspended in water, and air dried onto a quartz microscope slide for Raman analysis. Hence differences observed between spectra resulted from biochemical differences with the cell. In Chapter 2, we showed how the physiological state of cells can affect the Raman spectra. Here we have demonstrated how altered metabolic processes within bacteria can produce different Raman spectra.

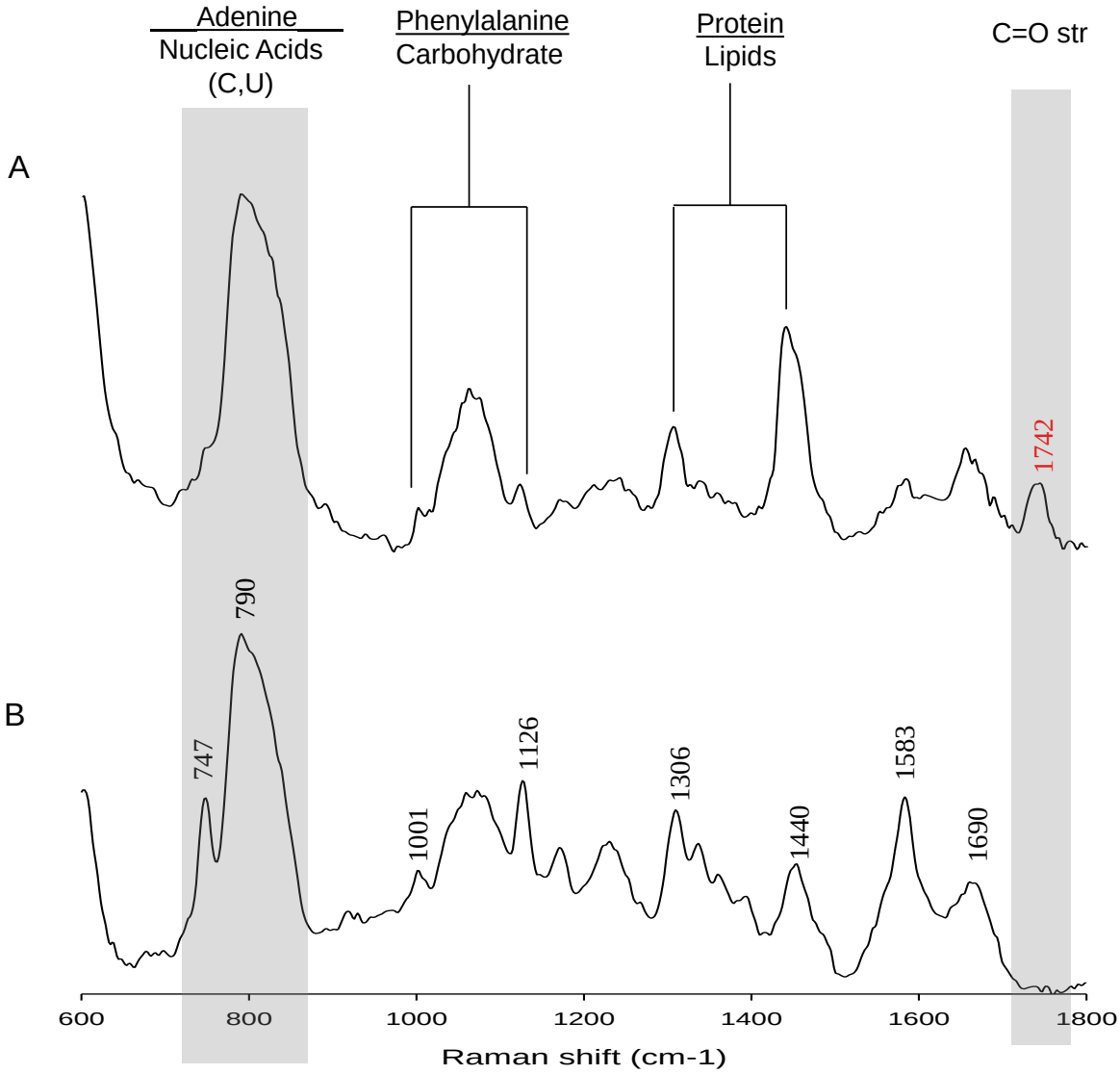

Figure 4:10: Normalized Raman spectra of *Pseudomonas* sp. strain ADP A) cultivated on minimal salt medium containing 50 ppm atrazine and B) cultivated on Luria-Bertani medium. Spectra were collected with 532 nm laser, 60 second exposure, 2 accumulations, and 0.6 µm spot size.

Table 4:5: Comparison of relative peak intensity ratios of selected molecular components of *Pseudomonas* sp. strain ADP grown on minimal salt (MS) medium containing 50 ppm atrazine to cells grown on Luria-Bertani (LB) medium. The ± values represent the 95% confidence levels (n=3).

	ADP cultured on MS		ADP cultured on LB	
Band Assignments	Ratio	Value	Ratio	Value
Phenylalanine/Carbohydrates	$\frac{I_{1002}}{I_{1127}}$	0.8 ± 0.2	$\frac{I_{1002}}{I_{1127}}$	0.7 ± 0.3
Lipids (CH_2) /Amide III	$\frac{I_{1440}}{I_{1304}}$	1.9 ± 0.1	$\frac{I_{1448}}{I_{1308}}$	1.0 ± 0.3
Amide I/Nucleic acids (A,G)	$\frac{I_{1663}}{I_{1582}}$	1.9 ± 0.2	$\frac{I_{1663}}{I_{1582}}$	0.9 ± 0.3

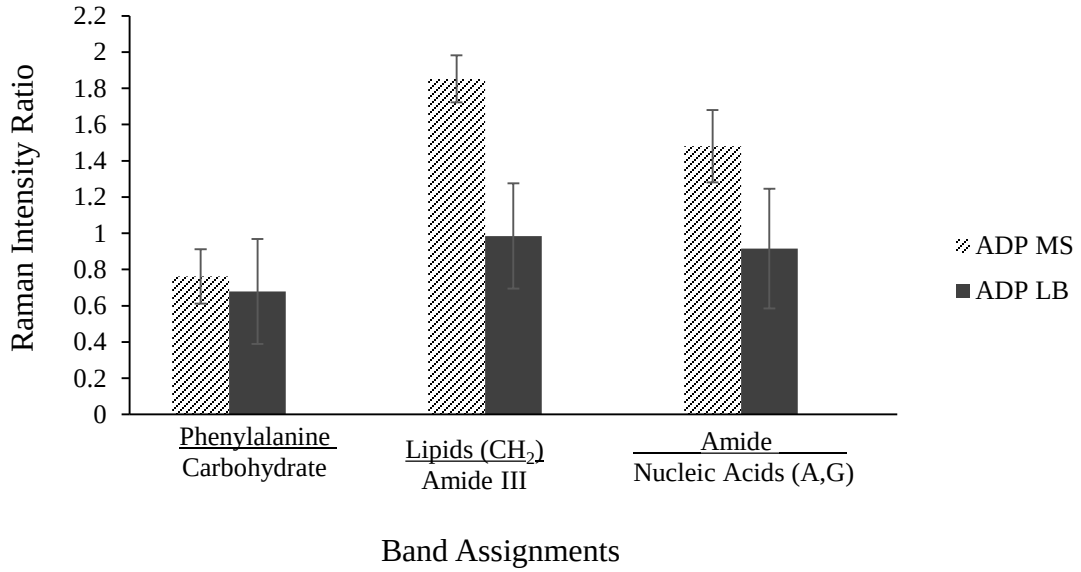

Figure 4:11: Relative Raman peak intensity ratios of ADP grown on minimal salt (MS) medium containing 50 ppm compared to ADP grown on nutrient rich medium, Luria-Bertani (LB). The error bars represent 95% confidence intervals.

Effluent Analysis

To track atrazine degradation qualitatively by detection of intermediates, Raman spectra were collected of effluent leaving the biofilm reactor every 24 h for 10 d. For the first 5 d, MS media containing 50 ppm atrazine flowed through the reactor at 0.8 mL/min. Atrazine was used as the sole nitrogen source in MS media to ensure bacterial use of atrazine as a nutrient source for survival and growth. Atrazine, in the presence of other nitrogen sources that support fast growth, will not induce the degradation pathway of interest in Figure 1:3.[30] Due to the fully oxidized state of the s-triazine ring carbon atoms, atrazine, along with hydroxyatrazine and cyanuric acid, cannot be used as carbon sources.[30]

As the biofilm grew in each chamber, some atrazine was used for assimilation, some atrazine was caught in the EPS matrix as seen in Figure 4:6, and some atrazine flowed out of the reactor. Stoichiometric ratios for the atrazine degradation pathway of atrazine to biuret are 1:1:1:1. The reaction continues to the final products of 2 moles of ammonia and 2 moles of carbon dioxide.

The stacked Raman spectra of influent entering the reactor and 24-110 h effluent leaving the reactor, showed the reduction in atrazine content leaving the bioreactor as a function of time (Figure 4:12). Initially, intense peaks were detected at 963-996 cm^{-1} on Days 0-3, but over time those peaks disappeared. The Raman spectrum of influent entering the biofilm reactor at t=0 is comparable to the Raman spectrum of atrazine. Having most notably Raman bands at 646, 684, 838, 23, 963, 992, 1254, 1550, and 1612 cm^{-1}; it is clear that atrazine is present in the matrix. After 24 h of flow through the biofilm reactor containing ADP cells, the Raman spectra of the effluent showed a strong band at 975 cm^{-1}, and the CH_2 twisting and triazine ring mode (6a) at 646 and 684 cm^{-1} were no longer visible. Prominent peaks appeared at 1071 and 1123 cm^{-1}, which were only detected in trace amounts

in the influent. The intense peak that was originally detected at 950 cm^{-1} in the influent, appeared to have shifted to 975 cm^{-1} and broadened in the 24 h effluent spectra. The shift and increase in peak width is indicative of structural disorder and change in the microevironment.[62] Since all samples were handled in the same manner for Raman analysis, these spectral differences are due to chemical changes.

On Day 2 (48 h), peaks 923 and 963 are no longer detected; the prominent peak is at 996 cm^{-1}. At 72 h, peak 996 cm^{-1} remains prominent, the relative intensity of 795 to 995 cm^{-1} begins to increase, and amide II is detected at 1522 cm^{-1}. At 96 h, the relative intensity of 793 to 992 cm^{-1} continued to increase. Then on Day 5 (120 h) the 992 cm^{-1} band was no longer detected. Combining these results, it appears as though the triazine ring opened, and the NH_2 deformation and C-N stretching became more prominent as time increased. Eventually characteristic bands of atrazine, 963 and 1254 cm^{-1}, became less visible due to decrease in atrazine content leaving the bioreactor as the biofilm matured.

The Raman spectrum of atrazine contains peaks at 924 (CH_3 twisting), 963 (ring mode 12 and C-C stretching), and 992 cm^{-1} (ring mode 19b, NH deformation and C-N stretching) (Table 4:1). Biuret does not contain the triazine ring, but also has peaks similar to atrazine at 951 and 998 cm^{-1}, resulting from NH_2 deformation. Thus, examination of the effluent spectrum leads one to assume that the triazine ring opened, with the loss of the 923 and 963 cm^{-1} peaks and an increase in the relative intensity of the 992 cm^{-1} band, which is also characteristic of NH_2 deformation. This assumption could not be substantiated because the chemical maker established early in the research to signal the detection of biuret, $\frac{I_{1513}}{I_{1691}}$, was not seen. However, it is clear that the atrazine content in the effluent did decrease over time. The entering influent contained peaks at 992, 963, and 992 cm^{-1}, similar to atrazine;

however, over time as the influent passed through the reactor as a nutrient source and an additional substrata to grow biofilm, the spectra from the exiting effluent lost the 923, 963, and 992 cm^{-1} peaks. Using the simultaneous appearance of 707 and 1729 cm^{-1} Raman bands as a chemical marker, cyanuric acid was never confirmed as an intermediate product in the effluent. Since the metabolic products are intermediates in the path to complete mineralization, they may be transient in the reactor.

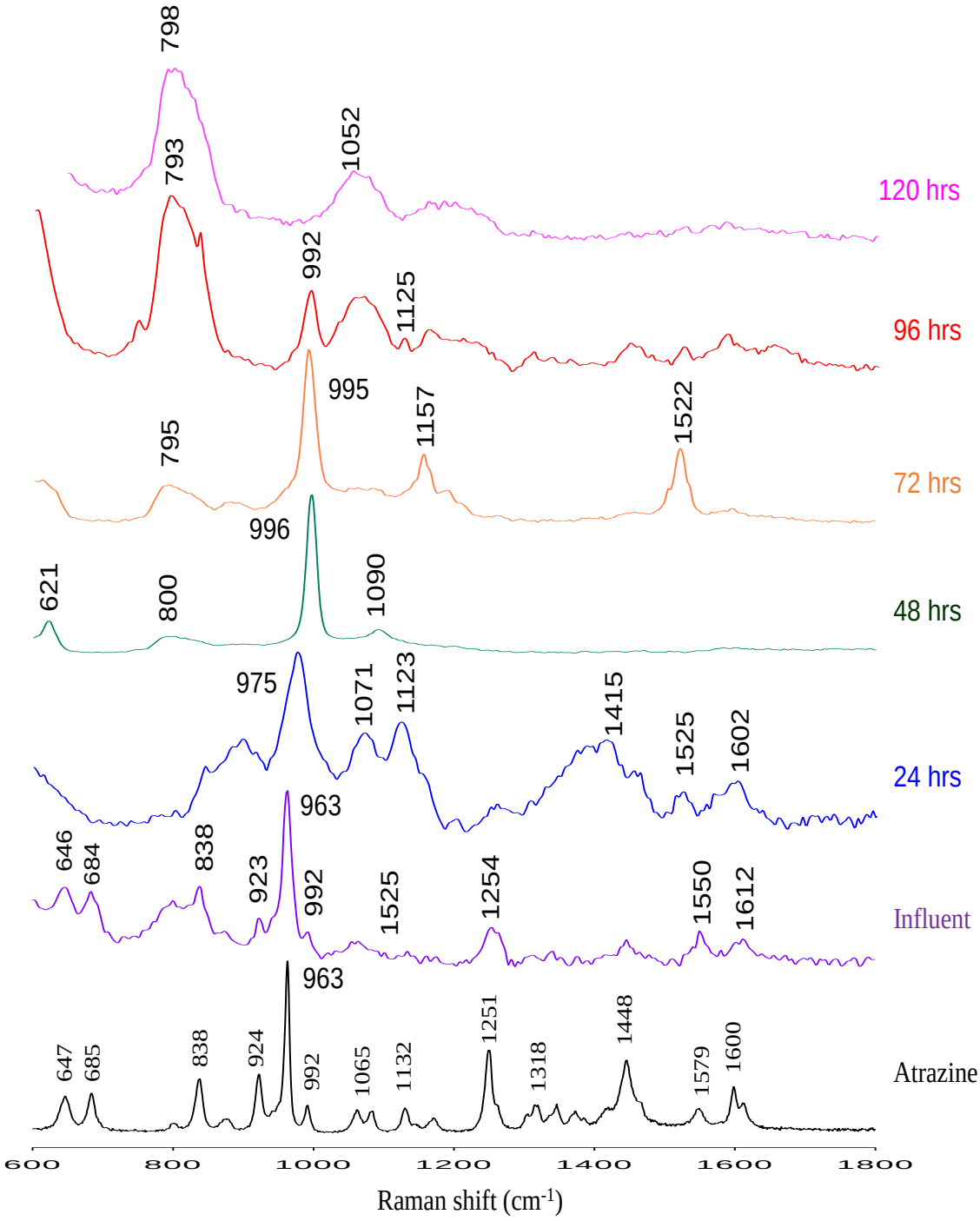

Figure 4:12: Stacked normalized Raman spectra of effluent over 5 days. Effluent was collected from a drip flow biofilm reactor with minimal salt medium containing 50 ppm atrazine flowing (0.8 mL/min) over *Pseudomonas* sp. strain ADP as a nutrient source to bacteria.

GC-MS Analysis

In efforts to determine the rate of accumulation and rate of degradation of atrazine in an ADP biofilm, GC-MS analysis was performed every 24 h on the effluent leaving the bioreactor for 10 d. The degradation rate was compared to 10 d analysis of suspended cells in MS media containing 50 ppm atrazine. Atrazine content of both the effluent leaving the bioreactor and shake flask media reduced to 0 ppm within 10 d (Figure 4:13). The calibration curve used to quantify atrazine concentration in solution is in Appendix E.

Biorector Effluent

Sterile MS media containing 50 ppm atrazine was fed into rectangular chambers (10 cm x 2.5 cm x 2 cm) containing microscope slides (7.5 cm x 2.5 cm x 0.1 cm) for biofilm growth, for the first 5 d (120 h). Immediately following day 5, sterile media without atrazine flowed through the reactor day 5-10. Media was pumped at a flow rate of 0.8 mL/min. Referring to Figure 4:14a, an immediate decrease in atrazine content was detected on day 1-2. However, atrazine concentration increased on day 2-5; then began to decrease again on day 5-7. Based on results, it appears as though 1 or 2 events are occurring or a combination of both. 1) After the initial cellular uptake of atrazine (day 1-2), cells begin to utilize more metabolically favorable intermediate products for nitrogen assimilation than atrazine (day 2-5). Other nitrogen sources that support fast growth are known to inhibit atrazine degradation by ADP.[30] When intermediate products are no longer available, cells revert back to utilizing atrazine as a nutrient source (day 5-7). 2) By day two, the EPS matrix was becoming saturated with atrazine and less incoming atrazine particles adhered to the matrix, resulting in increased atrazine concentration leaving the bioreactor (day 2-5). When atrazine was removed from the MS media flowing through the reactor, loosely attached atrazine particles washed away (day 5-6) as the system approached steady state, $C_o=C_t$ (day 7-10). The

Concentration entering the reactor was C_o, and concentration leaving the rector at specific time was C_t.

Shake Flask Broth

Erlenmeyer shake flasks, containing 50 mL of sterile MS media with 50 ppm atrazine were inoculated with 10% ADP cells. Atrazine concentrations were measured every 24 h for 8 d. The rate of degradation on day 1-2 was slower in shake flasks than in the bioreactor (Figure 4:13). However, the initial cellular uptake of atrazine on day 0-1, assuming 100% extraction, was 28% higher in shake flasks compared to the effluent. Atrazine degradation on day 1-8 was slow, but steady; no increase in atrazine was observed as with the effluent on day 2-5. Due to the sharp initial decrease of atrazine content on day 0-1, then slow steady decay on day 1-8; it is apparent that cells are utilizing another more favorable intermediate product generated from atrazine mineralization. Unlike the biofilm matrix, there is minimal sticky matrix for atrazine particles to adhere to in shake flasks experiments.

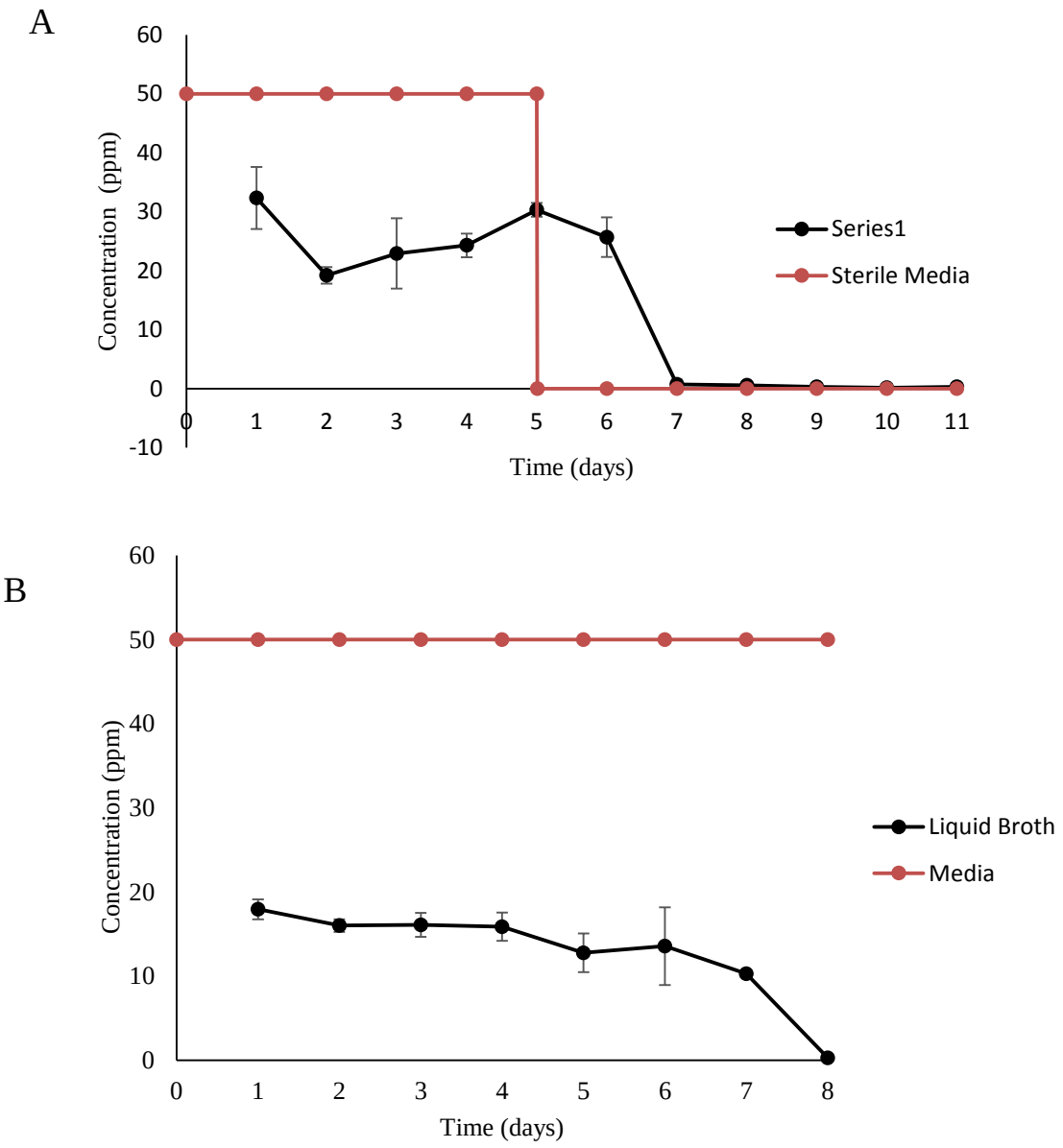

Figure 4:13: A) Concentration of atrazine in effluent leaving drip biofilm reactor over 10 d at a continuous flow rate (0.8 mL/min) of sterile minimal salt media containing 50 ppm atrazine initially for 5 d and an additional 5 d without atrazine in the media. B) Concentration of atrazine in shake flask over 8 d, which was initially inoculated with 50 ppm atrazine in sterile minimal salt medium. The error bars represent 95% confidence intervals (n=3).

Conclusion

Pseudomonas sp. strain ADP proved to be effective at degrading atrazine as determined by Raman and GC-MS analyses. Not only did cells mineralize atrazine as a nitrogen source, but the extracellular matrix functioned as an immobilizing agent encouraging the adsorption of atrazine particles under laminar flow conditions. Atrazine provided an additional substrata for cellular adhesion, which encouraged the maintenance of the biofilm's architecture. When atrazine was removed from the liquid media, the infrastructure of the biofilm matrix showed visible degeneration by day 10 under 5 d of flow without atrazine. These observations have positive implications in bioremediation applications in the removal of atrazine from liquid aquifers.

Of the three EPS fractions, atrazine appears to have the strongest affinity for SEPS. By Raman analysis, the biochemistry of cells grown on MS media containing atrazine was notably different from cells grown with nutrient-rich media. This phenomena is expected, because upon the induction of the atrazine degradation pathway, genes atzABCDEF are expressed at concurrent and variant times. Under nutrient rich conditions atzABCDEF are basally expressed. Further analysis of atz gene expression is evaluated in Chapter 5.

CHAPTER 5: IDENTIFYING ATRAZINE CATABOLISM GENES ATZA AND ATZD IN *PSEUDOMONAS* SP. STRAIN ADP BY *IN SITU* REVERSE TRANSCRIPTION

Introduction

The gram-negative bacterium, *Pseudomonas* sp. strain ADP, was isolated from a herbicide spill site in 1995 and found to have the ability to completely mineralize atrazine to ammonia and carbon dioxide through a series of hydrolytic reactions.[27, 70] The degradation pathway begins with the hydrolytic dechlorination of atrazine, proceeds with two amidohydrolytic reactions to cyanuric acid, and ends with three additional hydrolases to carbon dioxide and ammonia (Figure 5:1b).[29, 50] The six-step degradation pathway is encoded by the atzABCDEF genes located on a 108 kb transmissible catabolic plasmid, pADP-1 (Figure 5:1a).[29, 50] Genes atzA, atzB, and atzC exist on individual transcriptional units occupying nearly half of the plasmid sequence in the 47 kb region.[31] These units are flanked by transposable elements and insertion sequences (IS), making that portion of the plasmid unstable.[29] Transposable elements, in addition to IS elements, facilitate movement of the already mobile atzABC genes, thus resulting in the spontaneous loss of atzA, atzB, or atzC or deletion of all three genes from the plasmid. Genes atzA, atzB, and atzC encode enzymes AtzA, AtzB, and AtzC, which catalyze the catabolic removal of chlorine and aminoalkyl side chains of atrazine. However, with the increased mobility of these genes, ADP often loses its ability to degrade atrazine, resulting in the frequent appearance of Atr- derivatives (cells that can no longer metabolize atrazine).[30] ADP mutants that are unable to degrade cyanuric acid, Cya- , also sometimes arise from the spontaneous loss of the entire pADP-1 plasmid.

Genes atzDEF, on the other hand, are organized in an operon under a LysR-type transcriptional regulator, atzR (Figure 5:1a). These genes encode for the enzymes, AtzDEF,

which catalyze the hydrolysis of cyanuric acid to ammonia and carbon dioxide. The atzR-atzDEF cluster is physically separated from the unstable 47 kb region, containing atzABC, by two large gene clusters that include functions for replication, segregation and conjugational transfer of pADP-1. Genes atzD, atzE, and atzF do not share the genetic instability of atzABC. There is no evidence supporting spontaneous loss of atzDEF or associating these genes with the loss of the pADP-1 plasmid.[30]

For the purposes of this research, experiments were designed to probe for plasmid retention and loss in ADP cells by probing for atzA and atzD gene expression by *in situ* reverse transcription (ISRT). Since genes atzDEF exist on one operon and are genetically stable, the absence of atzD gene expression may be indicative of loss of the pADP-1 plasmid, which can be confirmed by PCR analysis. To ensure the degradation pathway has been induced, it is desirable to probe for atzA gene expression in response to atrazine.

The degradation pathway, which is induced by the presence of atrazine as the sole nitrogen source, has been extensively studied. Martinez et al. completed the entire sequencing and annotation of pADP-1.[29] Prior to her work, many thought genes involved in cyanuric acid degradation (genes atzDEF) were not located on the pADP-1 plasmid.[33] Govantes et al. explored ADP genetic response to nitrogen availability.[30] Sadowsky and Wackett, cloned and sequenced atzABC and over-expressed these proteins in *E.coli*.[69] Denvers et al. studied the expression of atz genes in ADP by real-time reverse transcription-PCR and found that atzABCDE genes significantly increased in the presence of atrazine.[50] In this work, atz gene expression in ADP cells was explored using ISRT.

ISRT can be used to determine when genes for atrazine degradation are converted to RNA and then to protein.[77] For ISRT, only one primer is needed to sufficiently incorporate labeled nucleotides into cDNA by hybridizing with the target mRNA. The primer is extended

with reverse transcriptase in the presence of fluorescently-labeled nucleotides.[77] In this research, two primers that specifically bind to genes encoding atrazine chlorohydrolase (atzA) and cyanuric acid aminohydrolase (atzD) are being applied to facilitate the analysis of pADP-1 retention or loss. This approach requires cell fixation and permeabilization of primers into cells by *in situ* hybridization. This method is attractive because it allows detection of low copy number RNA and avoids the need for gene amplification, drastically reducing the amount of time needed to detect genes present.[77] Previously, Chen et al. successfully applied ISRT in detecting the mRNA of the toluene degrading gene, todC1, in *Pseudomonas putida* F1.[77]

A)

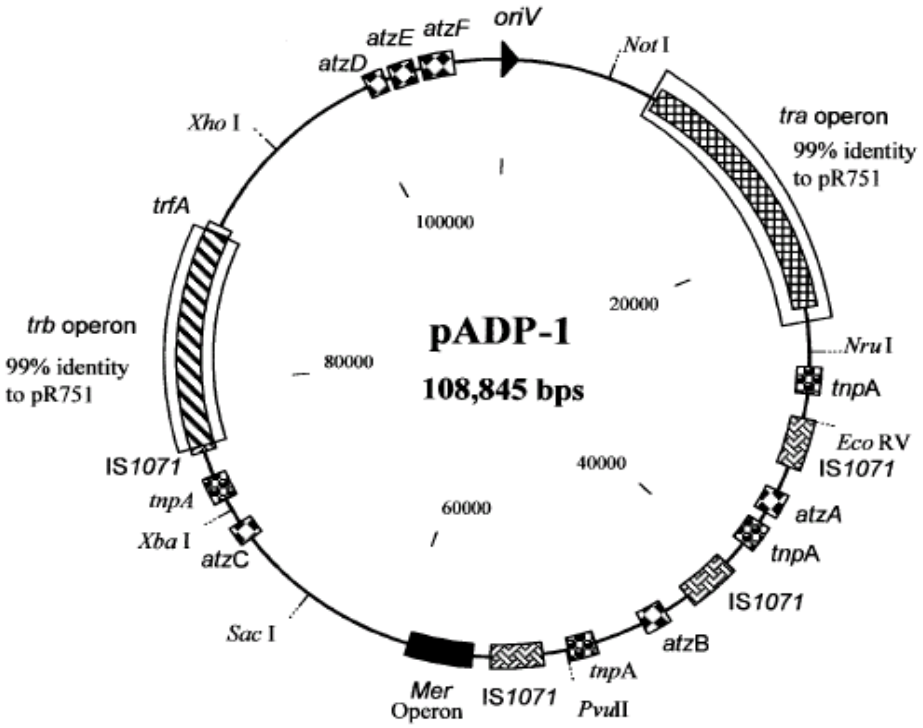

B)

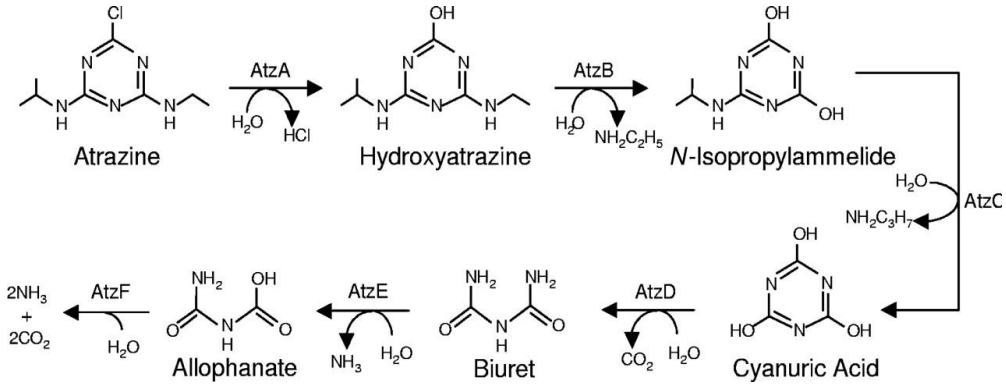

Figure 5:1: Schematic of A) the catabolic plasmid, pADP-1 and B) the catabolic pathway for atrazine degradation by *Pseudomonas* sp. strain ADP.

Source: Martinez, B.; Tomkins, J.; Wackett, L. P.; Wing, R.; Sadowsky, M. J., Complete nucleotide sequence and organization of the atrazine catabolic plasmid pADP-1 from *Pseudomonas* sp. strain ADP. *Journal of Bacteriology* **2001**, 183, 5684.

Materials and Methods

Chemicals

Atrazine was donated by Monsanto (Muscatine, Iowa). Control probe, EUB338, and gene-specific primers (Table 5:1) were purchased from Integrated DNA Technologies (Coralville, IA). SuperScriptase III Reverse Transcriptase and Qubit Assays were purchased from Life Technologies (Carlsbad, CA). DAPI and Alexa Fluor-5-dUTP were purchased from Molecular Probes (Eugene, OR). Chemicals used for media preparation and buffers were reagent grade and purchased from Fisher Scientific (Pittsburgh, Pennsylvania), Sigma Aldrich, and Mallinckrodt (St. Louis, Missouri). All water used for experimentation was purified using a Thermo Scientific Barnstead NANOpure DIamond ultrapure water system (Waltham, Massachusetts) and diethyl pyrocarbonate (DEPC)-treated prior to use.

Primers Design

Published primers, 19-20 bases long, were selected for ISRT.[50] Primers were located at least 200 bases downstream from the 5' end of the RNA sequence to ensure sufficient incorporation of labeled nucleotides into cDNA.[77] Primer A1r was designed to specifically bind to atzA gene encoding chlorohydrolase in the atrazine hydrolase system encoded on pADP-1 of ADP. Dr was designed to specifically bind to the atzD gene encoding amidohydroase on pADP-1 of ADP. Upon cell fixation and permeabilization, primers were incorporated into cells by *in situ* hybridization. Alexa Fluor 488-dUTP nucleotide was added to the reverse transcriptase mixture to allow atzA and atzD genes to fluorescence under microscopy.

Table 5:1: Selected primers design for targeting atrazine degrading genes as per Devers et al.[46]

Target Gene	Primer	Nucleotide Sequence (5'-3')	Annealing Temperature
atzA	A1r	CAC CCA CCT CAC CAT AGA CC	60°C
atzD	Dr	GGG TCT CGA GGT TTG ATT G	60°C

Cultures

Pseudomonas sp. strain ADP was purchased from Deutsche Sammlung von Mikrooganismen und Zelkulturen (Braunschweig, Germany) and prepared as described in the material and methods section of Chapter 4. As a negative control, suspended cells were also grown with ammonium nitrate instead of atrazine as a nitrogen source. The expression of the atrazine chlorohydrolase, atzA, is not induced in the absence of atrazine. The presence of atrazine or other triazine compounds induces the expression of atrazine genes, while the presence of more readily metabolized nitrogen sources represses the expression of atz genes.[19]

Suspended cells were grown in Erlenmeyer flasks in 1:10 dilution ratio of inoculum to media at 30°C and 180 rpm (Orbit Environ-Shaker Lab-line Instruments, Melrose, IL). Biofilms were grown as described in Chapter 4 for 5 days under continuous flow conditions containing 50 ppm atrazine.

Cell Fixation for ISRT

As per Chen et al. with some modifications, cells were harvested by centrifugation at 2,500 g for 10 min, then washed twice in phosphate buffer saline (PBS) pH 7.6.[77] Cell pellets were resuspended in 4% paraformaldehyde in PBS for 3 hours in the refrigerator (4°C), then transferred to 5 mL of 50% ethanol in PBS. For cell permeabilization, 5 µL

samples of fixed cells were air-dried onto silane-coated glass slides and treated with lysozyme (100 mM Tris, 50 mM EDTA [pH 8.0]) for 15 min at room temperature. Cells were dehydrated sequentially in 50, 80, 98% ethanol by volume in PBS for *in situ* hybridization. All water, buffers, and washing solutions were pretreated with DEPC to remove RNase activity, which might result in degradation of cellular RNA. See Appendix E for more information on solution recipes used for cell fixation.[77]

In situ Hybridization

Hybridization solution (20 µL) containing 100 ng of atzA primer was placed on cells. The slides, containing cells covered with hybridization solution, were incubated in a humid chamber for 2 h at 45°C and then washed with sodium chloride with 0.5 x trisodium citrate solution (45°C). A humid chamber was created by placing a 2L beaker filled with DI water into an enclosed incubator set at 45°C. Finally, cells were dehydrated sequentially in 50, 80, and 98% ethanol by volume in PBS before reverse transcriptase (SupersSriptase III) mixture including Alexa Fluor 488-dUTP was added. Cells were further counterstained with 100 µL of DAPI (0.5 µg/mL) for 5 min.[77] Cells were then washed once with distilled water and air dried. As a positive control, hybridization solution containing the EUB338 primer, in the absence of the atzA primer, was applied to fixed cells on slide. ISH with no primer was applied as a negative control.

Fluorescence microscopy using the Zeiss 710LSM confocal microscope with the DAPI/AF 488 excitation filters were used to visualize total cell population, control probe EUB388, and atzA expression in cells. Samples were viewed using the 63x oil objective lens.

Results and Discussion

Preliminary data are presented that were used to design experiments for detecting atz gene expression by ISRT. No atzA gene expression was observed in the free cell analysis (Figure 5:2). There are several possible reasons that can explain why atrazine chlorohydrolase was not detected: 1) the atrazine degradation pathway was not induced, 2) the mRNA copy number was significantly low, or 3) cell permeabilization was not sufficient to incorporate the probe. Mid log-phase cell samples were harvested from overnight cell cultures in minimal salt (MS) media containing 50 ppm atrazine. Prior to incubation in MS media containing atrazine (MSA), frozen cells were revived in Luria Bertani (LB) media. An immediate decrease in atrazine content has been noted when resting and exponential phase cells are transferred to buffer containing atrazine.[27, 50] In one study, cells were grown on MS media containing atrazine, then transferred to nutrient-rich Tryptic Soy Broth to collect cells in late exponential growth phase prior to suspension in MS buffer containing atrazine for atrazine degradation analysis.[50] In another study, atrazine grown culture was transferred to sterile MS medium containing atrazine and within 24 hours atrazine content was depleted.[27] Non-growing cultures, harvested in the late exponential phase, washed and then transferred to fresh media, showed similar results by metabolizing 100 ppm atrazine content within 5 hours.[27] Based on these results, it is highly unlikely that the atrazine degradation pathway was not induced at the time of analysis. With atrazine still available in the MSA as a nitrogen source, the atrazine chlorohydrolase should have been induced. Atr-derivatives are well known to appear among ADP cells, but it is highly unlikely for an entire population to become derivatives all at the same time. Going forward, to ensure that the atrazine degradation pathway is induced at the time of analysis, frozen cells will be revived in MSA instead of LB media, then transferred to fresh MSA for cell generation and finally

suspended in sterile MS media containing atrazine to collect exponential cells for ISRT analysis.

Reflecting on Devers et al. RT-PCR data, it is possible that the atzA gene was not detected by microscopy due to a significantly low copy mRNA. Similar to real-time reverse transcription PCR, ISRT relies on reverse transcription targeting mRNA using a forward primer. However, PCR involves gene amplification, while ISRT includes fluorescently labeled nucleotides with primers. With amplification, Devers et al. was able to observe a significant increase in atzA gene expression in cells exposed to atrazine compared to non-exposed cells (Figure 5:3).[50] Even though ISRT is a technique that eliminates the need for amplification by detecting target low copy mRNA, the limit of detection is unknown. Hence, there is a slight possibility that atz A gene expression was not detected by ISRT because sufficient mRNA was not present to adequately incorporate the primer. Further research is underway to extract and quantify RNA content in ADP cells.

To evaluate whether negative results were a reflection of the specific primer-RNA interaction, ISRT was repeated using a control probe, EUB338. EUB338 is complementary to a portion of the 16S rRNA gene conserved in the domain *Bacteria*.[78, 79] EUB338 is typically used for direct *in situ* analysis of complex natural and engineered systems.[78, 79] Ideally, most ADP cells should fluoresce during microscopic analysis with incorporation of the EUB338 probe by the ISRT method outlined. In Figure 5:4, about 10% of the cells did fluoresce during microscopic analysis and almost 100% of the cells in the sample fluoresced with the DAPI counterstain (Figure 5:4 a,c). The ISRT technique outlined in the methods section needs to be adjusted because more cells were expected to fluoresce with the EUB338 probe. Since only a few cells took up the probe following current ISRT methods, opportunities of viewing atzA gene expression were drastically reduced. Since ADP can be

detected by the EUB338 probe, of the three possibilities outlined for not detecting atzA gene expression in Figure 5:2, limited cell permeability is the most likely reason why atrazine chlorohydrolases were not detected.

To optimize cell permeability protocol, multiple variables will need to be addressed, including paraformaldehyde concentration, lysozyme concentration, sample exposure time to lysozyme, and incubation temperature. Every microbial system behaves differently, so it is important to identify optimal conditions required specifically for ADP under nutrient-limited conditions. There is also the appearance of background fluorescence not linked to gene expression to be mindful of when evaluating probe uptake. In Figure 5:4b, some non-specific binding of Alexa Fluor-488 was detected in the negative control sample not containing any primer.

A

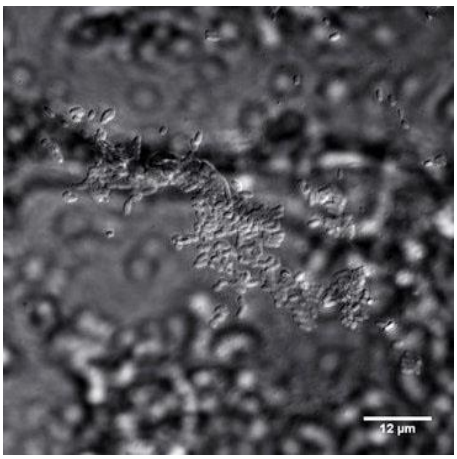

B

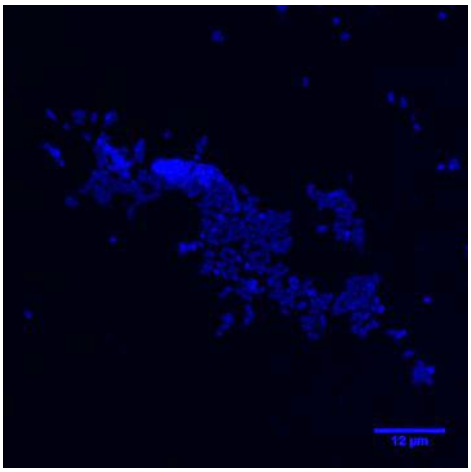

Figure 5:2: Microscopic analysis of ISH *Pseudomonas* sp. train ADP cells A) transmitted image and B) image under DAPI/488 filter. Notice that only DAPI fluorescence is detected; no atzA gene expression was observed (green fluorescence).

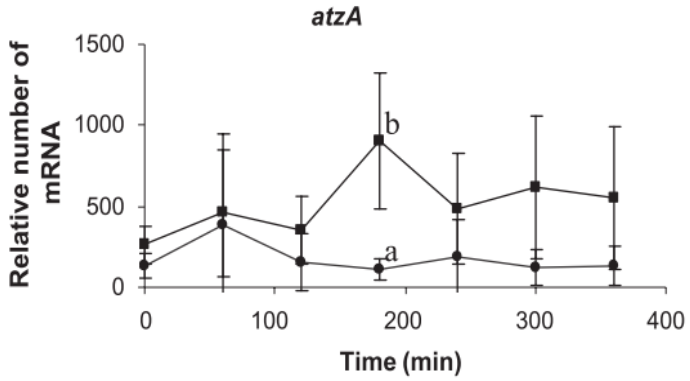

Figure 5:3: Relative number of atz mRNA measured in *Pseudomonas* sp. ADP incubated with 0 mg/L (circles) or 55 mg/L of atrazine (squares). mRNA was measured by RT-qPCR. A Fisher's test was performed at each sampling point of the kinetic to compare the relative number of atz transcripts in atrazine-treated and control samples (n=3, $p<0.05$). Results are expressed in mRNA number per 10^6 16S rRNA.

Source: Devers, M.; Soulas, G.; Martin-Laurent, F., Real-time reverse transcription PCR analysis of expression of atrazine catabolism genes in two bacterial strains isolated from soil. *Journal of microbiological methods* **2004**, 56, 3.

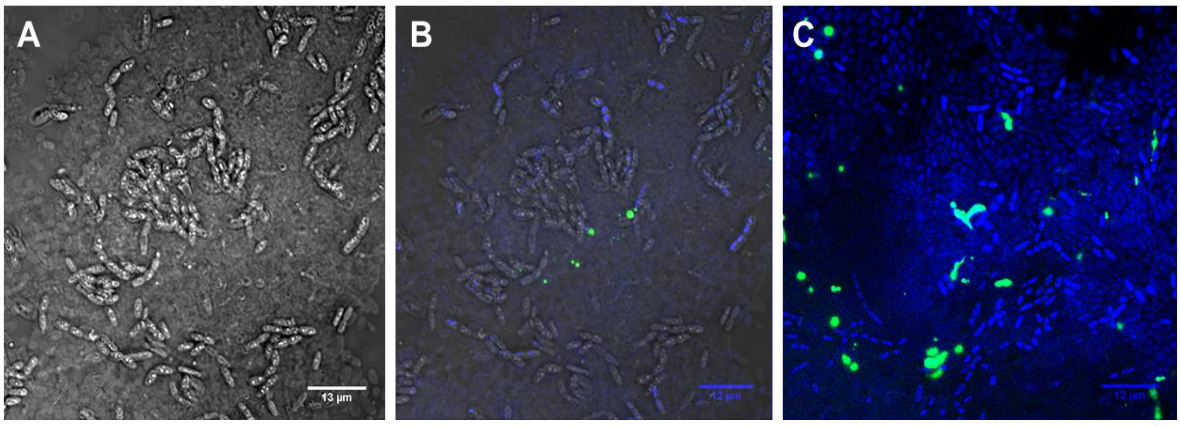

Figure 5:4: Analysis of ISRT method on *Pseudomonas* sp. strain ADP cells. A) Transmitted image of cells without filters, B) negative control containing cells without any primers added, and C) positive control with EUB338 probe.

Conclusion

The gene encoding atrazine chlorohydrolase was not detected by the current ISRT protocol. Previously, ISRT was demonstrated as a method for detecting the toluene degrading gene, todC1, in *Pseudomonas putida* F1.[77] However, after applying similar protocol to ADP cells in MSA, atz gene expression was not detected. By repeating the protocol with EUB388, it became apparent that the cell permeability was limited. By adjusting multiple individual parameters of the permeability protocol, such as fixative and detergent concentration, it is believed that the protocol can be optimized over time. However, calibrating an entire ISRT protocol may be time consuming because there are other variables, such as the hybridization solution, reverse transcriptase (RT) enzyme, and RT mixture to consider, in addition to cell permeability, for the overall success of ISRT.

The ultimate goal of this study was to detect plasmid retention and loss in ADP by detecting atzA and atzD gene expression. Since the atzA and EUB338 probes failed to detect gene expression in ADP by ISRT methods, analysis of atzD expression was not pursued. Before investing time to repeat numerous trials of ISRT while changing only one variable at time, reverse transcription polymerase chain reactions will be explored as an alternative method to meet research goals. Devers et al. was successful in quantifying atzABCDEF genes in ADP cells using real-time reverse transcription-PCR.[50] This method should be sufficient for detecting atzA and atzD to monitor pADP-1 retention and loss in the planktonic ADP cells.

Working towards the analysis of more complex systems, such as biofilms, ISRT still is the preferred method to use in identifying plasmid transfer within an intact biofilm matrix. Having the ability to view spatially, where within the biofilm specific atz genes are expressed, is beneficial in understanding how layers within the biofilm contribute to the

degradation process and may provide insight on how atrazine transports from the bulk media to layers closest to the substrata. The atzA gene is only expressed when cells have access to atrazine and are able to mineralize the compound. Areas exhibiting atzA gene expression would be indicative of areas that have access to atrazine. Appendix E contains a proposed experimental design of probing for atz gene expression in a biofilm matrix using ISRT. RT-qPCR is applicable to cells harvested from a biofilm matrix; however, the matrix will have to be disrupted to harvest the cells for analysis, thereby eliminating possibilities of spatial analysis.

CHAPTER 6: CONCLUSION AND FUTURE PERSPECTIVES

Thesis Conclusion

In this dissertation, functional group characteristics and physicochemical properties of atrazine degrading *Pseudomonas* sp. strain ADP biofilm were explored to gain insight to molecular and chemical distribution of compounds within a biofilm matrix. In scholarly articles, ADP has been primarily characterized in its freely suspended planktonic state. However, in natural environments most bacteria congregate at interfaces to form polymicrobial aggregates, such as films, mats, flocs, sludge, or biofilms.

ADP was found to readily form biofilms in a custom-made Teflon drip biofilm reactor on both glass and quartz substrata. SEM imaging showed how mature biofilm developed with intricate architecture, made up mostly of extracellular polymeric substances by Day 5. When atrazine was introduced as a nitrogen source for cellular assimilation, atrazine was observed on the surface of the EPS matrix, demonstrating the immobilizing property of biofilms when in contact with atrazine. The particles observed on the matrix were spherical and much smaller, than the original crystalline atrazine substrate. This immobilizing feature of the biofilm matrix may be useful in bioremediation, reducing pollutant infiltration into the environment. Undissolved atrazine also served as an additional substratum for cellular adhesion. When atrazine was removed from minimal salt (MS) media feed to the reactor, cells sloughed away, and the biofilm matrix readily broke down over 5 days.

Raman analysis allowed for rapid identification of biochemical properties in cells. In one scan at low resolution, molecular components were identified. By comparison of relative peak intensity ratios, the relative distribution of molecular components among samples was determined without principal component analysis of data. Cells grown on

nutrient-rich Luria-Bertani (LB) media generated a different Raman spectrum than cells grown on a minimal salt media. Planktonic cells emitted a different spectrum than cells in biofilms. Differences in samples were quantified by comparing the relative peak intensity ratio among samples, and it was possible to characterize the biofilm matrix. EPS proved to be the dominating feature in the biofilm grown on LB media. After fractionating EPS into soluble, lightly bound, and tightly bound EPS fractions, soluble EPS (SEPS) emitted the Raman signal most similar to biofilms, indicating that EPS is mostly made up of SEPS.

Raman spectroscopy appeared to also be promising in tracking atrazine degradation qualitatively by probing for intermediates and disappearance of functional groups in effluent leaving the bioreactor. Atrazine has characteristic peaks at 924, 963, and 992 cm^{-1}. Over 5 days, the 923 and 963 Raman bands disappeared from effluent samples, while the relative intensity of the 992 cm^{-1} peak decreased, signifying decreasing atrazine concentration. GC-MS analysis confirmed decrease in atrazine effluent over time. Although the intermediates biuret and cyanuric acid were not identified in the effluent with confidence, there were reasons to believe that biuret was present during sampling. The unassigned peak at 1513 cm^{-1}, unique to biuret, was also detected in the 5 day biofilm grown with MS media containing 50 ppm atrazine. However, ISRT did not validate the induction of atrazine chlorohydrolase by atzA gene identification. The atzA gene expression was not detected by fluorescently labeled primers perhaps due to low copy number mRNA in sample and/or inefficient cell permeabilization.

Scientific Impact

The studies presented in this dissertation have provided fundamental material to aid in the experimental design for analyzing complex biological systems using Raman spectroscopy, analyzing particle uptake in a biofilm matrix, and detecting gene expression

in biofilms. This work has contributed to the Raman microbial library and provided valuable images of xenobiotic degrading cells in contact with a pollutant. Though reputable fingerprints of ADP are presented in this thesis, attention should be made to growth media and phenotype when referencing spectra. Changes in media and method of growing cells will cause changes in the cellular make up, which are noticeable in spectra.

Future Work

Future work should involve: 1) exploring real-time analysis of effluent by Raman spectroscopy and 2) calibrating methods for detecting atz gene expression in ADP biofilm. Studies presented in this thesis have demonstrated the advantages of using Raman spectroscopy for the analysis of complex biosystems. On-line monitoring of effluent will provide further understanding of the kinetics involved in substrate degradation via intermediate product generation.

Real Time Analysis by Raman spectroscopy

Catabolic reactions involving enzymes typically have a turnover over number (k_{cat}) of 1-10,000 molecules per second. The catabolism of atrazine to carbon dioxide and ammonia occurs rapidly through a series of hydrolytic reactions that are facilitated by AtzABCDEF enzymes (Table 6:1). [29, 30] The stoichiometry of the reactions involved are all 1:1. However, with reactions occurring in fractions of a second, it is difficult to capture intermediate products in effluent on 24-h intervals by Raman spectroscopy. On-line Raman spectroscopy appears to be a more promising approach for detecting intermediate products in effluent and in shake-flask experiments.

On-line Raman spectroscopy allows non-invasive spectra acquisition of reactions over a time course.[80] Since the enzyme-catalyzed hydrolysis of atrazine occurs rapidly

(Table 6:1), we stand a better chance of capturing intermediate products by continuously probing the effluent leaving the reactor over an allotted time. As cells metabolize atrazine and intermediate products are produced, some products will wash out into the effluent from the continuous flow of media through the reactor. For shake-flasks experiments, cells grown in batch mode liquid cultures can also be analyzed over an allotted time. There should be more opportunities of detecting intermediate products with shake-flask experiments since measurements can be made on the actual liquid media containing reactions with cells.

Previously, Shaw et al. applied on-line monitoring of glucose fermentation by yeast to ethanol using a dispersive Raman spectrometer with a 780 nm diode laser.[81] A 780 nm diode laser was used to minimize fluorescence that is commonly known to accompany biological samples and improve sensitivity in comparison to the previously applied 1064 nm laser.[81] In monitoring air-dried biological samples, however, the 532 nm laser produced higher signal-to-noise ratio compared to the 780 nm laser. With the 6th order polynomial correction applied, background fluorescence is not problematic. To collect Raman spectra, Shaw et al. created a flow through set up by pulling the culture media, using a peristaltic pump, from a glass conical flask through a side arm at the bottom of the flask connected to a silicon tubing.[81] Culture was passed through a filter and into a quartz tube that was mounted on the Raman microscope stage, then recycled back into the conical flask. Samples were filtered prior to entering the quartz tube for Raman analysis, to reduce background disturbances from cellular material.[82] Raman spectra were collected as 3 scans of 60 s each using a 10x objective.[81]

Cannizzaro et al. used an *in situ* Raman spectroscopic probe, on the other hand, to monitor intracellular carotenoid production in *Phaffia rhodozyma* fed-batch experiments.[82] Raman spectra were collected directly in the fermentation broth of a bioreactor operating

under physiological conditions. A 12.5 mm probe attached to the control unit via a 3 m fiber-optic cable, was inserted into the bioreactor. A Teflon shutter encased the probe to block the laser light, 785 nm excitation, from the exiting probe tip. Raman spectra were collected with 30 sec exposure time and 4-10 accumulations every 15 min. The peak heights of 3 characteristic bands of carotenoid were linearly correlated with intracellular carotenoid content.

Schuster et al. studied starch hydrolases, i.e. α-amylase and amyloglucosidase, using FT-Raman spectroscopy.[80] Similar to Shaw, a flow-through setup was created routing media from the reactor, to the spectrometer, and back into the reactor. Instead of using quartz tubing as the flow cell, a rectangular flow cell made of PTFE (22 mm wide and 2 mm deep) with a calcium fluoride window was used and a palladium mirror was placed at the back of the flow channel to increase Raman scattering. Raman spectra were collected by co-adding 200 scans in 2 min using a 1064 nm excitation source.[80]

Moving forward, it may be valuable to conduct on-line monitoring of effluent for 24 h with a 0.2 μm filter insert on the outlet of the bioreactor to track atrazine degradation via intermediate products generation. Insertion of a filter will aid in withholding undissolved atrazine and cells from entering into the effluent being tested. This filtration will aid in reducing background disturbances and improve visibility of intermediates in Raman spectra. Since atrazine is continuously routed into the biofilm reactor, it is natural for larger quantities to be present in the effluent than the intermediate products, thus causing atrazine to dominate the Raman spectra. To avoid having the atrazine signal overpower other compounds' signal in the spectra, it will help to remove large particulates from the effluent prior to analysis.

Similar to Shaw and Schuster with some modifications, a flow-through setup can be created to route effluent leaving the bioreactor through size 13 silicon tubing, pass a filter,

into a flow cell mounted on the Raman microscope stage, then out to a waste container. Flow will be maintained with two peristaltic pumps operating at 0.8 mL/min. Pump 1 will control the flow of sterile media entering the biofilm reactor, and Pump 2 will be placed on the outlet of the flow cell to maintain steady flow of effluent through the flow cell. An open rectangular quartz box (10 mm x 22 x 4 mm) with an inlet and outlet port, mounted on top of a quartz plate (75 mm x 25 mm x 5 mm) can be used as the flow cell (Figure 6:1). An open box is ideal rather than an enclosed boxed with a coverslip attachment since the objectives on the Thermo Nicolet Almega XR Raman microscope operate in non-contact mode. Spectra can be collected using a 50x objective, 4 accumulations and 60 sec exposure.

Since high quality Raman spectra have been presented in this thesis with the 532 nm laser, it is reasonable to begin experimentation with the same wavelength. In efforts of simplifying the system, the reactor can be maintained at room temperature. Previous experimentation with cultivating ADP cells have demonstrated that cells can survive and grow at 28^{o}C; therefore, we assume cells will also survive at 25^{o}C. Characteristic Raman bands of cyanuric acid (705 and 1731 cm^{-1}) and biuret (1513 and 1691 cm^{-1}) can be used to linearly correlate intermediate products produced. Similar experimental design can be implemented for shake-flask experiments containing freely suspended cells, with the inclusion of a recycling loop to feed media back into the flask after Raman analysis.

Being able to monitor atrazine hydrolysis by ADP using on-line Raman spectroscopy will not only allow detection of atrazine degradation, but will also provide valuable information on the kinetics occurring. Coupling atz gene analysis with on-line Raman spectroscopy will aid interpretation of Raman data and validate the induction of the atrazine degradation pathway in ADP cells.

Table 6:1: The rates of enzymes AtzABCDEF acting on their relative substrates ($\frac{k_{cat}}{K_m}$). k_{cat} represents the number of molecules each enzyme site converts to product per unit time (turnover number) and K_m is indicative of the substrate concentration required for catalysis to occur.[83, 84]

Enzyme	Substrate	Product	k_{cat} (s^{-1})	k_m (μM)	$\frac{k_{cat}}{k_m}$ ($s^{-1}M^{-1}$)
AtzA (atrazine chlorohydrolase)[85]	atrazine	Hydroxyatrarzine	2.2[a]	> 153[a]	1.5 x 10^4
AtzB (hydroxyatrazine ethylaminohydrolase)	Hydroxyatrazine	N-isopropylammelide	Unknown	Unknown	Unknown
AtzC (N-isopropylammelide isopropylamino hydrolase)	N-isopropylammelide	Cyanuric acid	Unknown	Unknown	Unknown
AtzD (cyanuric acid amidohydrolase)[86]	Cyanuric acid	Biuret	6.8[b]	57[b]	1.2 x 10^5
Biuret hydrolase[87]	Biuret	Allophanate	4.0[b]*	23[b]*	1.7 X 10^5
AtzF (allophanate hydrolase)[88]	Allophanate	Ammonia and carbon dioxide	16.4[b]	1.5[b]	1.1 x 10^4

Kinetic data are derived from [a]wild type ADP and [b]recombinant *E.Coli*. *Biuret hydrolase kinetics are based on a modified enzyme from the cysteine family, not AtzE.

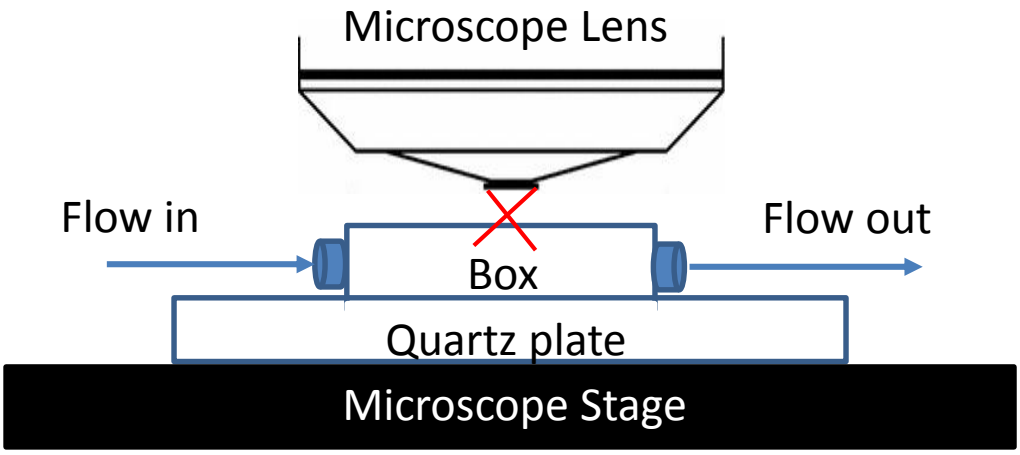

Figure 6:1: Schematic of flow-through flow cell setup for on-line Raman analysis. A quartz plate with a three-dimensional quartz box mounted onto the plate that allows flow of medium into and out of the box will be mounted onto the Raman microscope stage within the focal plane for analysis.

Probing for atz Gene Expression

In the current work, the EUB338 probe was detected minimally in the cell population, and atzA gene expression was not detected by ISRT methods. Data suggest inadequate cell permeabilization and/or low copy number mRNA. Cell wall permeability is critical for successful *in situ* techniques involving the uptake of probes. Cell membranes have to be permeable enough to allow entry of labeled probes, but resistant enough to retard the diffusion of products out of the cell at the same time.[89, 90] There are many factors that affect cell permeability, such as fixative strength, detergent concentration, exposure time, and temperature.[90] Amidzadeh et al. explored six different permeabilization methods to optimize detection of 18S rRNA in HeLa cells that were fixed in 2% paraformaldehyde in phosphate buffer saline.[90] They found cells that were treated with 0.2% Tween-20 and incubated for 30 min showed the highest fluorescent intensity. There is no one permeabilization method that suits all cell lines. Therefore, it is important to optimize procedures that will determine conditions required for efficient cell permeability of the cell line of interest before proceeding with *in situ* hybirdization.[89] Hybridization conditions also have to be optimized accordingly.[90]

In this study, cells were fixed in 4% paraformaldehyde and further permeabilized with 0.5% lysozyme in Tris/EDTA buffer. Moving forward, it will be beneficial to create a study to determine optimal conditions required for ADP uptake of the EUB338 probe by testing 4 conditions: 1) paraformaldehyde concentration (1, 2, 3, 4, and 5 %); 2) lysozyme concentration (0.2, 0.4, 0.6 %); 3) exposure time (10, 15, 20, 30 min); and 4) temperature (RT, 30^{o}, 40^{o}). However, only one variable can be altered at a time, so a series of 15 x 3 experiments will have to be conducted. The EUB338 probe will be inserted via RT mixture as described in Chapter 5, and cells will be counterstained with DAPI. Cell permeability can

be evaluated by fluorescence microscopy. Upon conclusion, hybridization conditions should also be evaluated by altering NaCl, Tris-HCl, sodium dodecyl sulfate, and primers concentration at different pHs. The hybridization solution currently used in our lab includes 100 ng unlabeled primer and 0.01% sodium dodecyl sulfate with salts (pH 7.2). Once the permeabilization protocol and hybridization solution have been optimized for the ADP system, then the PCR technique can be explored to address low copy number mRNA.

If ADP cells are minimally expressing atzABCDEF genes, even if permeability procedures are optimized, it will still be difficult to identify atz gene expression via ISRT. Including a PCR step will aid in amplifying the cDNA content, which will make it easier to identify cells expressing latent genes under microscopy. The two types of PCR techniques to consider are: prokaryotic *in situ* PCR (PI-PCR) and *in vitro* PCR (RT-PCR). PI-PCR allows indirect amplification of RNA within cells by amplifying the cDNA copy generated after the targeted RNA is converted into double-stranded cDNA by reverse transcriptase.[91] The cell membrane acts a container for amplified products, allowing direct viewing of particular metabolic activity within a population.[89] RT-PCR, behaves similarly to PI-PCR; however, amplification is performed on bulk extracted nucleic acids. Upon reverse transcription on extracted RNA, cDNA is amplified. Devers et al. was successful at quantifying atz gene expression in ADP cells using RT-qPCR.[50] However, RT-PCR techniques are limited because they cannot provide information on the spatial distribution of particular catabolic activity within a population.

Going forward, it will be best to perform PI-PCR on ADP cells, if the permeability protocol and hybridization solution are optimized early on. Researchers often state that *in situ* amplification is cumbersome, especially if working independently. However, if the study on cell permeability and hybridization solution is conducted as described and optimal

conditions for probe uptake is defined, then PI-PCR will be a good approach for detecting atz gene expression in ADP cells. In the event that inconclusive data are collected from the study, then RT-PCR is an alternative route to pursue. There are many reputable RNA extraction kits from which to select to perform RT-PCR. With the correct enzyme buffer, which usually accompanies purchased reverse transcriptase enzymes, RT-PCR should be successful.

Developing techniques for probing for atz gene expression in ADP free cells will aid in experimental design for detecting gene expression in more complex systems, such as biofilms. Recall from Chapter 1 that there are positive implications for growing ADP cells in a biofilm matrix. As a biofilm, there are increased opportunities for conserving the atrazine degradation pathway by horizontal gene transfer and homologous recombination mediated by insertion sequences.[2, 31] Since organisms are in close proximity to each other, instead of losing the atzABC genes and/or the pADP-1 plasmid, genes and plasmid can be transferred among organisms and remain entrapped in the extracellular matrix, thus reducing the appearance of Atr-derivatives and conserving the degradation pathway. Increased cellular density means increased bioavailability to atrazine, which should lead to higher atrazine consumption rates and improved bioremediation applications.

APPENDIX A: NICOLET ALMEGA XR DISPERSIVE RAMAN SPECTROMETER

Thermo Scientific Nicolet Almega XR Dispersive Raman Spectrometer equipped with Olympus BX 51 was used to collect all spectra. The focal length of spectrograph is 260 mm. Samples were illuminated with a frequency-doubled 532 nm Nd:YV04 laser or 785 nm diode laser with a spatial resolution at 100x objective of 1.4 µm or 2.0 µm, respectively. Spectra were processed using OMNIC 8 software, offering high and low resolution settings dependent on gratings and laser. Video images were taken by a CCD camera and stored and processed using the OMNIC software.

A1: Alignment

The instrument was aligned daily at the beginning of each experimental run to ensure that the viewing path, excitation laser, and Raman emissions path from sample to spectrograph were all aligned to the same spot on the sample. To begin alignment, the alignment tool was turned on by selecting the alignment tab in the experimental setup. Spectrograph was aligned to pinhole by centering cross hairs on red LED light in the center of field view on alignment tool using 10x objective. The laser was aligned to silicon by focusing cross hairs on surface of silicon wafer on the alignment tool using 50x objective. After a single peak spectrum was resolved and side/side and up/down values became constant, alignment was complete.

A2: Calibration

Calibration was performed every three months. Calibration of wavelength (X-axis), white light (Y-axis), and laser frequency was automated. Once calibration was complete, followed by alignment, then the Visible Raman Microscope (VRM) test was done. The VRM test was performed using polystyrene as an internal standard to test that the signal to noise ratio (SNR) was equal to or greater than 1,000 Pkh/rms. If SNR was below 1,000 then

calibration was repeated, followed by alignment, then VRM test. Calibration may take several hours. When time is limited, calibration may be bypassed by simply doing a VRM test. Once SNR is equal to or greater than 1000 Pkh/rms, then the instrument is working accurately. However, full calibrations, should be performed periodically.

A3: Fluorescence Correction

Fluorescence from samples distorts the baseline of Raman spectrum such that spectrum appears to be sitting on something abnormal. Polynomial functions are used for baseline corrections (see Figure A:3). In the Thermo Scientific OMNIC software 1-6 order polynomials may be assigned while collecting spectra. All spectra presented in thesis were corrected using 6th order polynomials.

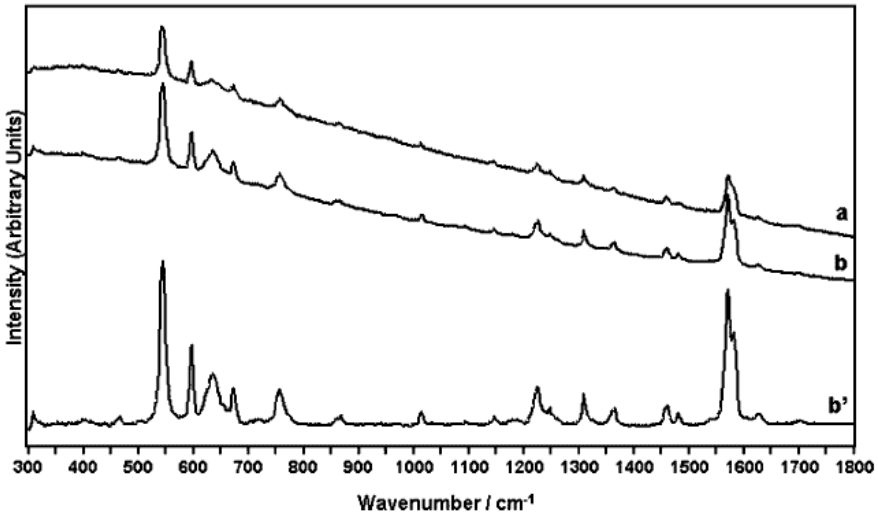

Figure A3:1: Example of fluorescence correction. Raman spectra of a) natural and b) synthetic indigo. In spectrum b') synthetic indigo spectrum was baseline corrected by subtraction of a 6th degree polynomial. Notice the smoothing of baseline.[92]

Source: Vandenabeele, P.; Moens, L., Micro-Raman spectroscopy of natural and synthetic indigo samples. *Analyst* **2003**, 128, 187-193.

A4: Time and Accumulation

Longer exposure time and increased number of accumulations increase signal-to-noise (S/N) ratio, but does not affect the Raman shift (refer to Figure A2:1). Longer exposure time and accumulations may be needed to resolve peaks for identification and quantification. For non-biological samples, such as atrazine, exposure time under 30 sec, is enough to collect high quality Raman spectrum. For microbial samples, on the other hand, 60 seconds in required to collect spectra with distinguishable Raman bands. At least 2 accumulations should be collected for all samples; more accumulations yields cleaner spectra with higher S/N ratios. On the downside, too much exposure to laser can heat and burn samples or saturate the detector.

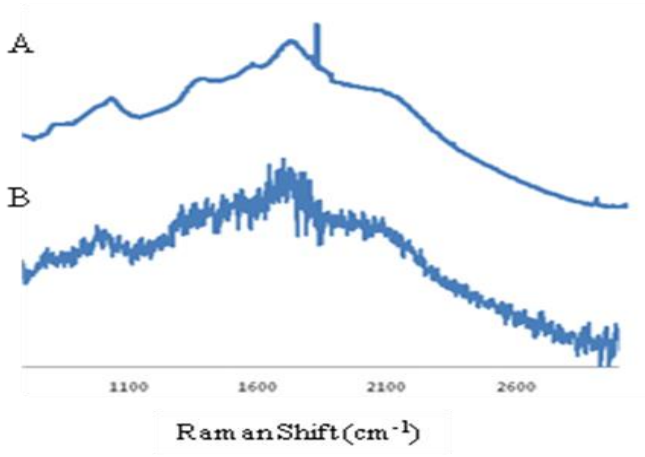

Figure A4:1: Raman spectra of 33 ppm atrazine in deionized water with A) 1 minute laser exposure and B) 250 milliseconds laser exposure. Sample was collected using Raman probe, 785 nm laser and 100 µm fiber optic. Spectrum A has a higher signal to noise ratio than spectrum B.

A5: Laser Wavelength

Shorter wavelength produced spectra with higher signal to noise ratio, making it easier to identify peaks from samples. In the early stages of this research, the 785 nm Raman excitation wavelength was employed, under the assumption that a shorter wavelength would burn samples and add to fluorescence emission. Many organisms produce fluorescence signals orders of magnitude more intensive than Raman signals due to existing chromophores.[93] A shorter wavelength was assumed to aid in the fluorescence disturbance, making it difficult to extract chemical information from Raman spectra. This assumption, proved to be incorrect upon collecting the first Raman spectrum of ADP free cell using both 785 and 532 nm laser (Figure A3:2). Using the 532 nm laser, biological samples did not burn and background fluoresce did not interfere with peak identification for chemical analysis. Higher quality Raman spectra with improved S/N ratio was obtained with the 532 nm laser compared to the 785 nm laser.

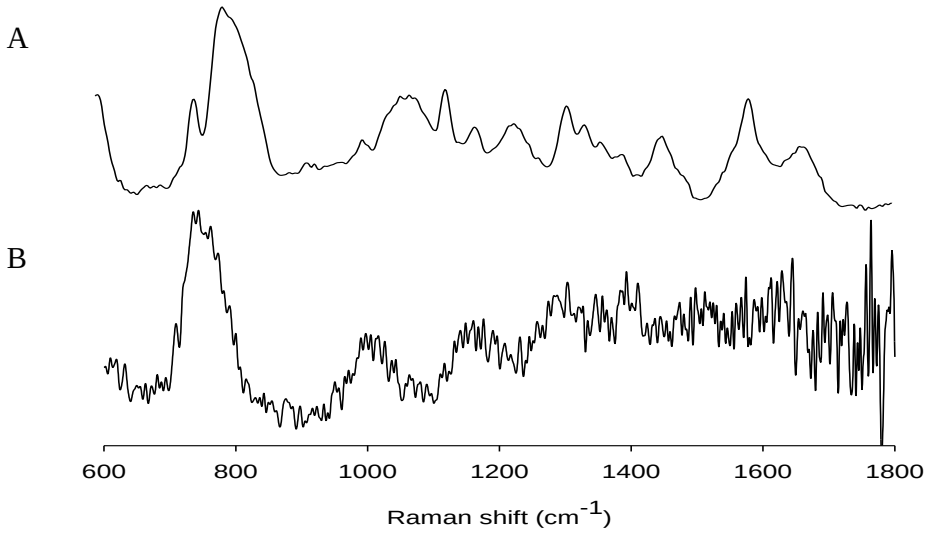

Figure A5:1: Raman spectra of *Pseudomonas* sp. strain ADP free cell A) collected with 532 nm laser and B) collected with 785 nm laser. Higher signal to noise ratio was obtained with the 532 nm laser.

APPENDIX B: DRIP BIOFILM REACTOR DESIGN

Pseudomonas sp. strain ADP readily forms biofilm. Even while growing cells in shaker flasks, light films became visible on walls of flask at the air-liquid interface by day 2, especially in the presence of atrazine (Figure B:1). For the purposes of this research, a modified plug flow reactor, adapted from Goeres's drip flow reactor design was used under laminar flow conditions.[94]

Figure B:1: Biofilm formation on upper inner side of shaker flask where liquid level breaks with air under 200 rpm movement. Flask contains 48 hours *Pseudomonas* sp. strain ADP broth grown at 27°C in orbital shaker.

Reactor Design

Through experimentation with different materials, Teflon was found to be best for growing biofilms since it is inert with respect to cells, thermally resistant to temperatures as high as 121°C, and chemically resistant to detergents, acids, and bases. A custom made10 x 2.5x 2 cm four channel Teflon drip biofilm reactor that could be adjusted to different angels and accommodate varying substrata was made by the University of Iowa Medical Shop (see Figure B:2). Each channel had polycarbonate lids, 0.25 µm bacterial vents, and rubber inlet stoppers. To achieve low shear at the air-liquid interface, media dripped continuously at 0.8

mL/min on a slight incline.[94]

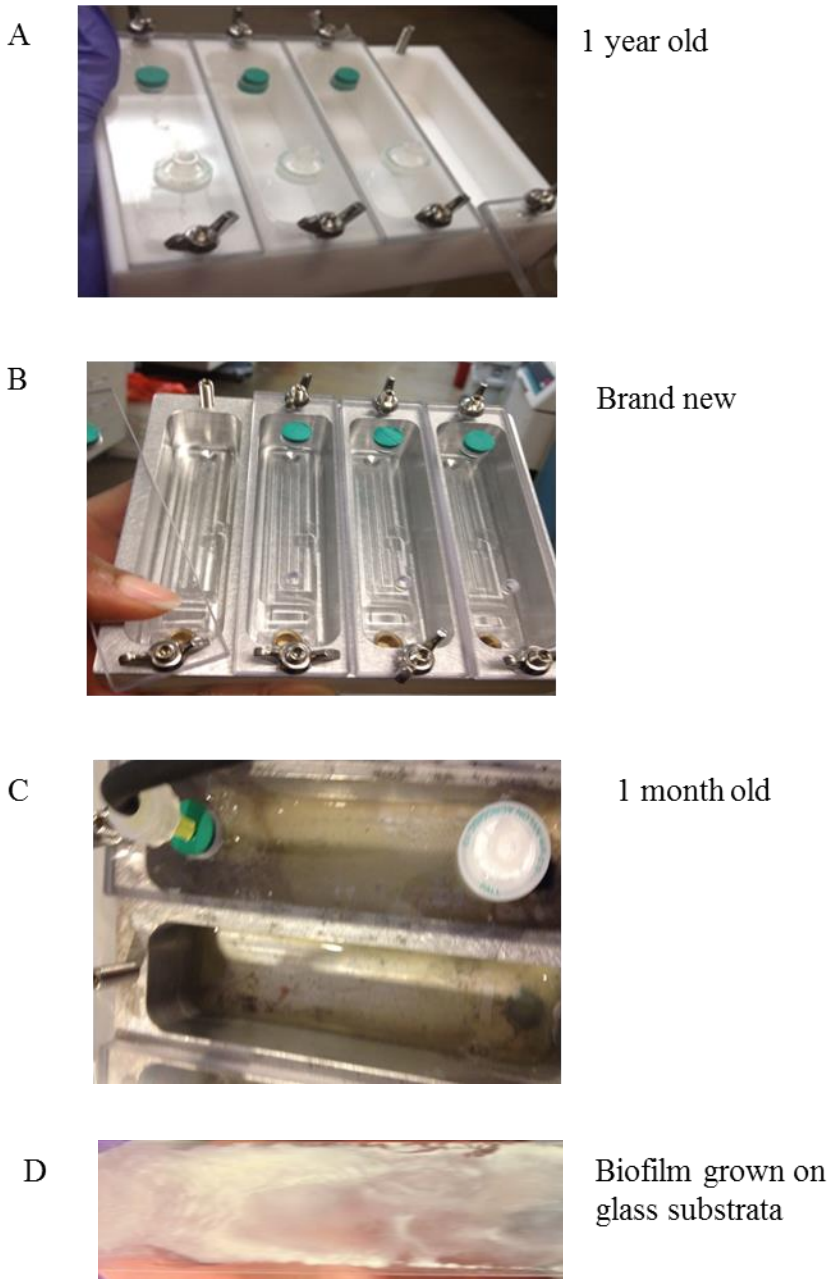

Figure B:2: Drip biofilm reactor A) made of Teflon, b) aluminum, and c) aluminum reactor after growing two sets of biofilms. D) 5-day old biofilm generated from one channel in the reactor. The aluminum reactor was more affordable, however, the reusability was inadequate. The aluminum reactor corroded easily. The Teflon reactor was more durable, saving money in the long run.

APPENDIX C: PROTEIN ASSAY

Modified lowery assay was performed using the Bio Rad RC DC Protein Assay Kit as per manufacturer's instructions. Bovine serum albumin (BVA) was used as the protein standard to generate the calibration curve (Figure C:1). Protein content was found by measuring sample's optical density/absorbance at 750 nm wavelength using the BioMate spectrophotometer. The equation generated from the plot was used to calculate the concentration of protein in EPS fractions based on absorbance.

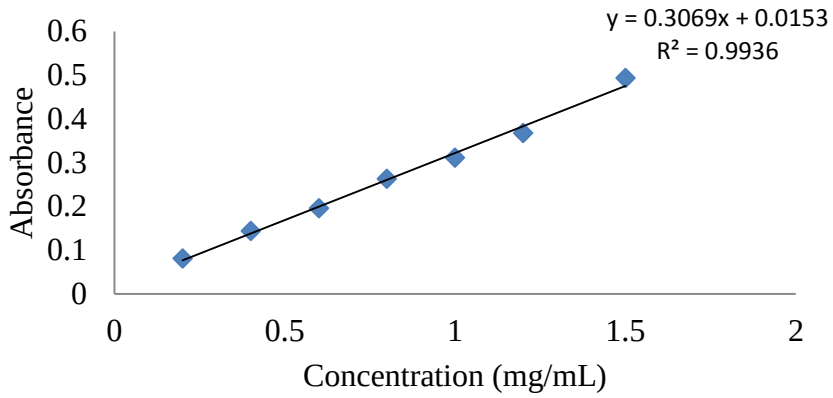

Figure C:1: Calibration curve of BSA standards for protein assay.

APPENDIX D: RNA ASSAY

Thermo Fisher Scientific Qubit RNA HS Assay Kit as per manufacturer's instructions were used to quantify RNA in EPS fractions using a Qubit 3.0 Fluorometer. The Qubit assay is highly selective for RNA and tolerates common contaminants such as free nucleotides, protein, and detergents, without quantifying interferences. A calibration curve was generated using the Qubit prediluted standards provided. RNA content in EPS fractions were quantified automatically based on the internal standards provided.

APPENDIX E: CALIBRATION CURVE FOR GC-MS ANALYSIS

A calibration curve of the response of varying concentrations of atrazine was generated to quantify atrazine contents in effluent and shake flasks. Data was collected using the Waters GCT Premier and a 30 meter Db-1701 column at the High Resolution Mass Spectrometry Facility at the University of Iowa.

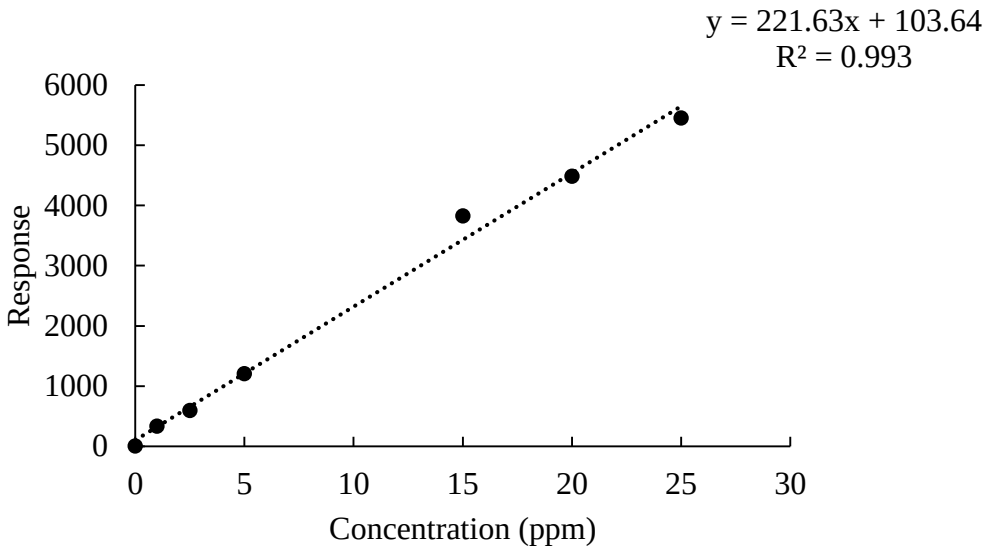

Figure E:1: Calibration curve of atrazine standards for GC-MS analysis.

APPENDIX F: SOLUTIONS USED FOR ISRT

Table E:1: Hybirdization solution recipe

Compound	Concentration (mmol/L)	Concentration (g/L)
NaCl	900	52.60
Tris-HCl	20	2.42
Sodium dodecyl Sulfate	0.01%	0.1
pH	7.2	7.2

Table E:2: Sodium chloride with trisodium citrate (SSC) solution (0.5 x SSC)

Compound	Concentration (mmol/L)	Concentration (g/L)
NaCl	750	43.83
Trisodium Citrate	75	19.35
pH	7.0	7.0

Table E:3: Lysozyme solution

Compound	Concentration (mmol/L)	Mass (g)	Volume of water	pH	Final
Tris	100	1.211	20 mL	8	14 mL
EDTA	50	1.461	20 mL	8	7 mL

Table E:4: 4% Paraformaldehyde in PBS

Compound	Mass (g)	Volume of water (DEPC treated)
Paraformaldehyde	2	40 mL
1 x PBS		5 mL

Table E:5: Reverse transcription mixture

Concentration	Compound
1 x	Enzyme buffer
200 µM	dATP
200 µM	dCTP
190 µM	dTTP
10 µM	Alexa Fluor dUTP
0.02%	Bovine serum albumin
5 mM	dithiothreitol
1 U µ/L	Reverse transciptase SuperScriptase III

Final volume of 20 µL needed to cover cells

APPENDIX G: PROPOSED METHOD FOR ISTRT ON BIOFILMS

Cells in intact biofilms can be fixed as per Tolker-Neilsen with slight modifications.[42] Paraformaldehyde can be pumped into the flow chamber at a flow rate of 0.2 mL/sec for 15 min and allowed 1 hour to work. Then wash the fixed biofilm for 20 min with PBS at a flow rate of 0.2 mL/sec. To make biofilm rigid for three dimensional analyses, acrylamide solution will need to be pumped in at a flow rate of 0.5 mL/sec for one minute, and then allowed at least 1 hour to rest. Solidified acrylamide slab of biofilm can then be cut and placed downward in a well on a microscope slide, then covered with FISH prehybridization buffer and incubated in a formamide-saturated incubation chamber for 30 min at 37^{o}C.[42]

Hybridization solution containing 100 ng of atzA and atzD primers can then be placed on slides containing biofilm. Incubate slides in a humid chamber for two hours at 45^{o}C, and then washed with sodium chloride with trisodium citrate (SSC) solution.[22] Finally slides can be washed with deionized water and covered in reverse transcriptase mixture containing Alexa Fluor 488-dUTP. All incubations and washing should be performed in a formamide-saturated incubation chamber at 37^{o}C in the dark for biofilms.[42]

REFERENCES

1. Flemming, H.-C.; Wingender, J., The biofilm matrix. *Nature Reviews Microbiology* **2010**, 8, 623.

2. Singh, R.; Paul, D.; Jain, R. K., Biofilms: implications in bioremediation. *Trends in microbiology* **2006**, 14, 389.

3. Huang, W. E.; Ude, S.; Spiers, A. J., Pseudomonas fluorescens SBW25 biofilm and planktonic cells have differentiable Raman spectral profiles. *Microbial ecology* **2007**, 53, 471.

4. Schwartz, T.; Jungfer, C.; Heissler, S.; Friedrich, F.; Faubel, W.; Obst, U., Combined use of molecular biology taxonomy, Raman spectrometry, and ESEM imaging to study natural biofilms grown on filter materials at waterworks. *Chemosphere* **2009**, 77, 249.

5. Bernsmann, F.; Laube, N.; Baldsiefen, G.; Castellucci, M.; Iop Hydrogenated amorphous carbon coatings on implants drastically reduce biofilm formation and water permeation. In 7th Symposium on Vacuum-based Science and Technology (SVBST), Kolobrzeg, POLAND, Nov 19-21, 2013; Kolobrzeg, POLAND, 2013; Vol. 564.

6. Pasvolsky, R.; Zakin, V.; Ostrova, I.; Shemesh, M., Butyric acid released during milk lipolysis triggers biofilm formation of Bacillus species. *International Journal of Food Microbiology* **2014**, 181, 19-27.

7. Usher, K. M.; Kaksonen, A. H.; Cole, I.; Marney, D., Critical review: Microbially influenced corrosion of buried carbon steel pipes. *International Biodeterioration & Biodegradation* **2014**, 93, 84-106.

8. Veerachamy, S.; Yarlagadda, T.; Manivasagam, G.; Yarlagadda, P., Bacterial adherence and biofilm formation on medical implants: A review. *Proceedings of the Institution of Mechanical Engineers Part H-Journal of Engineering in Medicine* **2014**, 228, 1083-1099.

9. Nadell, C. D.; Xavier, J. B.; Levin, S. A.; Foster, K. R., The evolution of quorum sensing in bacterial biofilms. *Plos Biology* **2008**, 6, 171.

10. Pamp, S. J.; Gjermansen, M.; Tolker-Nielsen, T. The Biofilm Matrix: A Sticky Framework. In *The Biofilm Mode of Life: Mechanisms and Adapations*, Kjelleberg, S.; Givskov, M., Eds.; 2007; Chapter 4, pp 37-69.

11. Beyenal, H.; Lewandowski, Z., Internal and external mass transfer in biofilms grown at various flow velocities. *Biotechnology progress* **2002**, 18, 55.

12. Francolini, I.; Donelli, G., Prevention and control of biofilm-based medical-device-related infections. *Fems Immunology and Medical Microbiology* **2010**, 59, 227-238.

13. Shrout, J. D.; Tolker-Nielsen, T.; Givskov, M.; Parsek, M. R., The contribution of cell-cell signaling and motility to bacterial biofilm formation. *MRS Bulletin* **2011**, 36, 367.

14. Mikkelsen, H.; Duck, Z.; Lilley, K. S.; Welch, M., Interrelationships between colonies, biofilms, and planktonic cells of Pseudomonas aeruginosa. *Journal of Bacteriology* **2007**, 189, 2411-2416.

15. Stoodley, P.; Sauer, K.; Davies, D. G.; Costerton, J. W., Biofilms as complex differentiated communities. *Annual Review of Microbiology* **2002**, 56, 187-209.

16. Galluzzo, M. J.; Banerji, S. K.; Bajpai, R.; Surampalli, R. Y., Atrazine removal through biofiltration. *Practice Periodical of Hazardous, Toxic, and Radioactive Waste Management* **1999**, 3, 163.

17. Syngenta United, S. Internal and external mass transfer in biofilms grown at various flow velocities. http://www.atrazine.com/AtraMain.aspx (May 10)

18. Hancock, J. Iowa community sues atrazine maker for contaminated drinking water. http://iowaindependent.com/29518/iowa-community-sues-atrazine-maker-for-contaminated-drinking-water http://dx.doi.org/10.1061/(ASCE)1090-025X(1999)3:4(163) (Apri 15).

19. Natural Resources Defense, C. Atrazine: Poisoning the Well. http://www.nrdc.org/health/atrazine/ (April 10).

20. Sciarillo, E. Geocommons. http://geocommons.com/maps/7808 (February 11).

21. Rey, F.; Gonzalez, M.; Zayas, M. A.; Stoker, C.; Durando, M.; Luque, E. H.; Munoz-de-Toro, M., Prenatal exposure to pesticides disrupts testicular histoarchitecture and alters testosterone levels in male Caiman latirostris. *General and comparative endocrinology* **2009**, 162, 286.

22. Hayes, T. B.; Collins, A.; Lee, M.; Mendoza, M.; Noriega, N.; Stuart, A. A.; Vonk, A., Hermaphroditic, demasculinized frogs after exposure to the herbicide atrazine at low ecologically relevant doses. *Proceedings of the National Academy of Sciences of the United States of America* **2002**, 99, 5476.

23. Hayes, T. B.; Khoury, V.; Narayan, A.; Nazir, M.; Park, A.; Brown, T.; Adame, L.; Chan, E.; Buchholz, D.; Stueve, T.; Gallipeau, S., Atrazine induces complete feminization and chemical castration in male African clawed frogs (Xenopus laevis). *Proceedings of the National Academy of Sciences of the United States of America* **2010**, 107, 4612.

24. Cragin, L. A.; Kesner, J. S.; Bachand, A. M.; Barr, D. B.; Meadows, J. W.; Krieg, E. F.; Reif, J. S., Menstrual cycle characteristics and reproductive hormone levels in women exposed to atrazine in drinking water. *Environmental research* **2011**, 111, 1293.

25. Wang, D.; Shin, J. Y.; Cheney, M. A.; Sposito, G.; Spiro, T. G., Manganese dioxide as a catalyst for oxygen-independent atrazine dealkylation. *Environmental Science and Technology* **1999**, 33, 3160.

26. Murphy, M. B.; Hecker, M.; Coady, K. K.; Tompsett, A. R.; Jones, P. D.; Du Preez, L. H.; Everson, G. J.; Solomon, K. R.; Carr, J. A.; Smith, E. E.; Kendall, R. J.; Van der Kraak, G.; Giesy, J. P., Atrazine concentrations, gonadal gross morphology and histology in ranid frogs collected in Michigan agricultural areas. *Aquatic Toxicology* **2006**, 76, 230.

27. Mandelbaum, R. T.; Allan, D. L.; Wackett, L. P., Isolation and Characterization of a Pseudomonas Sp that Mineralizes the S-Triazine Herbicide Atrazine. *Applied and Environmental Microbiology* **1995**, 61, 1451.

28. Biglione, N.; Rodgers, V. G. J.; Peeples, T. L. Determining design and scale-up parameters for degradation of atrazine with suspended Pseudomonas sp. ADP in aqueous bioreactors. 2540 Olentangy River Road, P.O. Box 3337, Columbus, OH 43210-3337, United States, 2008; American Chemical Society: 2540 Olentangy River Road, P.O. Box 3337, Columbus, OH 43210-3337, United States, 2008; Vol. 24; p 588.

29. Martinez, B.; Tomkins, J.; Wackett, L. P.; Wing, R.; Sadowsky, M. J., Complete nucleotide sequence and organization of the atrazine catabolic plasmid pADP-1 from Pseudomonas sp. strain ADP. *Journal of Bacteriology* **2001**, 183, 5684.

30. Govantes, F.; Garcia-Gonzalez, V.; Porrua, O.; Isabel Platero, A.; Jimenez-Fernandez, A.; Santero, E., Regulation of the atrazine-degradative genes in Pseudomonas sp strain ADP. *FEMS microbiology letters* **2010**, 310, 1.

31. Changey, F.; Devers-Lamrani, M.; Rouard, N.; Martin-Laurent, F., In vitro evolution of an atrazine-degrading population under cyanuric acid selection pressure: Evidence for the selective loss of a 47 kb region on the plasmid ADP1 containing the atzA, B and C genes. *Gene* **2011**, 490, 18.

32. Devers, M.; Rouard, N.; Martin-Laurent, F., Fitness drift of an atrazine-degrading population under atrazine selection pressure. *Environmental Microbiology* **2008**, 10, 676-684.

33. de Souza, M. L.; Wackett, L. P.; Sadowsky, M. J., The atzABC genes encoding atrazine catabolism are located on a self-transmissible plasmid in Pseudomonas sp. strain ADP. *Applied and Environmental Microbiology* **1998**, 64, 2323.

34. Schuster, K. C.; Reese, I.; Urlaub, E.; Gapes, J. R.; Lendl, B., Multidimensional information on the chemical composition of single bacterial cells by confocal Raman microspectroscopy. *Analytical Chemistry* **2000**, 72, 5529.

35. Huang, W. E.; Griffiths, R. I.; Thompson, I. P.; Bailey, M. J.; Whiteley, A. S., Raman microscopic analysis of single microbial cells. *Analytical Chemistry* **2004**, 76.

36. Kaiser Optical Systems, I. Raman Spectroscopy-A Tutorial. http://www.kosi.com/na_en/products/raman-spectroscopy/raman-technical-resources/raman-tutorial.php (November 2014)

37. Leeds, S. M. Characterization of the Gas-Phase Environment in a Microwave Plasma Enhanced Diamond Chemical Vapour Deposition Reactor Using Molecular Beam Mass Spectroscopy. University of Bristol, 1999.

38. Larkin, P., In *IR and raman spectroscopy*; Amsterdam ; Boston : Elsevier: Amsterdam ; Boston, 2011.

39. Choo-Smith, L.; Maquelin, K.; Van, V. T.; Bruining, H. A.; Puppels, G. J.; Ngo, T. N. A.; Kirschner, C.; Naumann, D.; Ami, D.; Villa, A. M.; Orsini, F.; Doglia, S. M.; Lamfarraj, H.; Sockalingum, G. D.; Manfait, M.; Allouch, P.; Endtz, H. P., Investigating Microbial (Micro)colony Heterogeneity by Vibrational Spectroscopy. *Applied and Environmental Microbiology* **2001**, 67, 1461.

40. Wagner, M.; Ivleva, N. P.; Haisch, C.; Niessner, R.; Horn, H., Combined use of confocal laser scanning microscopy (CLSM) and Raman microscopy (RM): Investigations on EPS - Matrix. *Water research* **2009**, 43, 63.

41. Sandt, C.; Smith-Palmer, T.; Pink, J.; Brennan, L.; Pink, D., Confocal Raman microspectroscopy as a tool for studying the chemical heterogeneities of biofilms in situ. *Journal of applied microbiology* **2007**, 103, 1808.

42. Abu-Absi, N. R.; Kenty, B. M.; Cuellar, M. E.; Borys, M. C.; Sakhamuri, S.; Strachan, D. J.; Hausladen, M. C.; Li, Z. J., Real Time Monitoring of Multiple Parameters in Mammalian Cell Culture Bioreactors Using an In-Line Raman Spectroscopy Probe. *Biotechnology and Bioengineering* **2011**, 108, 1215-1221.

43. Li, B.; Ryan, P. W.; Ray, B. H.; Leister, K. J.; Sirimuthu, N. M. S.; Ryder, A. G., Rapid Characterization and Quality Control of Complex Cell Culture Media Solutions Using Raman Spectroscopy and Chemometrics. *Biotechnology and Bioengineering* **2010**, 107, 290-301.

44. Maquelin, K.; Kirschner, C.; Choo-Smith, L. P.; van den Braak, N.; Endtz, H. P.; Naumann, D.; Puppels, G. J., Identification of medically relevant microorganisms by vibrational spectroscopy. *Journal of microbiological methods* **2002**, 51, 255.

45. Mobili, P.; Londero, A.; De Antoni, G.; Gomez-Zavaglia, A.; Araujo-Andrade, C.; Avila-Donoso, H.; Ivanov-Tzonchev, R.; Moreno, I.; Frausto-Reyes, C., Multivariate analysis of Raman spectra applied to microbiology Discrimination of microorganisms at the species level. *Revista Mexicana De Fisica* **2010**, 56, 378.

46. Patzold, R.; Keuntje, M.; Anders-Von Ahlften, A., A new approach to non-destructive analysis of biofilms by confocal Raman microscopy. *Analytical and Bioanalytical Chemistry* **2006**, 386, 286.

47. Chen, Y.-P.; Zhang, P.; Guo, J.-S.; Fang, F.; Gao, X.; Li, C., Functional groups characteristics of EPS in biofilm growing on different carriers. *Chemosphere* **2013**, 92, 633.

48. Clausen, G. B.; Larsen, L.; Johnsen, K.; de Lipthay, J. R.; Aamand, J., Quantification of the atrazine-degrading Pseudomonas sp strain ADP in aquifer sediment by quantitative competitive polymerase chain reaction. *FEMS microbiology ecology* **2002**, 41, 221.

49. Katz, I.; Dosoretz, C. G.; Mandelbaum, R. T.; Green, M., Atrazine degradation under denitrifying conditions in continuous culture of Pseudomonas ADP. *Water research* **2001**, 35, 3272.

50. Devers, M.; Soulas, G.; Martin-Laurent, F., Real-time reverse transcription PCR analysis of expression of atrazine catabolism genes in two bacterial strains isolated from soil. *Journal of microbiological methods* **2004**, 56, 3.

51. Herzberg, M.; Dosoretz, C. G.; Tarre, S.; Beliavski, M.; Green, M., Biological granulated activated carbon fluidized bed reactor for atrazine remediation. *Water Science and Technology* **2004**, 49, 215-222.

52. Biglione, N. K. Fundamental Kinetic Parameters of Suspended and Biofilm Atrazine Degrading Cells. University of Iowa, University of Iowa, 2008.

53. Xie, C. G.; Li, Y. Q.; Tang, W.; Newton, R. J., Study of dynamical process of heat denaturation in optically trapped single microorganisms by near-infrared Raman spectroscopy. *Journal of Applied Physics* **2003**, 94, 6138-6142.

54. Ude, S.; Bailey, M. J.; Huang, W. E.; Spiers, A. J., The environmental plasmid pQBR103 alters the single-cell Raman spectral profile of Pseudomonas fluorescens SBW25. *Microbial ecology* **2007**, 53, 494.

55. Tolker-Nielsen, T.; Sternberg, C., Growing and analyzing biofilms in flow chambers. *Current protocols in microbiology* **2011**, Chapter 1.

56. Nielsen, P. H.; Jahn, A. Extraction of EPS. In *Microbial Extracellular Polymeric Substances*, Wingender, J.; Neu, T. R.; Flemming, H.-C., Eds.; Springer: 1999; Chapter 3.

57. Apicella, M. A.; Shao, J. Q.; Neil, R. B., Methods for Studying Neisseria meningitidis Biofilms. *Neisseria Meningitidis: Advanced Methods and Protocols* **2012**, 799, 169-184.

58. Sheng, G. P.; Yu, H. Q.; Li, X. Y., Extracellular polymeric substances (EPS) of microbial aggregates in biological wastewater treatment systems: A review. *Biotechnology Advances* **2010**, 28, 882-894.

59. Nielsen, P. H.; Andreas, J. Extraction of EPS. In *Microbial Extracellular Polymeric Substances*, Wingender, J., Ed.; Springer-Vaerlag Berlin Heidelberg: 1999; Chapter Chapter 3.

60. Liang, Z. W.; Li, W. H.; Yang, S. Y.; Du, P., Extraction and structural characteristics of extracellular polymeric substances (EPS), pellets in autotrophic nitrifying biofilm and activated sludge. *Chemosphere* **2010**, 81, 626-632.

61. Castro, L.; Zhang, R.; Munoz, J. A.; Gonzalez, F.; Luisa Blazquez, M.; Sand, W.; Ballester, A., Characterization of exopolymeric substances (EPS) produced by Aeromonas hydrophila under reducing conditions. *Biofouling* **2014**, 30, 501.

62. David, C. Raman spectroscopy for proteins. Horiba Scientific2012; www.horiba.com/scientific.(Februrary 2014).

63. McGrath, K.; Kaplan, D., *Protein-Based Materials*. Birkhauser: Boston, 1997.

64. Radosevich, M.; Traina, S. J.; Hao, Y. L.; Tuovinen, O. H., DEGRADATION AND MINERALIZATION OF ATRAZINE BY A SOIL BACTERIAL ISOLATE. *Applied and Environmental Microbiology* **1995**, 61, 297-302.

65. Yang, C. Y.; Li, Y.; Zhang, K.; Wang, X.; Ma, C. Q.; Tang, H. Z.; Xu, P., Atrazine degradation by a simple consortium of Klebsiella sp A1 and Comamonas sp A2 in nitrogen enriched medium. *Biodegradation* **2010**, 21, 97-105.

66. Guo, Q. W.; Zhang, J. X.; Wan, R.; Xie, S. G., Impacts of carbon sources on simazine biodegradation by Arthrobacter strain SD3-25 in liquid culture and soil microcosm. *International Biodeterioration & Biodegradation* **2014**, 89, 1-6.

67. Solomon, R. D. J.; Kumar, A.; Satheeja Santhi, V., Atrazine biodegradation efficiency, metabolite detection, and trzD gene expression by enrichment bacterial cultures from agricultural soil. *Journal of Zhejiang University-Science B* **2013**, 14, 1162-1172.

68. Al-Mailem, D. M.; Eliyas, M.; Khanafer, M.; Radwan, S. S., Biofilms constructed for the removal of hydrocarbon pollutants from hypersaline liquids. *Extremophiles* **2015**, 19, 189-196.

69. Sadowsky, M. J.; Wackett, L. P., Genetics and biochemistry of atrazine biodegradation by pseudomonas sp strain ADP and other gram-negative bacteria. *Abstracts of Papers of the American Chemical Society* **1999**, 218, U118-U118.

70. Mandelbaum, R. T.; Wackett, L. P.; Allan, D. L., Mineralization of the S-Triazine Ring of Atrazine by Stable Bacterial Mixed Cultures. *Applied and Environmental Microbiology* **1993**, 59, 1695.

71. University of Iowa Central of Microscopy Research Facilty. Scanning Electron Microscopy. http://cmrf.research.uiowa.edu/scanning-electron-microscopy (October 2013).

72. Costa, J. C. S.; Ando, R. A.; Camargo, P. H. C.; Corio, P., Understanding the Effect of Adsorption Geometry over Substrate Selectivity in the Surface-Enhanced Raman Scattering Spectra of Simazine and Atrazine. *Journal of Physical Chemistry C* **2011**, 115, 4184.

73. Socrates, G., *Infrared and Raman characteristic group frequencies : tables and charts / George Socrates*. 3rd ed.. ed.; Chichester : Wiley: Chichester, 2004.

74. Rastogi, V.; Jain, D.; Mital, H.; Sharma, S., LASER RAMAN AND INFRARED-ABSORPTION SPECTRA OF 2,4-DICHLORONITROBENZENE. *Acta Physica Polonica A* **1991**, 79, 765-774.

75. He, L.; Liu, Y.; Lin, M.; Awika, J.; Ledoux, D.; Li, H.; Mustapha, A., A new approach to measure melamine, cyanuric acid, and melamine cyanurate using surface enhanced Raman spectroscopy coupled with gold nanosubstrates. *Sens. & Instrumen. Food Qual.* **2008**, 2, 66-71.

76. Keuleers, R.; Desseyn, H. O.; Rousseau, B.; Van Alsenoy, C., Vibrational Analysis of Urea. *Journal of Physical Chemistry A* **1999**, 103, 4621-4630.

77. Chen, F.; Gonzalez, J. M.; Dustman, W. A.; Moran, M. A.; Hodson, R. E., In situ reverse transcription, an approach to characterize genetic diversity and activities of prokaryotes. *Applied and Environmental Microbiology* **1997**, 63, 4907.

78. Sunde, P. T.; Olsen, I.; Göbel, U. B.; Theegarten, D.; Winter, S.; Debelian, G. J.; Tronstad, L.; Moter, A., Fluorescence in situ hybridization (FISH) for direct visualization of bacteria in periapical lesions of asymptomatic root-filled teeth. *Microbiology (Reading, England)* **2003**, 149, 1095.

79. Daims, H.; Brühl, A.; Amann, R.; Schleifer, K.-H.; Wagner, M., The Domain-specific Probe EUB338 is Insufficient for the Detection of all Bacteria: Development and Evaluation of a more Comprehensive Probe Set. *Systematic and Applied Microbiology* **1999**, 22, 434-444.

80. Schuster, K. C.; Ehmoser, H.; Gapes, J. R.; Lendl, B., On-line FT-Raman spectroscopic monitoring of starch gelatinisation and enzyme catalysed starch hydrolysis. *Vibrational Spectroscopy* **2000**, 22, 181-190.

81. Shaw, A. D.; Kaderbhai, N.; Jones, A.; Woodward, A. M.; Goodacre, R.; Rowland, J. J.; Kell, D. B., Noninvasive, on-line monitoring of the biotransformation by yeast of glucose to ethanol using dispersive Raman spectroscopy and chemometrics. *Applied Spectroscopy* **1999**, 53, 1419-1428.

82. Cannizzaro, C.; Rhiel, M.; Marison, I.; von Stockar, U., On-line monitoring of Phaffia rhodozyma fed-batch process with in situ dispersive Raman spectroscopy. *Biotechnology and Bioengineering* **2003**, 83, 668-680.

83. Eisenthal, R.; Danson, M. J.; Hough, D. W., Catalytic efficiency and kcat/KM: a useful comparator? *Trends in biotechnology* **2007**, 25, 247.

84. Oregan State University, KM, Kcat, and kcat/km. http://oregonstate.edu/dept/biochem/hhmi/hhmiclasses/bb450/winter2002/ch11/c11kkkk.htm (September 2015).

85. Scott, C.; Jackson, C. J.; Coppin, C. W.; Mourant, R. G.; Hilton, M. E.; Sutherland, T. D.; Russell, R. J.; Oakeshott, J. G., Catalytic Improvement and Evolution of Atrazine Chlorohydrolase. *Applied and Environmental Microbiology* **2009**, 75, 2184-2191.

86. Fruchey, I.; Shapir, N.; Sadowsky, M. J.; Wackett, L. P., On the origins of cyanuric acid hydrolase: Purification, substrates, and prevalence of AtzD from Pseudomonas sp strain ADP. *Applied and Environmental Microbiology* **2003**, 69, 3653-3657.

87. Cameron, S. M.; Durchschein, K.; Richman, J. E.; Sadowsky, M. J.; Wackett, L. P., New Family of Biuret Hydrolases Involved in s-Triazine Ring Metabolism. *Acs Catalysis* **2011**, 1, 1075-1082.

88. Shapir, N.; Sadowsky, M. J.; Wackett, L. P., Purification and characterization of allophanate hydrolase (AtzF) from Pseudomonas sp strain ADP. *Journal of Bacteriology* **2005**, 187, 3731-3738.

89. Chen, F.; Hodson, R. E., In situ PCR/RT-PCR coupled with in situ hybridization for detection of functional gene and gene expression in prokaryotic cells. *Methods in Microbiology, Vol 30* **2001**, 30, 409.

90. Amidzadeh, Z.; Behbahani, A. B.; Erfani, N.; Sharifzadeh, S.; Ranjbaran, R.; Moezi, L.; Aboualizadeh, F.; Okzhovat, M. A.; Parniyan, A.; Azarpira, N., Assessment of different permeabilization methods of minimizing damage to the adherent cells for detection of intracellular RNA by flow cytometry.(Original Article)(Report). *Avicenna Journal of Medical Biotechnology (AJMB)* **2014**, 6, 38.

91. Bagasra, O.; Harris, T., Latest developments in in situ PCR. *Methods in molecular biology (Clifton, N.J.)* **2006**, 334, 221.

92. Vandenabeele, P.; Moens, L., Micro-Raman spectroscopy of natural and synthetic indigo samples. *Analyst* **2003**, 128, 187-193.

93. Hallmark, V. M.; Zimba, C. G.; Swalen, J. D.; Rabolt, J. F., Ft-Raman Spectroscopy of Biological Molecules. *Mikrochimica acta* **1988**, 2, 215.

94. Goeres, D. M.; Hamilton, M. A.; Beck, N. A.; Buckingham-Meyer, K.; Hilyard, J. D.; Loetterle, L. R.; Lorenz, L. A.; Walker, D. K.; Stewart, P. S., A method for growing a biofilm under low shear at the air-liquid interface using the drip flow biofilm reactor. *Nature Protocols* **2009**, 4, 783-788.